Supporting Information
Tuning the Mechanical Properties of Molecular Perovskites by Controlling Framework Distortions *via* A-site Substitution

Silva M. Kronawitter,[a] Shinjoo Park,[a] Sebastian A. Hallweger,[a] Emily Myatt,[b] Jem Pitcairn,[b] Matthew J. Cliffe,[b] Dominik Daisenberger,[c] Markus Drees[a] and Gregor Kieslich*[a]

[a] Technical University of Munich, TUM Natural School of Sciences, Lichtenbergstr. 4, 85748, Garching, Germany.
[b] School of Chemistry, University of Nottingham, Nottingham NG7 2RD, United Kingdom.
[c] Diamond Light Source Ltd., Diamond House, Harwell Campus, Didcot OX11 ODE, United Kingdom.
*gregor.kieslich@tum.de

Contents:

1. Material synthesis

All used chemicals for the A-site cation (A^+) precursor synthesis and molecular perovskite synthesis were purchased from Sigma Aldrich without further purification. Solvents and ultrapure (Millipore) water were in the quality of reagent grade.

Synthesis of the A-site precursor 1,1-diethylpiperidinium bromide – [DEP]Br:

12.30 mL (0.9 mol, 1 eq.) 1,5-dibromopentane was added in a three-necked flask setup to 20 ml acetonitrile under stirring. The solution was heated up to reflux, and 10.30 mL (1 mol, 1.1 eq.) diethylamine was added dropwise. After stirring overnight, 12 g of potassium carbonate was added, and the mixture was stirred overnight at reflux temperature. The mixture was filtered, and the excess solvent was removed *in vacuo*, yielding a white, crystalline precipitate recrystallised in isopropanol and dried *in vacuo*. 10.55 g (52.2% yield) of the product was obtained.

^{1}H NMR: (400 MHz, deuterated chloroform): δ / ppm = 3.65 (*t*, 4 H), 3.58 (*q*, 4 H), 1.88 (*q,* 4 H), 1.81 (*q,* 2 H), 1.33 (*t*, *J* = 7.3 Hz, 6 H).

^{13}C NMR:(100 MHz, deuterated chloroform): δ / ppm = 57.78, 52.82, 20.37, 19.42, 7.12.

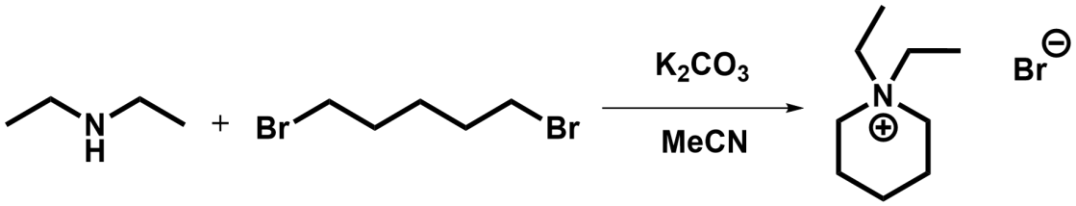

Figure S1: Nucleophilic substitution reaction scheme towards the synthesis of the A-site cation precursor salt [DEP]Br ($[DEP]^+ = [C_9H_{20}N]^+$).

Synthesis of the A-site precursor 1-ethyl-1-propylpiperidinium bromide – [PEP]Br:

In a three-necked flask, 9.11 mL (0.1 mol, 1 eq.) bromopropane was added dropwise to a stirring solution of 13.81 mL (0.1 mol, 1 eq.) ethylpiperidine in 40 mL acetonitrile. The mixture was heated to reflux overnight, and 14 g of potassium carbonate was added. The mixture was stirred at reflux temperature overnight. The solvent was removed *in vacuo*, and the crystalline product was washed using 70 mL ethyl acetate, yielding a pure product of 19.18 g (81.2%).

^{1}H NMR: (400 MHz, deuterium oxide): δ / ppm = 3.28 (*q*, 2 H), 3.22 (*m*, 4 H), 3.12 (*m*, 2 H), 1.77 (*m,* 4 H), 1.60 (*m,* 4 H), 1.18 (*t*, *J* = 1.8 Hz, 3 H), 0.88 (*t*, *J* = 7.3 Hz, 3 H).

^{13}C NMR: (100 MHz, deuterium oxide): δ / ppm = 59.01, 58.70, 53.78, 20.74, 19.06, 14.36, 9.91, 6.33.

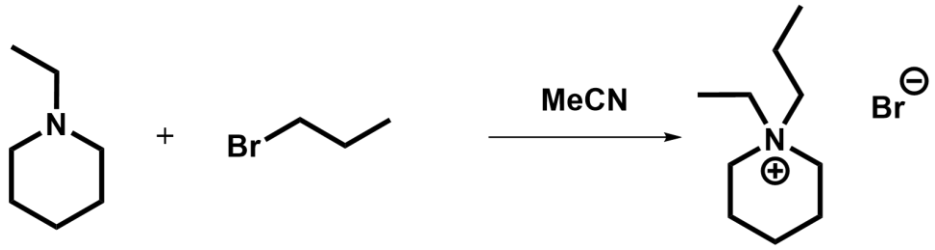

Figure S2: Nucleophilic substitution reaction scheme towards the synthesis of the A-site cation precursor salt [PEP]Br ($[PEP]^+ = [C_{10}H_{22}N]^+$).

Synthesis of the A-site precursor 1,1-diisopropylpiperidinium bromide – [DIP]Br:

12.30 mL (0.9 mol, 1 eq.) 1,5-dibromopentane was added in a three-necked flask to 40 ml methanol under stirring. The solution was heated to reflux, and 14.05 mL (1 mol, 1.1 eq.) di-isopropylamine was added dropwise. The mixture was stirred overnight. In the next step, 16 g potassium carbonate was added, and the mixture was stirred for 3 h at reflux temperature. After cooling down to room temperature, the base was filtered, forming a white, crystalline precipitate, which was recrystallised in isopropanol and dried *in vacuo*, yielding 3.77 g (16.5% yield).

^{1}H NMR: (400 MHz, deuterium oxide): δ / ppm = 3.98 (*p*, 2 H), 3.29 (*t*, 4 H), 1.79 (*m,* 4 H), 1.58 (*p,* 2 H), 1.35 (*dt*, *J* = 1.5 Hz, 12 H).

^{13}C NMR: (100 MHz, deuterium oxide): δ / ppm = 60.27, 53.47, 20.61, 19.46, 17.10.

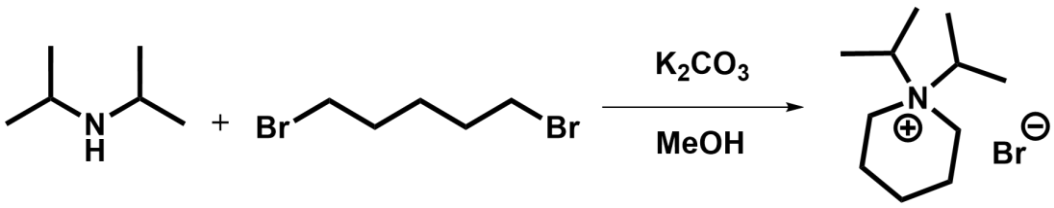

Figure S3: Nucleophilic substitution reaction scheme towards the synthesis of the A-site cation precursor salt [DIP]Br ($[DIP]^+ = [C_{11}H_{24}N]^+$).

Synthesis of the A-site precursor 1,1-dipropylpiperidinium bromide – [DPP]Br:

1,1-dipropylpiperidinium bromide was prepared in a two-step synthesis. First 1-propylpiperidinium bromide was synthesised starting from 4.10 mL (41.4 mmol, 1 eq.) piperidine and 4.15 mL (45.6 mmol, 1.1 eq.) bromopropane in 30 mL acetonitrile. Next, the solution was heated to reflux and stirred overnight. After cooling to room temperature, the solvent was removed *in vacuo*, followed by working up with 70 mL ethyl acetate to remove the solvent *via* decantation. The white crystalline product was recrystallised in 10 mL acetonitrile and washed with ethyl acetate, yielding 5.11 g (24.55% yield).

^{1}H NMR: (400 MHz, deuterium oxide): δ / ppm = 3.29 (d, 3*J* = 12.3 Hz, 2H), 3.00 (m, 2H), 2.87 (td, 3*J* = 12.6, 3.1 Hz, 2H), 1.91 (d, 3*J* = 14.7 Hz, 2H), 1.57 (m, 6H), 0.92 (t, *J* = 37.4 Hz, 3H).
^{13}C NMR: (100 MHz, deuterium oxide): δ / ppm = 58.42, 53.02, 22.76, 21.13, 17.04, 10.11.

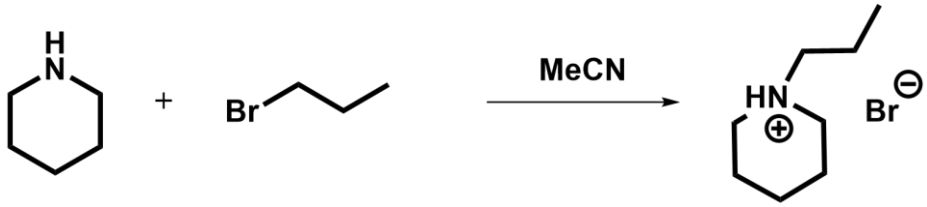

Figure S4: Synthesis of 1-propylpiperidinium bromide.

In a second step, 4.10 g (19.7 mmol, 1 eq.) 1-propylpiperidinium bromide was dissolved in 40 mL ethanol and 9 g potassium carbonate was added. Next, the solution was heated to reflux temperature and 3.85 mL (39.4 mmol, 2 eq.) bromopropane was added dropwise followed by stirring under reflux overnight. After cooling down, the base was removed *via* filtration. The remaining solvent was removed, and the crystalline product was recrystallised in 30 mL ethyl acetate, yielding 4.032 g (81.7% yield).

^{1}H NMR: (400 MHz, deuterium oxide): δ / ppm = 3.29 (t, 3*J* = 5.8 Hz, 4H), 3.19 (m, 4H), 1.82 (m, 4H), 1.65 (m, 6H), 0.92 (t, 3*J* = 7.3 Hz, 6H).
^{13}C NMR: (100 MHz, deuterium oxide): δ / ppm = 61.66, 59.17, 20.71, 19.08, 14.40, 9.82.

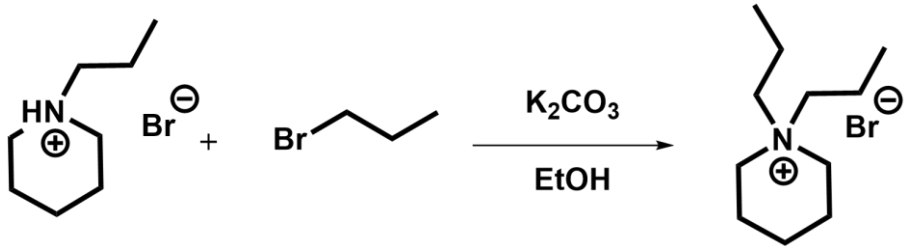

Figure S5: Synthesis towards 1,1-dipropylpiperidinium bromide used as A-site precursor salt [DPP]Br ($[DPP]^{+}$ = $[C_{11}H_{24}N]^{+}$).

Synthesis of molecular perovskites $[A]Ni(C_2N_3)_3$:

Single crystals of the family of molecular perovskites $[A]Ni(C_2N_3)_3$ (A^+ = $[DEP]^+$ = $[C_9H_{20}N]^+$, $[PEP]^+$ = $[C_{10}H_{22}N]^+$, $[DIP]^+$ = $[C_{11}H_{24}N]^+$ and $[DPP]^+$ = $[C_{11}H_{24}N]^+$) were synthesised following an established mild solution crystallisation method in aqueous solution from commercially available $Na(C_2N_3)$ (96 %, Sigma-Aldrich), $Ni(NO_3)_2{\cdot}6H_2O$ (98 %, Sigma-Aldrich) and ultrapure water.[1] In a typical crystallisation routine, 1 mL ultrapure water was placed in a glass vial, and the precursor solutions were layered on top in order of 0.5 mL of the respective aqueous [DIP]Br solution (0.2 M), 1.0 mL of an aqueous $Ni(NO_3)_2$ solution (0.4 M) and 0.3 mL of an aqueous sodium dicyanamide solution (2 M). After cooling in a refrigerator overnight, small, well-defined block single crystals with sizes between 2 and 4 mm were collected at ambient temperature, washed with ultrapure water, and dried (Fig. S6).

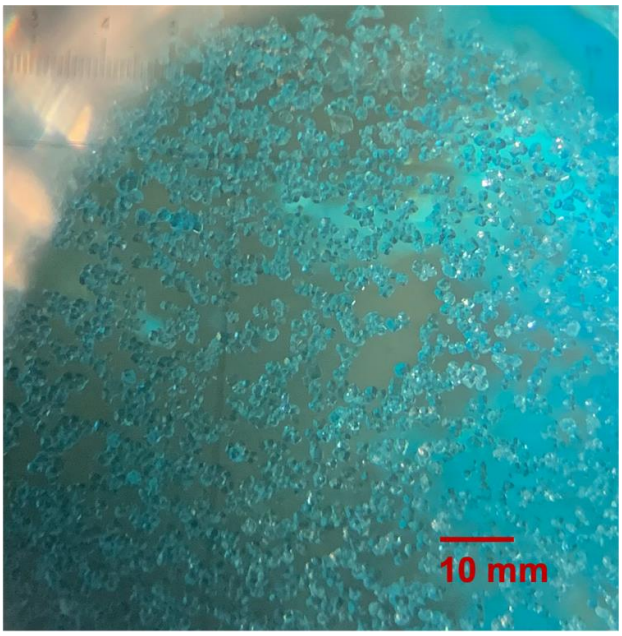

Figure S6: Microscopic image of the crystalline compound $[DIP]Ni(C_2N_3)_3$ showing small block-shaped blue crystals.

Elemental analysis:

The elemental analysis measurements and quantifications of the synthesised molecular perovskites $[A]Ni(C_2N_3)_3$ ($A^+ = [PEP]^+ = [C_{10}H_{22}N]^+$, $[DEP]^+ = [C_9H_{20}N]^+$, $[DIP]^+ = [C_{11}H_{24}N]^+$ and $[DPP]^+ = [C_{11}H_{24}N]^+$) were determined by the technical staff of the microanalytical laboratory at the Catalysis Research Center at the Technical University of Munich. The elemental composition (sample weight around 5 – 10 mg) was analysed using a *HEKAtech* Euro EA elemental analyser with flash combustion at 1800 °C and subsequent chromatographical separation and quantification with a thermal conductivity detector (TCD).

$[DEP]Ni(C_2N_3)_3$: calc. C 45.60 H 4.08 N 35.46 Ni 14.86, found C 45.63 H 4.09 N 35.02 Ni 14.71.

$[PEP]Ni(C_2N_3)_3$: calc. C 46.52 H 5.37 N 33.91 Ni 14.26, found C 46.23 H 5.32 N 33.23 Ni 14.20.

$[DIP]Ni(C_2N_3)_3$: calc. C 47.80 H 5.66 N 32.79 Ni 13.74, found C 46.82 H 5.51 N 32.41 Ni 13.42.

$[DPP]Ni(C_2N_3)_3$: calc. C 47.80 H 5.66 N 32.79 Ni 13.74, found C 47.56 H 5.48 N 32.73 Ni 13.89.

Synthesis of $[PEP]_{1-x}[DPP]_xNi(C_2N_3)_3$ solid solutions:

Similar to the described synthesis of the pure molecular perovskite compounds $[A]Ni(C_2N_3)_3$, the solid solutions were prepared *via* a mild solution route in aqueous solution using commercially available $Na(C_2N_3)$ (96 %, Sigma-Aldrich), $Ni(NO_3)_2 \cdot 6H_2O$ (98 %, Sigma-Aldrich) and ultrapure water. After adding 1 mL of ultrapure water to the bottom of a glass vial, a mixture of the A-site precursors [PEP]Br/[DPP]Br (0.5/0 mL, 0.4/0.1 mL, 0.25/0.25 mL, 0.15/0.35 mL, 0.05/0.45 mL and 0/0.5 mL) in varying ratios was added, followed by 1 mL of an aqueous $Ni(NO_3)_2$ solution (0.4 M) and 0.3 mL of an aqueous sodium dicyanamide solution (2 M). After cooling overnight, small single crystals were obtained, which were not suitable for SCXRD analysis.

2. Single crystal X-ray diffraction (SCXRD) data

The single crystal X-ray diffraction experiments of the molecular perovskites $[A]Ni(C_2N_3)_3$ (A^+ = $[DEP]^+$ = $[C_9H_{20}N]^+$, $[PEP]^+$ = $[C_{10}H_{22}N]^+$, $[DIP]^+$ = $[C_{11}H_{24}N]^+$ and $[DPP]^+$ = $[C_{11}H_{24}N]^+$) were performed using a *Bruker* APEX-II CCD diffractometer equipped with a fine focus tube with a Mo K_a radiation source (λ = 0.71073 Å), a *Triumph* monochromator, a CMOS plate detector and an *Oxford Cryosystem* for temperature control. Suitable single crystals were selected and mounted onto a Kapton micro-sample loop in perfluorinated ether, fixed to the instrument goniometer and cooled to 100 K under a stream of cold nitrogen flow. A matrix scan for initial unit cell determination, data reduction and absorption correction (including odd and even ordered spherical harmonics was performed using SADABS[2]) was performed by using the APEX III software package.[3] Reflections were merged and corrected for Lorentz and polarisation effects, scan speed and background using SAINT.[4] The successful structure refinement and systematic absences were used as the basis for the respective space group assignments. The structure solution was performed by using SHELX[5,6] as integrated in Olex2.[7] Structures were solved by direct methods with the aid of successive difference Fourier maps and were refined against all data. The VESTA software package 3.4.0 was used to visualise the crystal structures (Fig. S7-S10).[8]

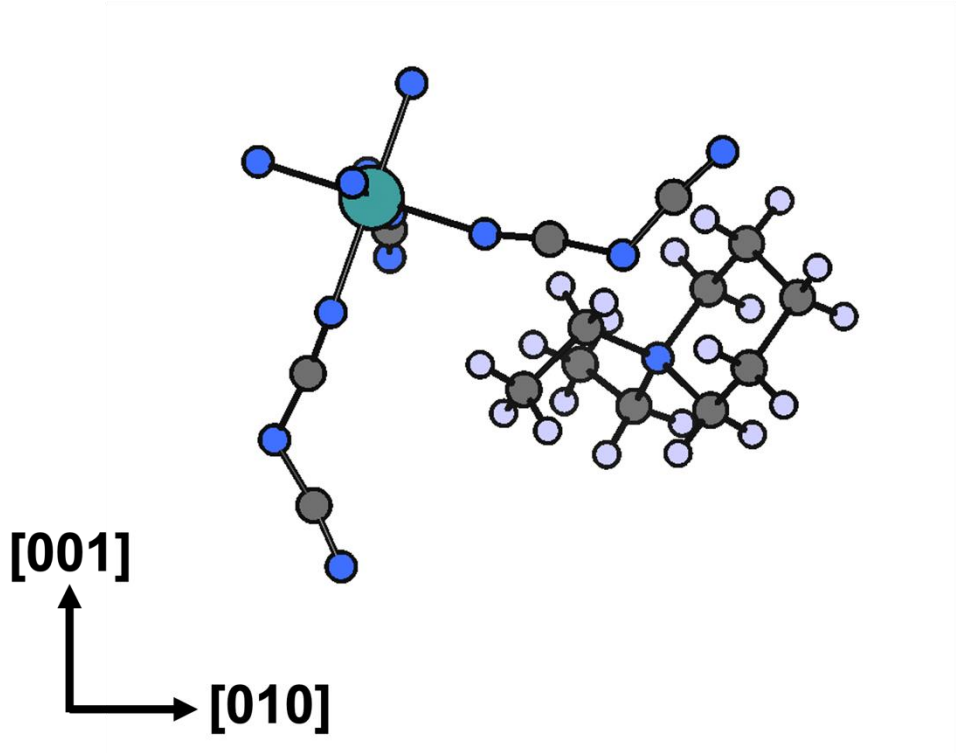

Figure S7: Structure of the asymmetric unit of [DEP]Ni(C_2N_3)$_3$ when looking along the [100] axis with $(C_2N_3)^-$ ligands acting as bridges between the Ni^{2+} cations while the $[DEP]^+$ cations occupy the void of the pseudo-cubic ReO_3 cavities. Colour code: Ni – green, N – blue, C – dark grey and H – light purple.

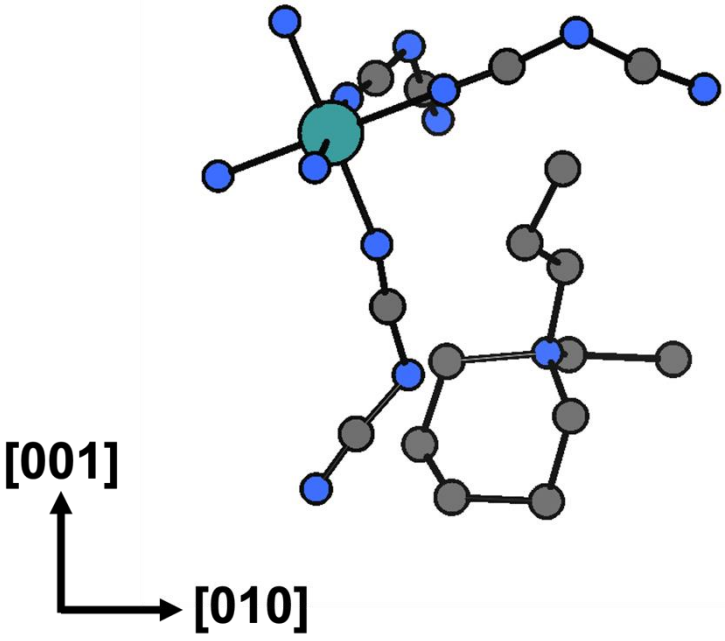

Figure S8: Structure of the asymmetric unit of [PEP]Ni(C_2N_3)$_3$ when looking along the [100] axis with $(C_2N_3)^-$ ligands acting as bridges between the Ni^{2+} cations while the $[PEP]^+$ cations occupy the void of the pseudo-cubic ReO_3 cavities. Colour code: Ni – green, N – blue, C – dark grey and H – atoms were neglected.

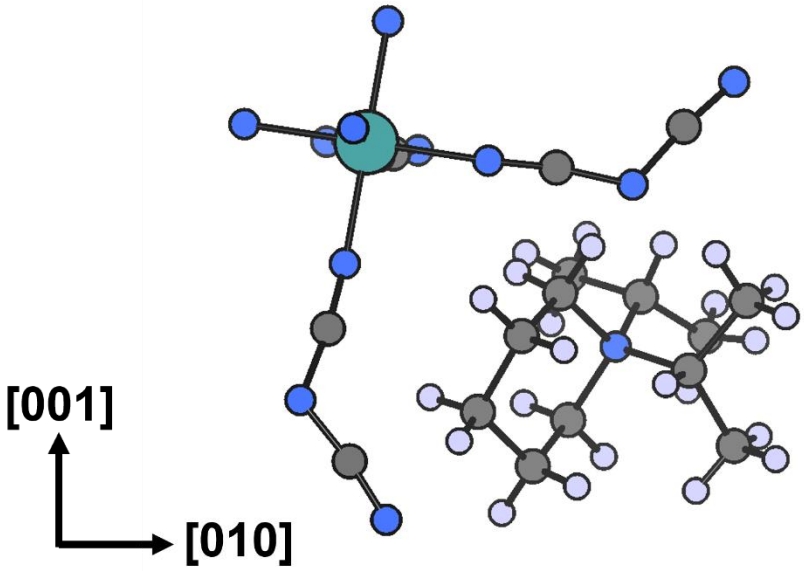

Figure S9: Structure of the asymmetric unit of [DIP]Ni(C_2N_3)$_3$ when looking along the [100] axis with $(C_2N_3)^-$ ligands acting as bridges between the Ni^{2+} cations while the $[DIP]^+$ cations occupy the void of the pseudo-cubic ReO_3 cavities, with the longer butyl group slightly extending into the neighbouring cavity. Colour code: Ni – green, N – blue, C – dark grey and H – light purple.

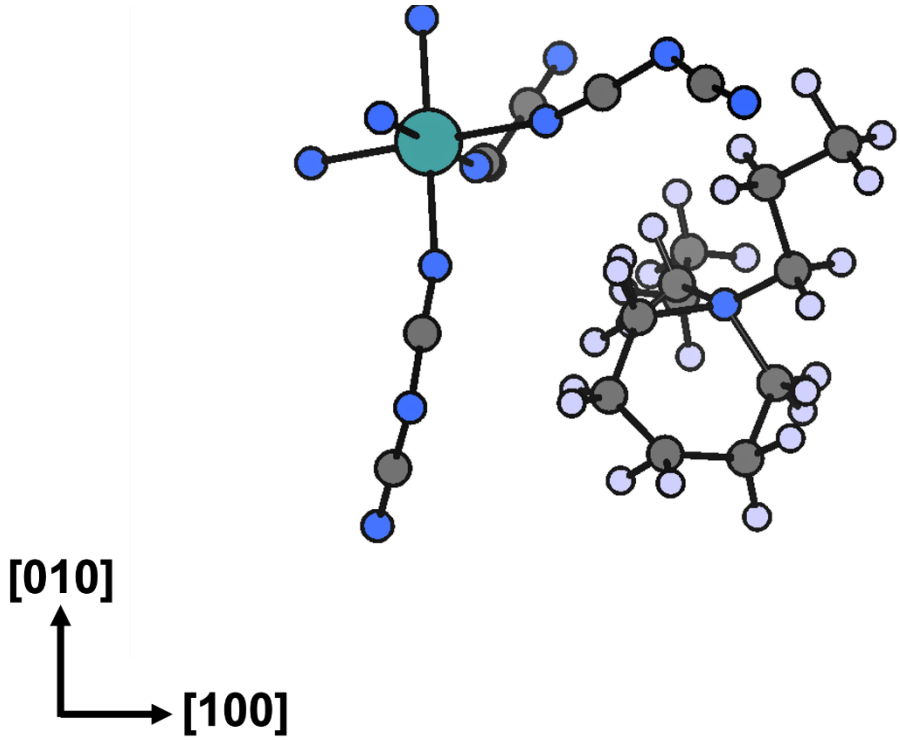

Figure S10: Structure of the asymmetric unit of [DPP]Ni(C_2N_3)$_3$ when looking along the [001] axis with $(C_2N_3)^-$ ligands acting as bridges between the Ni^{2+} cations while the $[DPP]^+$ cations occupy the void of the pseudo-cubic ReO_3 cavities, with the longer butyl group slightly extending into the neighbouring cavity. Colour code: Ni – green, N – blue, C – dark grey and H – light purple.

Table S1: Crystallographic data from SCXRD for the as-synthesised [DEP]Ni(C_2N_3)$_3$ at 100 K.

Compound	[DEP]Ni(C_2N_3)$_3$
Chemical Formula	$C_{15}H_{20}NiN_{10}$
Formula weight (g/mol)	399.12
Temperature (K)	100
Crystal system	monoclinic
Space group	$P2_1/c$
a (Å)	16.3161(17)
b (Å)	12.1389(13)
c (Å)	10.1679(11)
α (°)	90
β (°)	101.691(3)
γ (°)	90
Volume (Å^3)	1972.1(4)
Z	4
ρ_{calc} (g/cm^3)	1.344
μ (mm^{-1})	1.004
F (000)	832.0
Radiation	MoK_α (λ = 0.71073)
2θ range for data collection (°)	2.65 to 26.47
Index ranges	$-20 \le h \le 20$
	$-15 \le k \le 15$
	$-12 \le l \le 12$
Reflections collected	48266
Independent reflections	4029 [R_{int} = 0.0267, R_{sigma} = 0.0110]
Data/restraints/parameters	4029/0/198
Goodness of fit on F^2	1.048
Final R indexes [I > 2σ (I)]	R_1 = 0.0523, wR_2 = 0.1136
Final R indexes [all data]	R_1 = 0.0555, wR_2 = 0.1159
Largest diff. peak/hole/ (Å^{-3})	1.015/-0.709
Deposition number	CCDC 2309035

Table S2: Crystallographic data from SCXRD for the as-synthesised [PEP]Ni(C_2N_3)$_3$ at 100 K.

Compound	[PEP]Ni(C_2N_3)$_3$
Chemical Formula	$C_{16}H_{22}NiN_{10}$
Formula weight (g/mol)	413.14
Temperature (K)	100
Crystal system	monoclinic
Space group	$P2_1/c$
a (Å)	16.3743(14)
b (Å)	11.9171(9)
c (Å)	10.4761(8)
α (°)	90
β (°)	105.903(4)
γ (°)	90
Volume (Å^3)	1966.0(3)
Z	4
ρ_{calc} (g/cm^3)	1.396
μ (mm^{-1})	1.010
F (000)	864.0
Radiation	MoK_α (λ = 0.71073)
2θ range for data collection (°)	2.59 to 30.31
Index ranges	$-22 \leq h \leq 23$
	$-17 \leq k \leq 17$
	$-14 \leq l \leq 15$
Reflections collected	32134
Independent reflections	6028 [R_{int} = 0.0814, R_{sigma} = 0.0650]
Data/restraints/parameters	6028/0/239
Goodness of fit on F^2	1.054
Final R indexes [I > 2σ (I)]	R_1 = 0.0685, wR_2 = 0.1592
Final R indexes [all data]	R_1 = 0.1315, wR_2 = 0.1920
Largest diff. peak/hole/ (Å^{-3})	1.096/-1.163
Deposition number	CCDC 2309049

Table S3: Crystallographic data from SCXRD for the as-synthesised [DIP]Ni(C_2N_3)$_3$ at 100 K.

Compound	[DIP]Ni(C_2N_3)$_3$
Chemical Formula	$C_{17}H_{24}NiN_{10}$
Formula weight (g/mol)	427.15
Temperature (K)	100
Crystal system	monoclinic
Space group	$P2_1/c$
a (Å)	16.1247(8)
b (Å)	11.9812(5)
c (Å)	10.8829(5)
α (°)	90
β (°)	95.986(2)
γ (°)	90
Volume (Å^3)	2091.04(17)
Z	4
ρ_{calc} (g/cm^3)	1.281
μ (mm^{-1})	0.952
F (000)	896.0
Radiation	MoK_α (λ = 0.71073)
2θ range for data collection (°)	2.122 to 28.312
Index ranges	$-21 \leq h \leq 21$
	$-15 \leq k \leq 15$
	$-14 \leq l \leq 14$
Reflections collected	96894
Independent reflections	5203 [R_{int} = 0.0211, R_{sigma} = 0.0080]
Data/restraints/parameters	5203/0/260
Goodness of fit on F^2	1.037
Final R indexes [I > 2σ (I)]	R_1 = 0.0237, wR_2 = 0.0627
Final R indexes [all data]	R_1 = 0.0258, wR_2 = 0.0644
Largest diff. peak/hole/ (Å^{-3})	0.363/-0.247
Deposition number	CCDC 2309038

Table S4: Crystallographic data from SCXRD for the as-synthesised [DPP]Ni(C_2N_3)$_3$ at 100 K.

Compound	[DPP]Ni(C_2N_3)$_3$
Chemical Formula	$C_{17}H_{24}NiN_{10}$
Formula weight (g/mol)	427.15
Temperature (K)	100
Crystal system	monoclinic
Space group	*C2/c*
a (Å)	17.1198(15)
b (Å)	12.3344(10)
c (Å)	10.2007(9)
α (°)	90
β (°)	110.800(3)
γ (°)	90
Volume (Å^3)	2013.6(3)
Z	4
ρ_{calc} (g/cm^3)	1.409
μ (mm^{-1})	0.989
F (000)	896.0
Radiation	MoK_α (λ = 0.71073)
2θ range for data collection (°)	2.55 to 25.37
Index ranges	-20 ≤ *h* ≤ 20
	-14 ≤ *k* ≤ 14
	-12 ≤ *l* ≤ 12
Reflections collected	22253
Independent reflections	1847 [R_{int} = 0.0652, R_{sigma} = 0.0257]
Data/restraints/parameters	1847/0/153
Goodness of fit on F^2	1.074
Final R indexes [I > 2σ (I)]	R_1 = 0.0473, wR_2 = 0.1184
Final R indexes [all data]	R_1 = 0.0534, wR_2 = 0.1226
Largest diff. peak/hole/ (Å^{-3})	0.875/-0.789
Deposition number	CCDC 2309042

Table S5: Crystallographic data from SCXRD for the as-synthesised [DEP]Ni(C_2N_3)$_3$ at 300 K.

Compound	[DEP]Ni(C_2N_3)$_3$
Chemical Formula	$C_{15}H_{20}NiN_{10}$
Formula weight (g/mol)	399.12
Temperature (K)	300
Crystal system	monoclinic
Space group	$P2_1/c$
a (Å)	16.3871(7)
b (Å)	12.2076(5)
c (Å)	10.2673(4)
α (°)	90
β (°)	100.250(2)
γ (°)	90
Volume (Å^3)	2021.16(14)
Z	4
ρ_{calc} (g/cm^3)	1.312
μ (mm^{-1})	0.980
F (000)	832.0
Radiation	MoK_α (λ = 0.71073)
2θ range for data collection (°)	2.092 to 31.032
Index ranges	$-23 \leq h \leq 23$
	$-17 \leq k \leq 17$
	$-14 \leq l \leq 14$
Reflections collected	61583
Independent reflections	6371 [R_{int} = 0.0957, R_{sigma} = 0.0473]
Data/restraints/parameters	6371/0/240
Goodness of fit on F^2	1.172
Final R indexes [I > 2σ (I)]	R_1 = 0.0609, wR_2 = 0.1782
Final R indexes [all data]	R_1 = 0.1254, wR_2 = 0.2452
Largest diff. peak/hole/ (Å^{-3})	0.609/-0.593
Deposition number	CCDC 2309036

Table S6: Crystallographic data from SCXRD for the as-synthesised [PEP]Ni(C_2N_3)$_3$ at 300 K.

Compound	[PEP]Ni(C_2N_3)$_3$
Chemical Formula	$C_{16}H_{22}NiN_{10}$
Formula weight (g/mol)	413.14
Temperature (K)	300
Crystal system	monoclinic
Space group	$P2_1/c$
a (Å)	16.4756(7)
b (Å)	11.9516(5)
c (Å)	10.6587(4)
α (°)	90
β (°)	104.9160(10)
γ (°)	90
Volume (Å^3)	2028.08(14)
Z	4
ρ_{calc} (g/cm^3)	1.353
μ (mm^{-1})	0.979
F (000)	864.0
Radiation	MoK_α (λ = 0.71073)
2θ range for data collection (°)	2.56 to 24.09
Index ranges	$-18 \leq h \leq 18$
	$-13 \leq k \leq 13$
	$-12 \leq l \leq 12$
Reflections collected	30600
Independent reflections	3184 [R_{int} = 0.0737, R_{sigma} = 0.0362]
Data/restraints/parameters	3184/0/249
Goodness of fit on F^2	1.117
Final R indexes [I > 2σ (I)]	R_1 = 0.0606, wR_2 = 0.1630
Final R indexes [all data]	R_1 = 0.0943, wR_2 = 0.2082
Largest diff. peak/hole/ (Å^{-3})	0.603/-0.481
Deposition number	CCDC 2309050

Table S7: Crystallographic data from SCXRD for the as-synthesised [DIP]Ni(C_2N_3)$_3$ at 300 K.

Compound	[DIP]Ni(C_2N_3)$_3$
Chemical Formula	$C_{17}H_{24}NiN_{10}$
Formula weight (g/mol)	427.17
Temperature (K)	300
Crystal system	monoclinic
Space group	$P2_1/c$
a (Å)	16.346(2)
b (Å)	12.0065(16)
c (Å)	11.0462(17)
α (°)	90
β (°)	93.708(6)
γ (°)	90
Volume (Å^3)	2163.4(5)
Z	4
ρ_{calc} (g/cm^3)	1.312
μ (mm^{-1})	0.920
F (000)	896.0
Radiation	MoK_α (λ = 0.71073)
2θ range for data collection (°)	2.50 to 26.25
Index ranges	$-20 \le h \le 20$
	$-15 \le k \le 15$
	$-13 \le l \le 13$
Reflections collected	46500
Independent reflections	4227 [R_{int} = 0.0445, R_{sigma} = 0.0230]
Data/restraints/parameters	4227/0/260
Goodness of fit on F^2	2.669
Final R indexes [I > 2σ (I)]	R_1 = 0.1450, wR_2 = 0.5296
Final R indexes [all data]	R_1 = 0.1558, wR_2 = 0.5445
Largest diff. peak/hole/ (Å^{-3})	1.639/-0.765
Deposition number	CCDC 2309039

Table S8: Crystallographic data from SCXRD for the as-synthesised [DPP]Ni(C_2N_3)$_3$ at 300 K.

Compound	[DPP]Ni(C_2N_3)$_3$
Chemical Formula	$C_{17}H_{24}NiN_{10}$
Formula weight (g/mol)	427.15
Temperature (K)	300
Crystal system	monoclinic
Space group	C2/*c*
a (Å)	17.3196(5)
b (Å)	12.3357(3)
c (Å)	10.4909(3)
α (°)	90
β (°)	111.9170(10)
γ (°)	90
Volume (Å^3)	2079.38(10)
Z	4
ρ_{calc} (g/cm^3)	1.365
μ (mm^{-1})	0.957
F (000)	896.0
Radiation	MoK_α (λ = 0.71073)
2θ range for data collection (°)	2.081 to 29.145
Index ranges	-23 ≤ *h* ≤ 23
	-16 ≤ *k* ≤ 16
	-14 ≤ *l* ≤ 14
Reflections collected	52302
Independent reflections	2803 [R_{int} = 0.0502, R_{sigma} = 0.0194]
Data/restraints/parameters	2803/0/131
Goodness of fit on F^2	1.180
Final R indexes [I > 2σ (I)]	R_1 = 0.0592, wR_2 = 0.1756
Final R indexes [all data]	R_1 = 0.0848, wR_2 = 0.2271
Largest diff. peak/hole/ (Å^{-3})	0.736/-1.038
Deposition number	CCDC 2309043

3. NMR spectroscopy of the precursor A-site cations

To confirm the chemical composition of the A-site precursor salts ([DEP]Br, [PEP]Br, [DIP]Br and [DPP]Br), we used a combination of ^{1}H and ^{13}C NMR measurements. All NMR spectra were recorded on a *Bruker* AVIII 400 US spectrometer at ambient temperature (298 K). Chemical shifts are expressed as parts per million (δ / ppm) and are corrected for the strongest residual solvent shift as an internal standard for ^{1}H NMR spectra. The following descriptions of signal multiplicity are used: *t* = triplet, *dt* = doublet of triplets, *p* = pentet, *q* = quartet and *m* = multiplet. NMR data are reported in the order of chemical shifts (multiplicity, coupling constant and integral). The coupling constants are absolute values and are expressed in Hertz (Hz).[9]

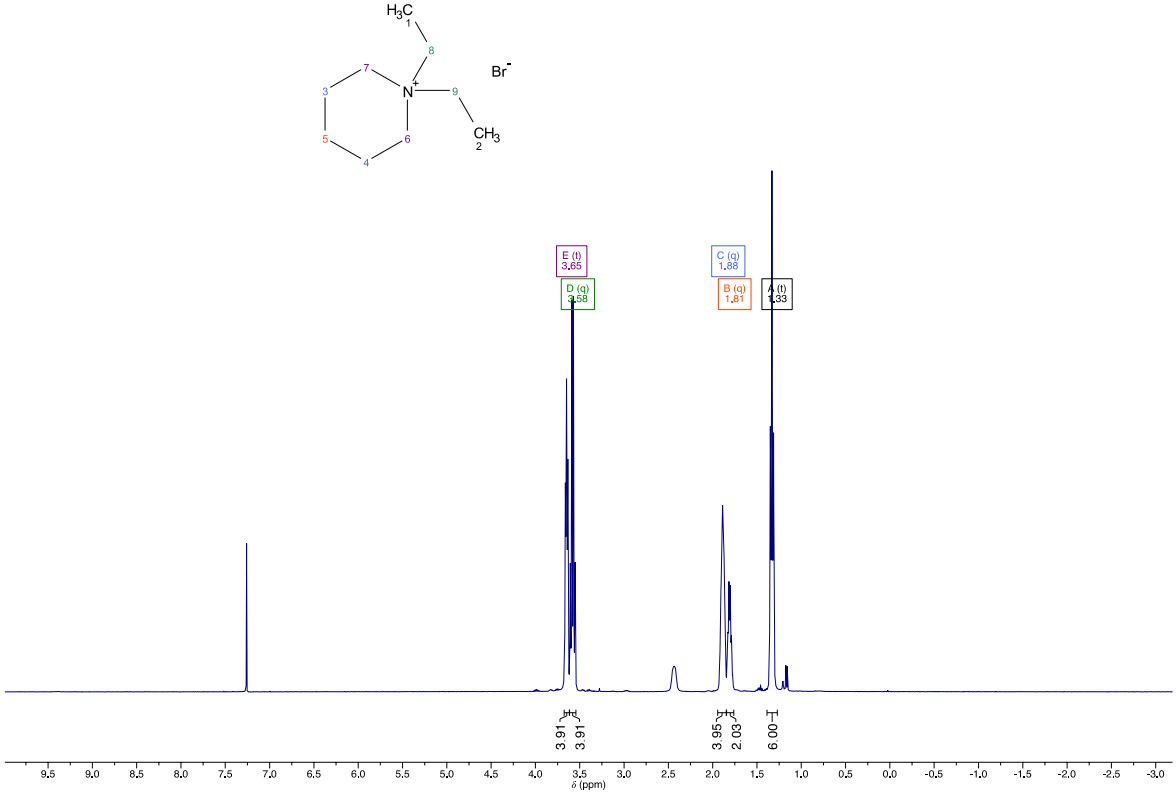

Figure S11: ^{1}H NMR spectrum of [DEP]Br in $CDCl_3$.

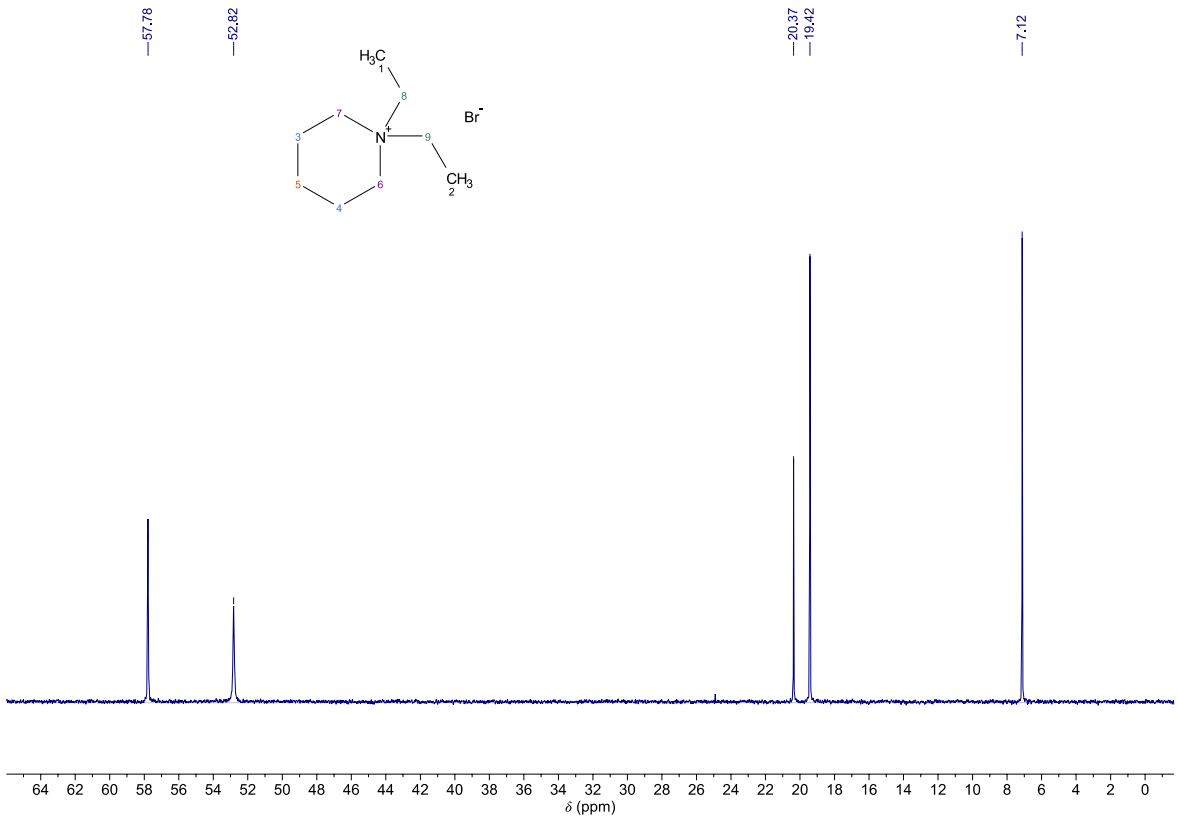

Figure S12: ^{13}C NMR spectrum of [DEP]Br in $CDCl_3$.

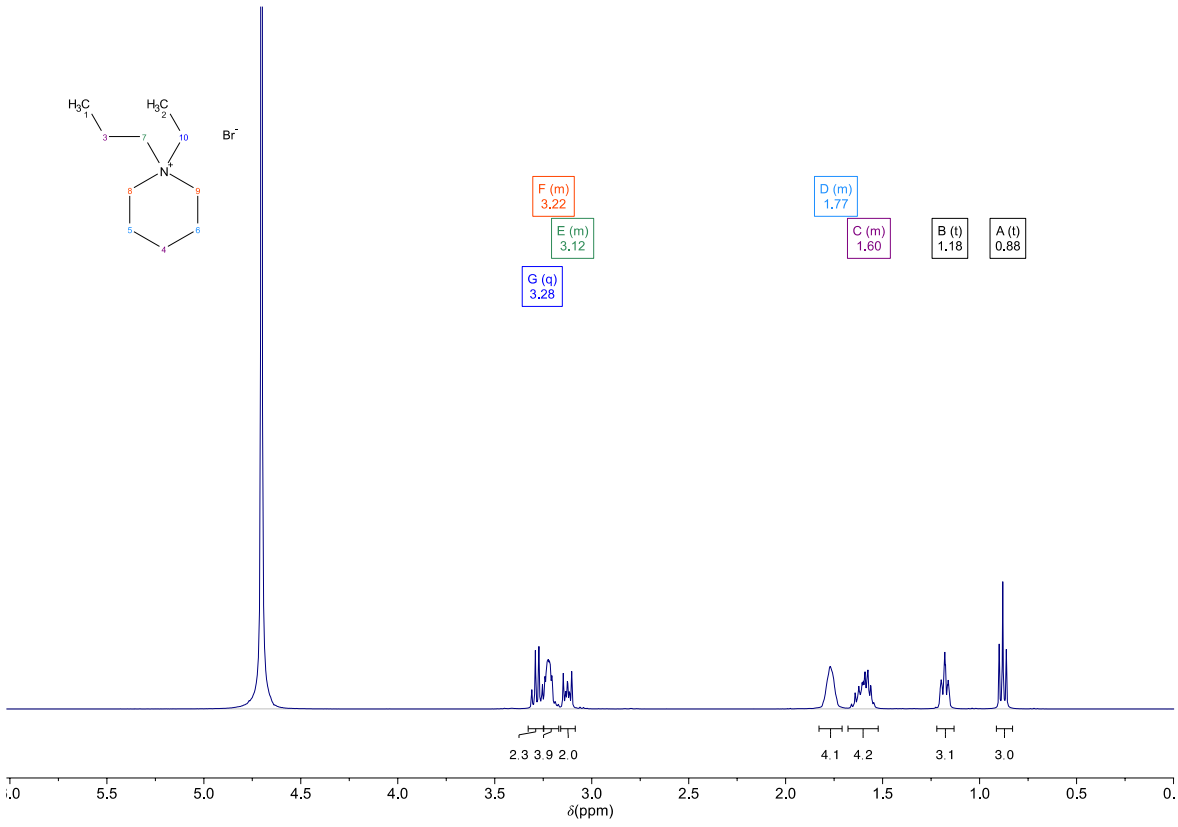

Figure S13: ^{1}H NMR spectrum of [PEP]Br in D_2O.

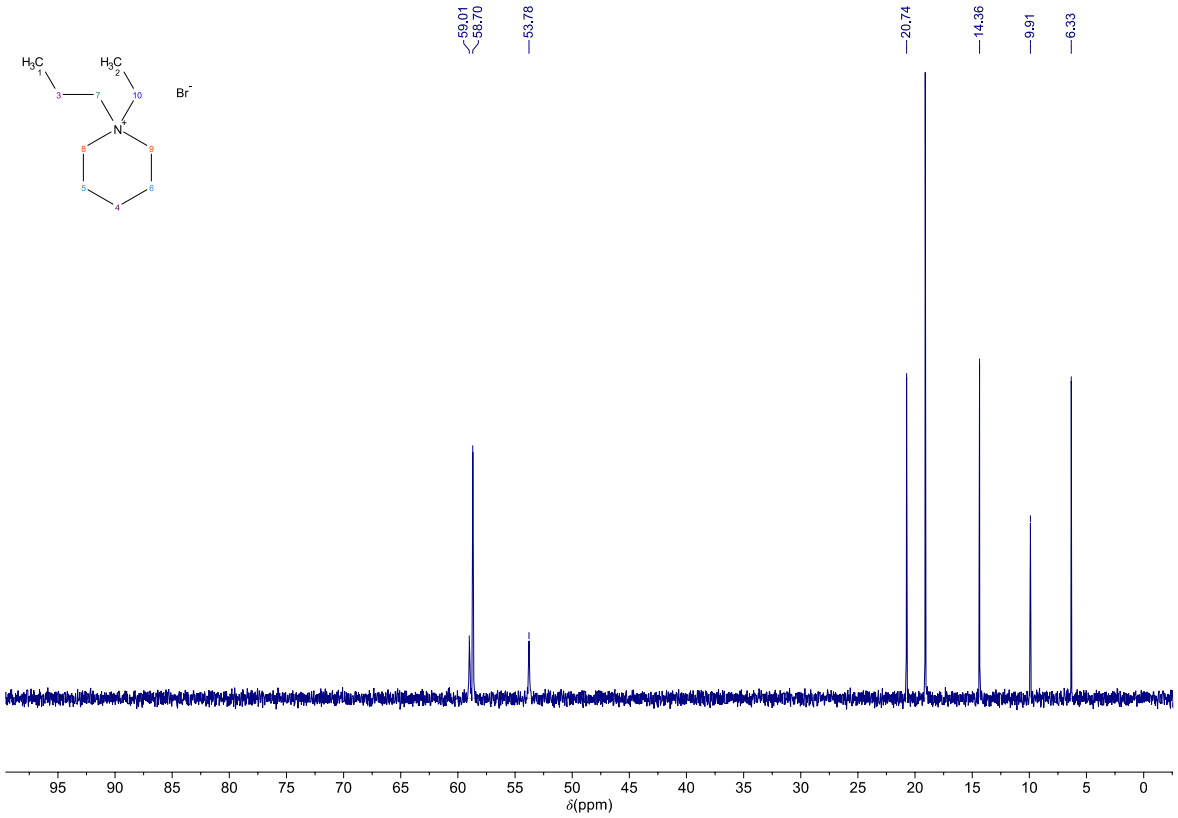

Figure S14: ^{13}C NMR spectrum of [PEP]Br in D_2O.

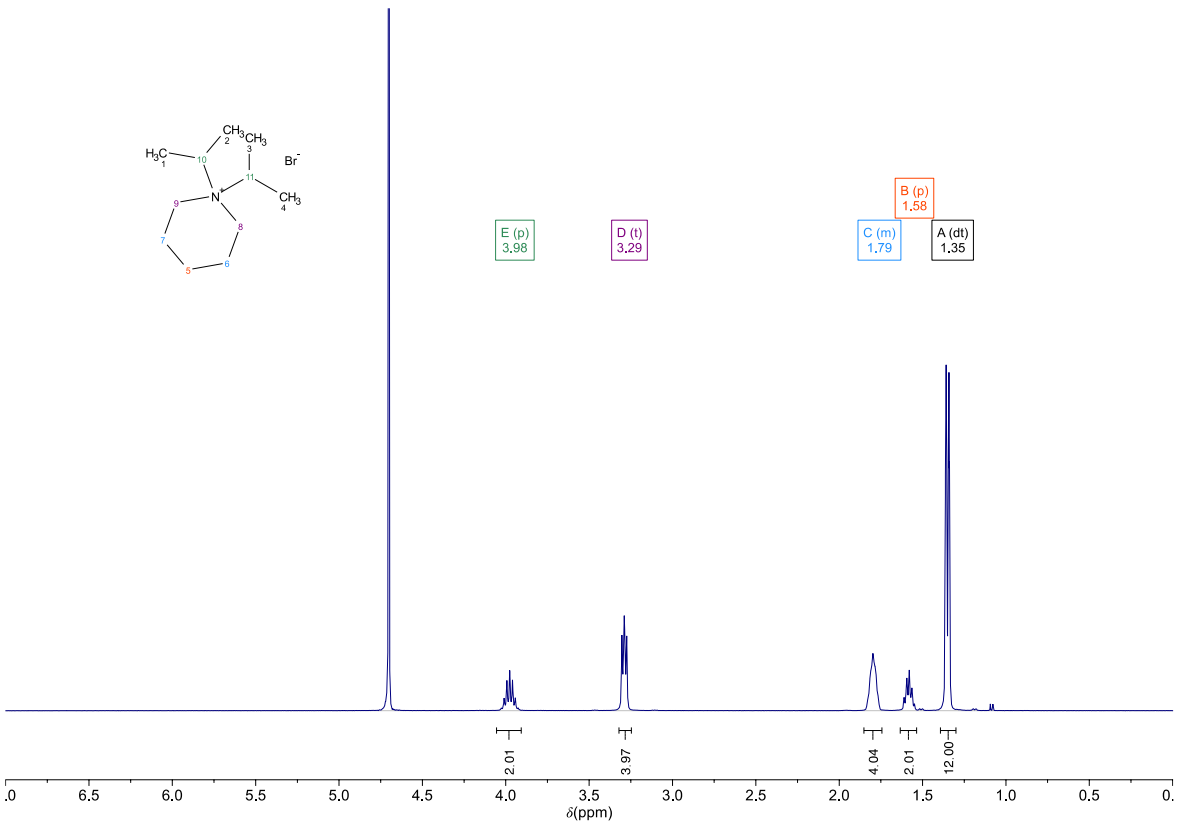

Figure S15: ^{1}H NMR spectrum of [DIP]Br in D_2O.

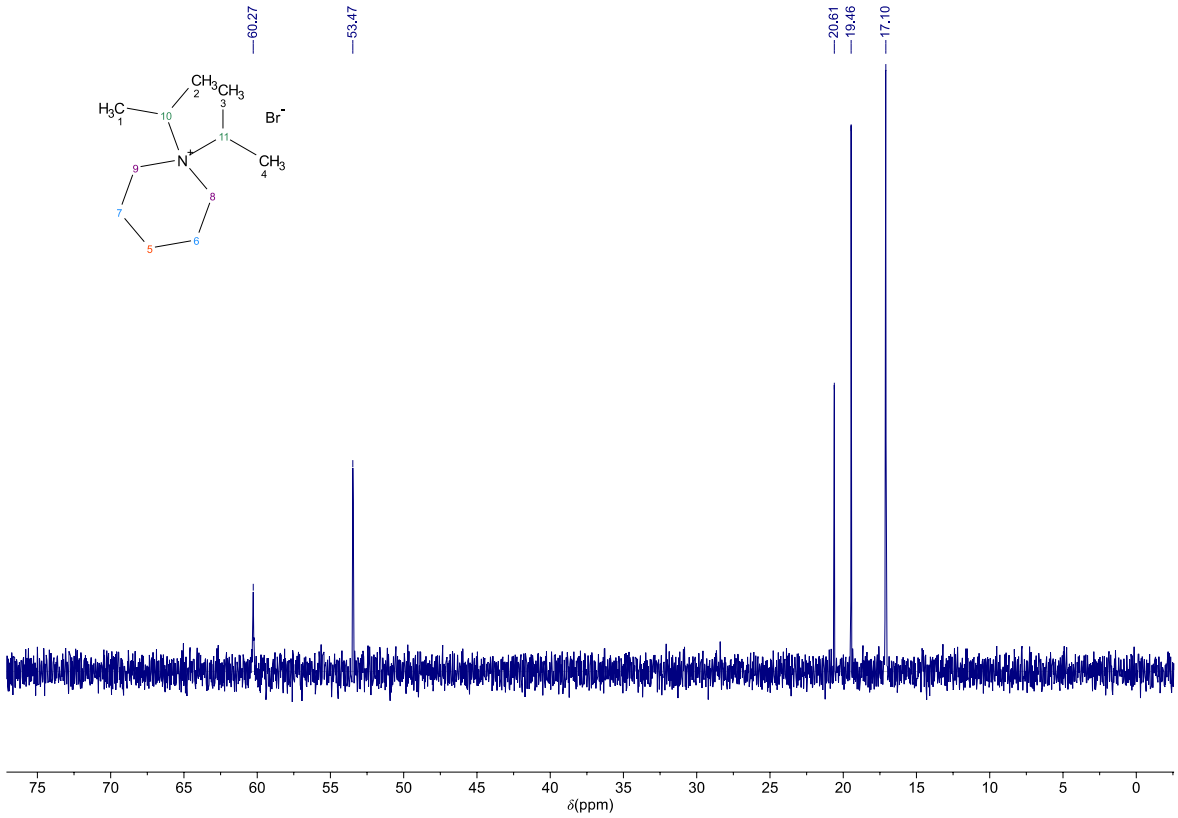

Figure S16: ^{13}C NMR spectrum of [DIP]Br in D_2O.

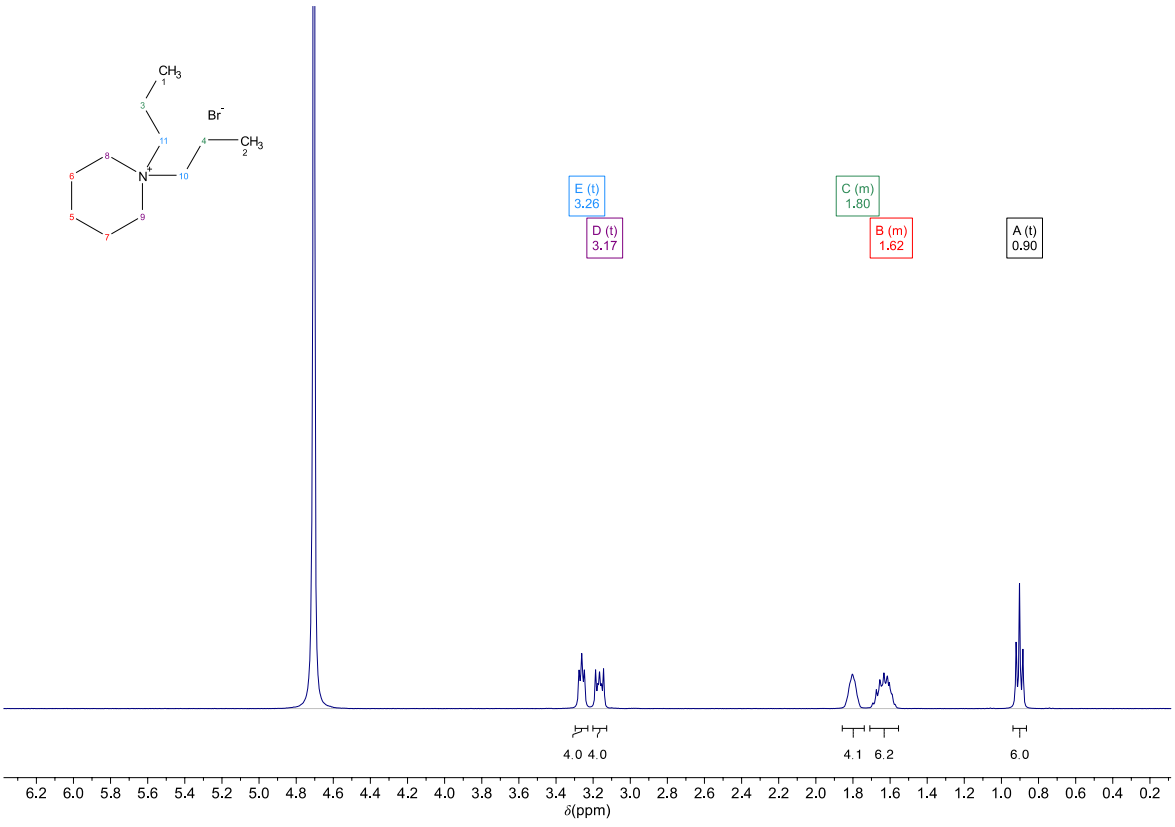

Figure S17: ^{1}H NMR spectrum of [DPP]Br in D_2O.

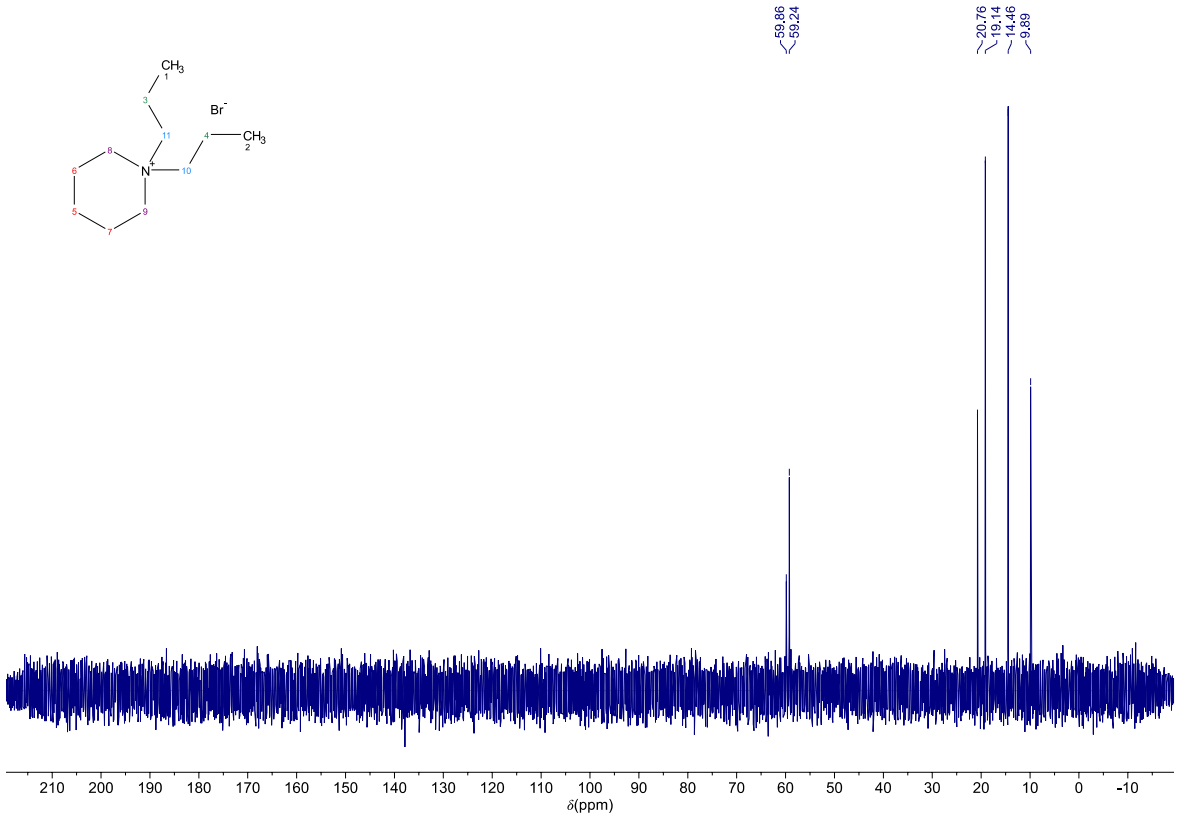

Figure S18: ^{13}C NMR spectrum of [DPP]Br in D_2O.

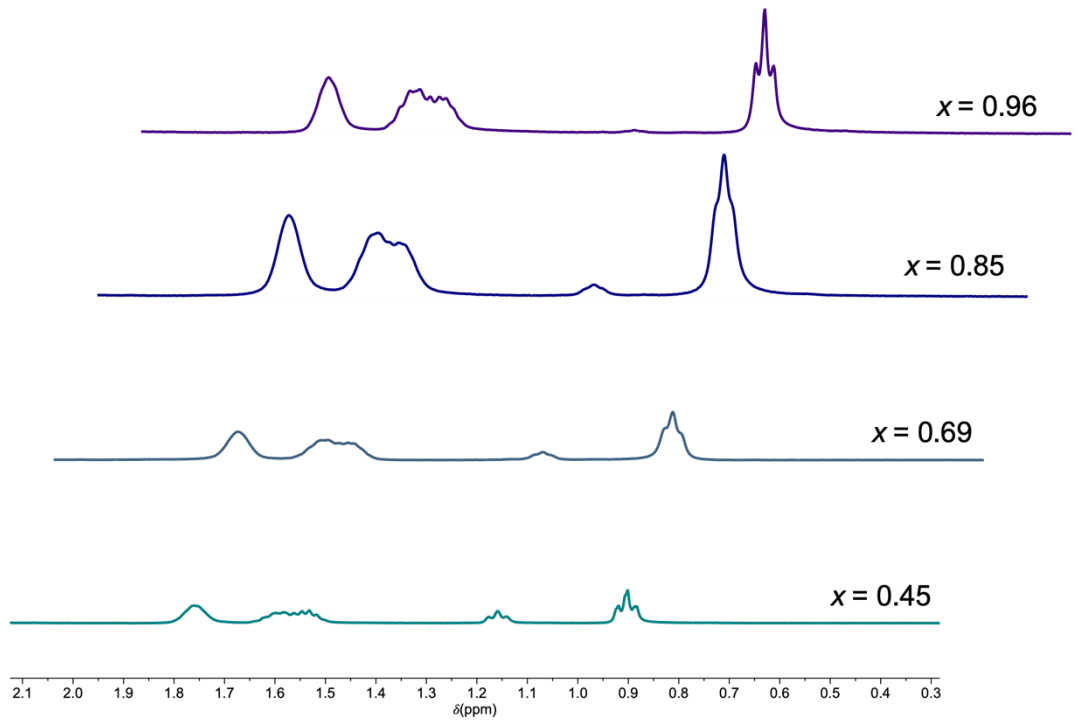

Figure S19: Stacked ^{1}H NMR spectra of the solid solutions $[PEP]_{1-x}[DPP^{i}]_xNi(C_2N_3)_3$ with x = 0.45, 0.69, 0.85 and 0.96 in D_2O including the chemical shift range (0.8 – 1.3 ppm) used for determination of x.

We performed ^{1}H NMR spectroscopy to calculate the composition of the A-site cations present in the solid solutions $[PEP]_{1-x}[DPP']_xNi(C_2N_3)_3$ (Table S9). The terminal carbon atoms of the propyl groups of $[PEP]^+$ and $[DPP]^+$ are both visible in the spectra as a triplet at around 0.9 ppm. The terminal carbon atom of the ethyl group of $[PEP]^+$ is also visible as a triplet, but at a much higher chemical shift, around 1.2 ppm. The triplet resulting from the terminal carbon of ethyl and propyl groups of the $[PEP]^+$ should hypothetically have the same integral size. Consequently, the size of the ethyl integral was subtracted from the propyl integral to calculate *x*, resulting in a value that is directly related only to the $[DPP]^+$ propyl groups. Compared to other possible analytical methods, we used NMR spectroscopy to avoid contamination by residual X- or M-site precursor salts.

Table S9: Overview of determined composition *via* ^{1}H NMR spectroscopy and the used stoichiometry during mild solution synthesis in the ratio of [PEP]Br/[DPP]Br.

***x* in $[PEP]_{1-x}[DPP']_xNi(C_2N_3)$**	***x* (^{1}H NMR)**	***x* (Synthesis)**
	0.45	0.2
	0.69	0.5
	0.85	0.7
	0.96	0.9

4. Thermogravimetric analysis and differential scanning calorimetry (TGA-DSC)

Thermal analysis (TGA-DSC experiments) of the molecular perovskites $[A]Ni(C_2N_3)_3$ (A^+ = $[DEP]^+$ = $[C_9H_{20}N]^+$, $[PEP]^+$ = $[C_{10}H_{22}N]^+$, $[DIP]^+$ = $[C_{11}H_{24}N]^+$ and $[DPP]^+$ = $[C_{11}H_{24}N]^+$) was performed on a *Netzsch* STA449F5 Jupiter TGA-DSC device using aluminium oxide pans with a lid (70 µL) under flowing argon (20 mL min^{-1}). The temperature calibration of the oven cell was carried out based on the melting points of metals (In, Sn, Bi, Zn, Al, Au and Ag). The baseline was corrected by screening an empty sample pan with the respective temperature program from room temperature to 1073.15 K using a heating rate of 10 K min^{-1}. The respective sample masses (m_0) are given below in the captions (Fig. S20-S23). The onset of significant thermal decomposition (T_d) was determined by extrapolating the linear range of the relative mass loss observed with a heating rate of 10 K min^{-1}. We observe the following decomposition temperatures: T_d of $[DEP]Ni(C_2N_3)_3$ = 595.15 K, T_d of $[PEP]Ni(C_2N_3)_3$ = 598.35 K, T_d of $[DIP]Ni(C_2N_3)_3$ = 568.95 K and T_d of $[DPP]Ni(C_2N_3)_3$ = 598.05 K.

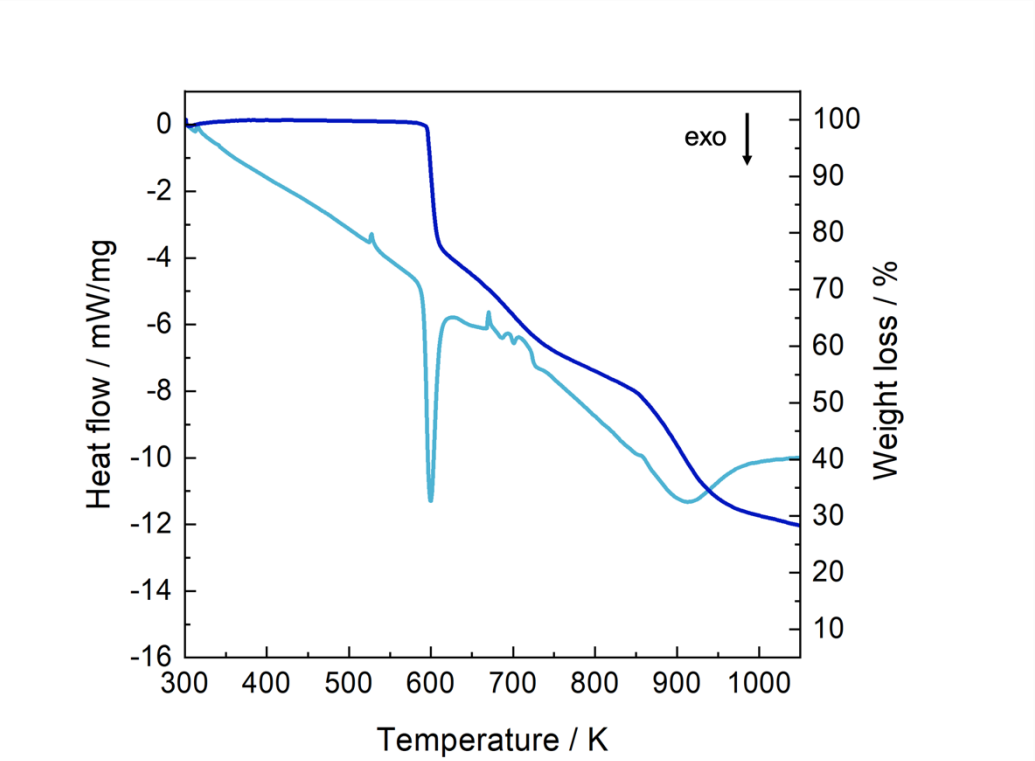

Figure S20: TGA-DSC of $[DEP]Ni(C_2N_3)_3$ with a sample mass of 5.0842 mg from room temperature to 1073.15 K with a heating rate of 10 K min^{-1}. TGA curve is shown in dark blue, indicating the thermal stability under constant argon flow before thermal decomposition, and the corresponding DSC curve is highlighted in light blue.

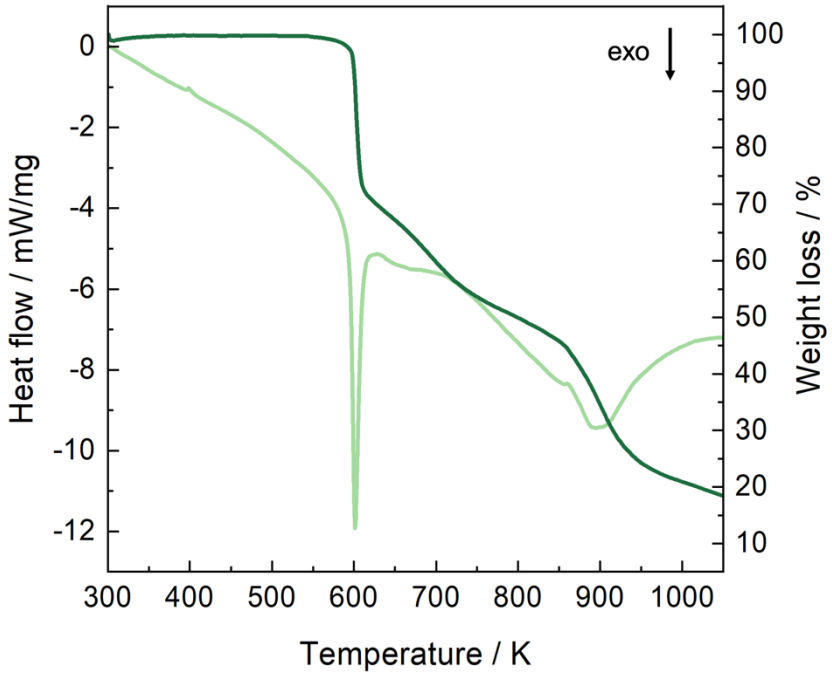

Figure S21: TGA-DSC of [PEP]Ni(C_2N_3)$_3$ with a sample mass of 5.608 mg from room temperature to 1073.15 K with a heating rate of 10 K min^{-1}. TGA curve is shown in dark green, indicating the thermal stability under constant argon flow before thermal decomposition, and the corresponding DSC curve is highlighted in light green.

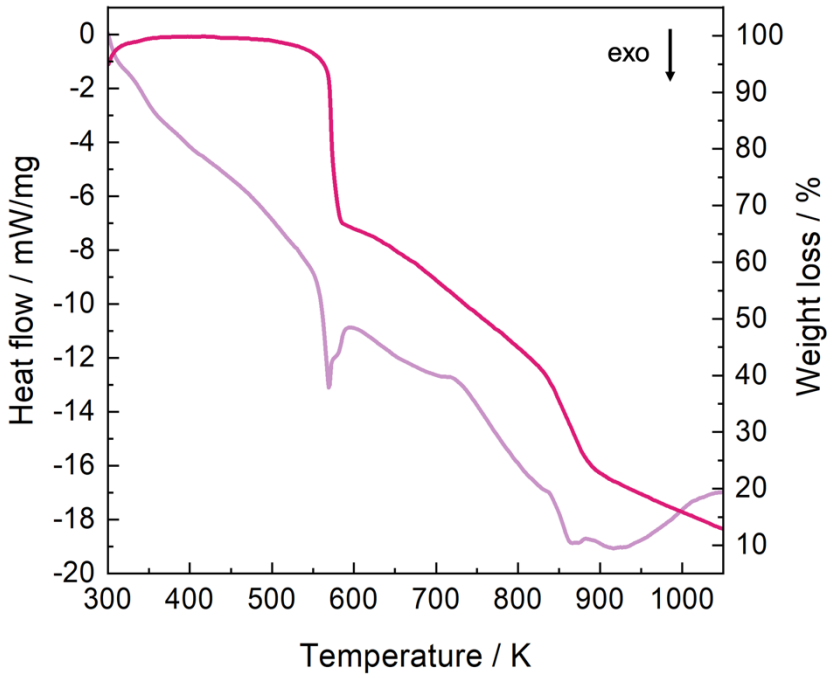

Figure S22: TGA-DSC of [DIP]Ni(C_2N_3)$_3$ with a sample mass of 3.1921 mg from room temperature to 1073.15 K with a heating rate of 10 K min^{-1}. TGA curve is shown in dark pink, indicating the thermal stability under constant argon flow before thermal decomposition, and the corresponding DSC curve is highlighted in light pink.

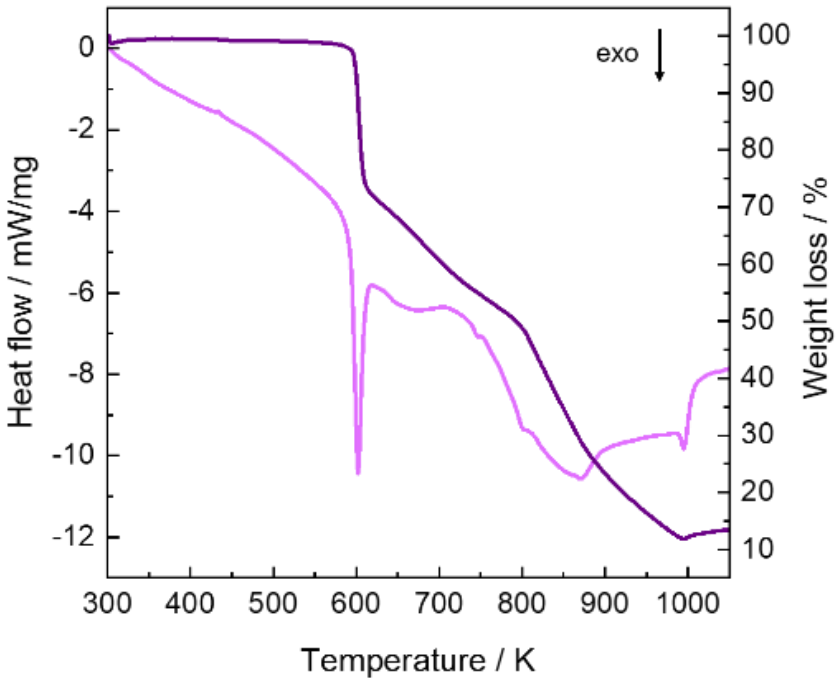

Figure S23: TGA-DSC of [DPP]Ni(C_2N_3)$_3$ with a sample mass of 6.238 mg from room temperature to 1073.15 K with a heating rate of 10 K min^{-1}. TGA curve is shown in dark purple, indicating the thermal stability under constant argon flow before thermal decomposition, and the corresponding DSC curve is highlighted in light purple.

5. Differential scanning calorimetry

DSC experiments of powder samples $[A]Ni(C_2N_3)_3$ (with A^+ = $[DEP]^+$ = $[C_9H_{20}N]^+$, $[PEP]^+$ = $[C_{10}H_{22}N]^+$, $[DIP]^+$ = $[C_{11}H_{24}N]^+$ and $[DPP]^+$ = $[C_{11}H_{24}N]^+$) were performed in a DSC (*TA Instruments* Q2000) under a constant He purging gas flow (25 mL min^{-1}) and a heating rate of 20 K min^{-1} in the temperature range between 173 and 423 K by using liquid nitrogen for cooling.

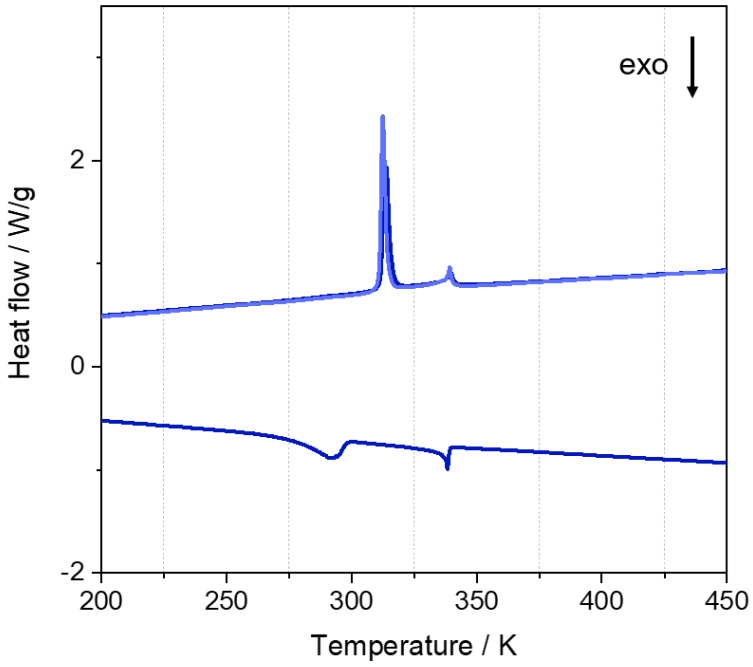

Figure S24: Reversible DSC measurement of $[DEP]Ni(C_2N_3)_3$ with an initial heating run and subsequent cooling shown as dark blue line and the re-heating run in light blue.

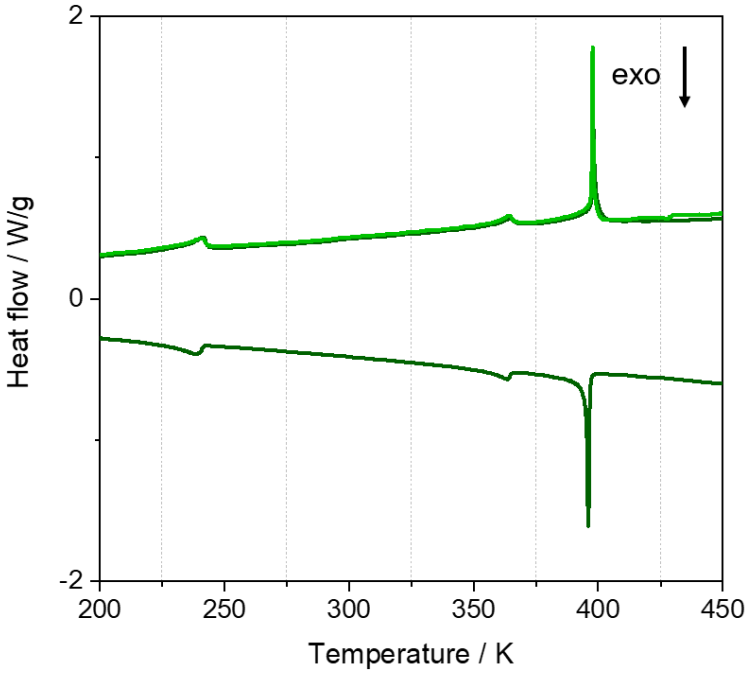

Figure S25: Reversible DSC measurement of $[PEP]Ni(C_2N_3)_3$ with an initial heating run and subsequent cooling shown as dark green line and the re-heating run in light green.

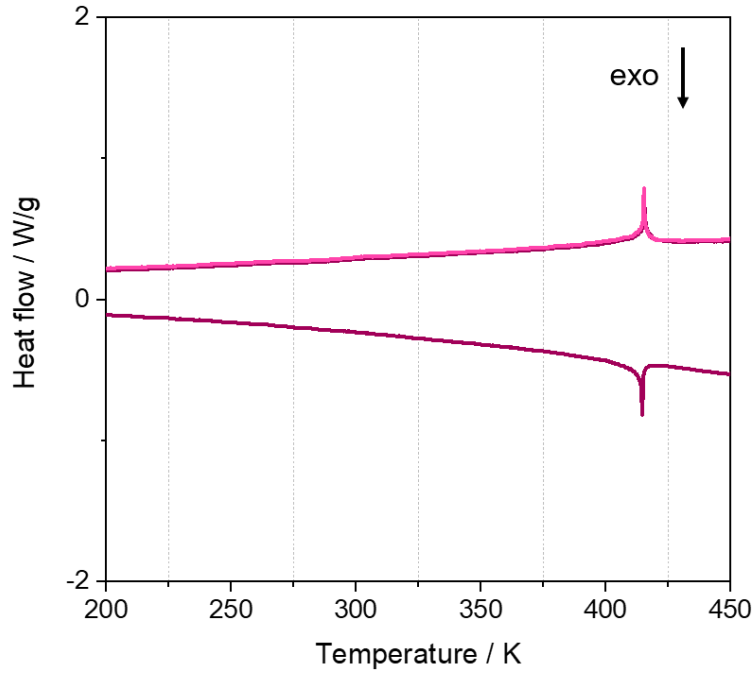

Figure S26: Reversible DSC measurement of [DIP]Ni(C_2N_3)$_3$ with an initial heating run and subsequent cooling shown as dark pink line and the re-heating run in light pink.

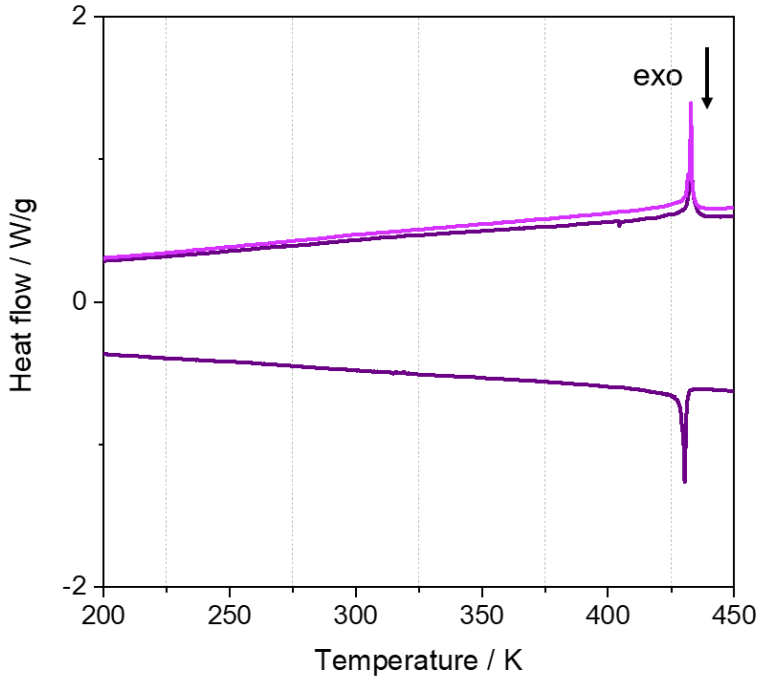

Figure S27: Reversible DSC measurement of [DPP]Ni(C_2N_3)$_3$ with an initial heating run and subsequent cooling shown as dark purple line and the re-heating run in light purple.

6. Powder X-ray diffraction (PXRD) data

Laboratory PXRD measurements of the molecular perovskites $[A]Ni(C_2N_3)_3$ (with $A^+ = [DEP]^+ = [C_9H_{20}N]^+$, $[PEP]^+ = [C_{10}H_{22}N]^+$, $[DIP]^+ = [C_{11}H_{24}N]^+$ and $[DPP]^+ = [C_{11}H_{24}N]^+$) were performed at ambient temperature using *Debye-Scherrer* geometry with borosilicate glass capillaries (0.8 mm diameter) in a *STOE* Stadi P diffractometer with a *DECTRIS* MYTHEN 1K / *DECTRIS* Multi-MYTHEN detector, a curved Ge(111) monochromator and a Mo K_α source (λ = 0.70926 Å). The measurement range was from 2° to 36.56° (2θ) with a step size of 0.015° (2θ). To verify the phase purity of the samples, we carried out a Pawley profile fit analysis of all PXRD patterns by using the TOPAS v6 software.[10] Standard deviations of all parameters were calculated, and "randomize_on_errors" was used to ensure that the refinement minimum was achieved.

Laboratory PXRD measurements of the series of solid solutions $[PEP]_{1-x}[DPP]_xNi(C_2N_3)_3$ with x = 0, 0.45, 0.69, 0.85, 0.96 and 1, and a 1:1 mixture of $[PEP]Ni(C_2N_3)_3$ and $[DPP]Ni(C_2N_3)_3$ were collected at ambient temperature on a silicon wafer using *Bragg-Brentano* geometry in a *Rigaku* MiniFlex 600-C diffractometer with X-ray Cu K_α radiation (λ_1 - 1.5406 Å, λ_2 - 1.5444 Å, I_2/I_1 - 0.5, K_β radiation was removed by a Ni-filter). The measurement range, unless stated otherwise, was from 2.0° to 50.0° (2θ) with a step size of 0.010° and a scan rate of 5° per min.

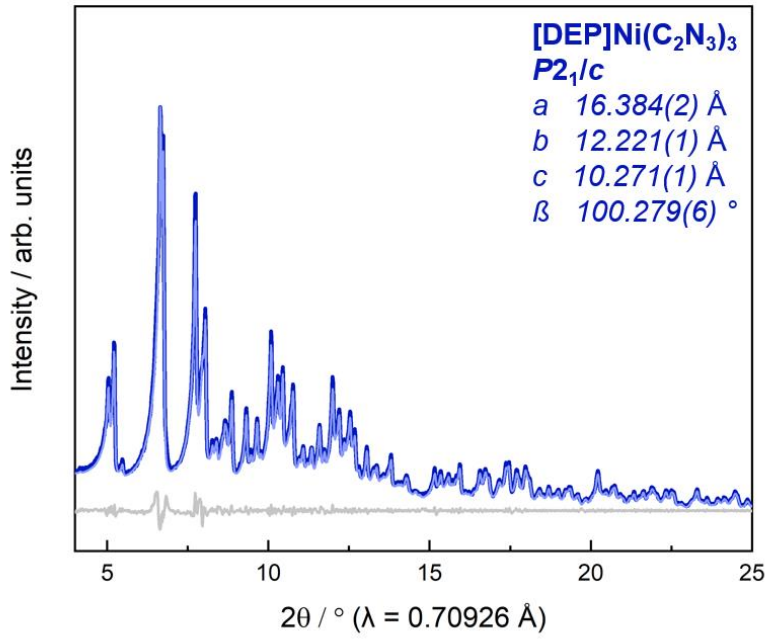

Figure S28: Powder X-ray diffraction data of $[DEP]Ni(C_2N_3)_3$ (dark blue) compared to the calculated data from Pawley profile fit analysis (light blue), with R_{wp} = 2.334, R_{exp} = 0.924 and GOF = 2.524. The grey difference curve (Pawley profile fit – experimental data) indicates phase purity.

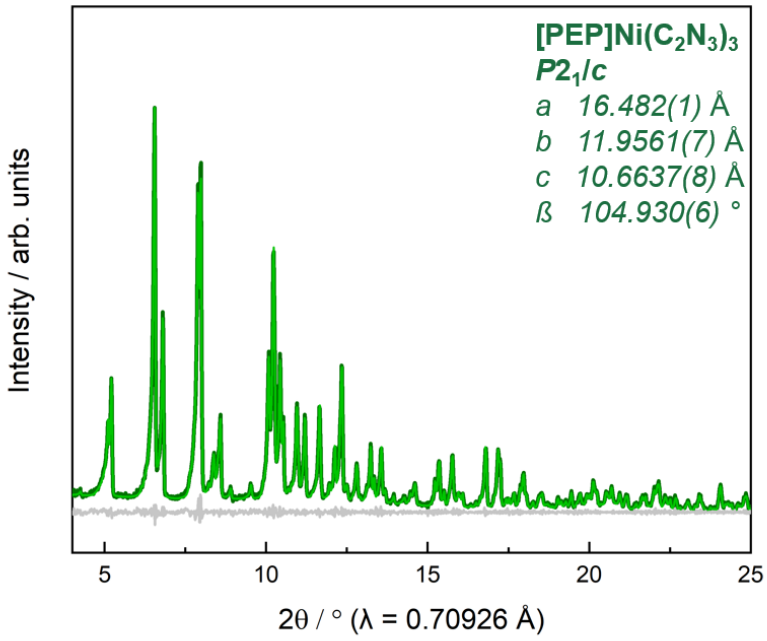

Figure S29: Powder X-ray diffraction data of $[PEP]Ni(C_2N_3)_3$ (dark green) compared to the calculated data from Pawley profile fit analysis (light green), with $R_{wp} = 3.555$, $R_{exp} = 3.244$ and GOF = 1.095. The grey difference curve (Pawley profile fit – experimental data) indicates phase purity.

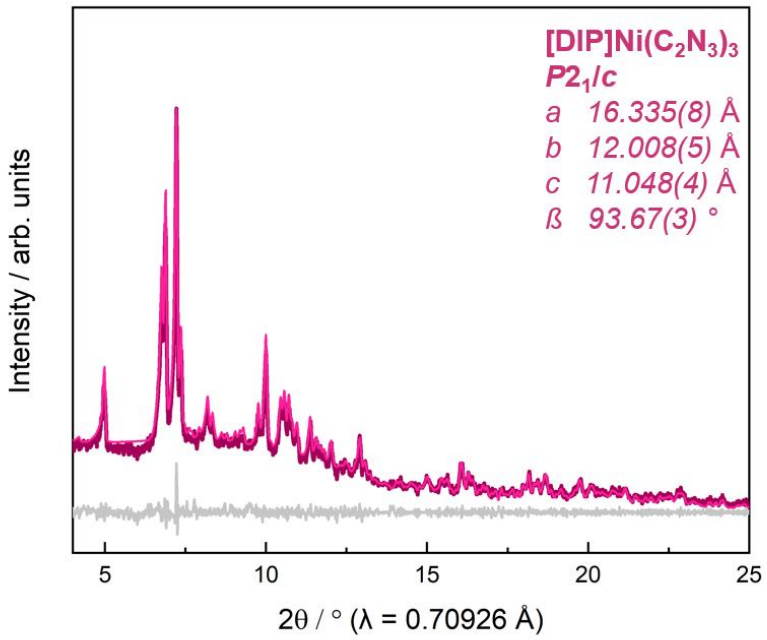

Figure S30: Powder X-ray diffraction data of $[DIP]Ni(C_2N_3)_3$ (dark pink) compared to the calculated data from Pawley profile fit analysis (light pink), with $R_{wp} = 4.759$, $R_{exp} = 3.959$ and GOF = 1.202. The grey difference curve (Pawley profile fit – experimental data) indicates phase purity.

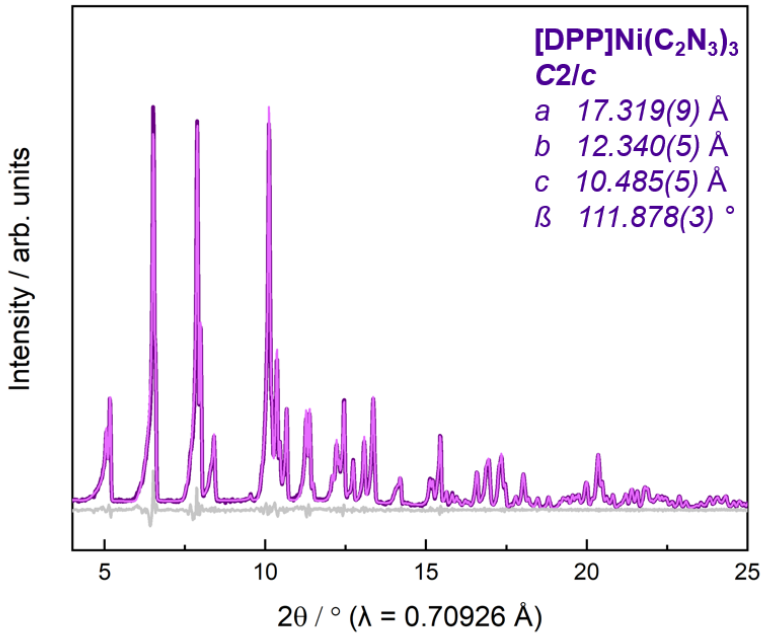

Figure S31: Powder X-ray diffraction data of $[DPP]Ni(C_2N_3)_3$ (dark purple) compared to the calculated data from Pawley profile fit analysis (light purple), with $R_{wp} = 3.635$, $R_{exp} = 2.450$ and GOF = 1.483. The grey difference curve (Pawley profile fit – experimental data) indicates phase purity.

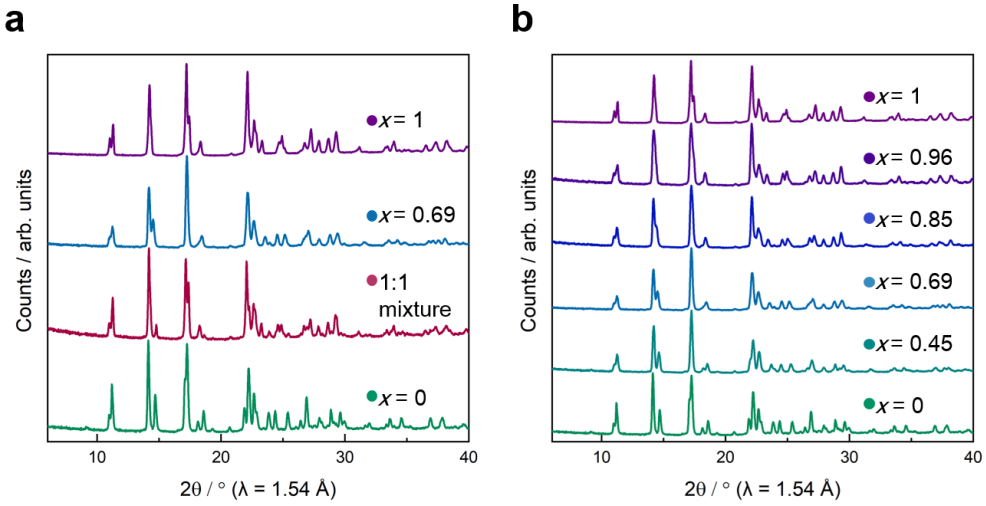

Figure S32: Collections of PXRD patterns of the pure perovskites $[PEP]Ni(C_2N_3)_3$, $[DPP]Ni(C_2N_3)_3$ and a 1:1 mixture compared to $[PEP]_{1-x}[DPP]_xNi(C_2N_3)_3$ (with x = 0.69) (a) and stacked PXRD patterns of the solid solution series (b).

7. High-pressure powder X-ray diffraction (HPXRD)

High-pressure powder X-ray diffraction (HPPXRD) data was collected at beamline I15 (within beamtime CY30815-2) at the Diamond Light Source (UK) using a fixed operating photon energy of 29.2 keV (λ = 0.4246 Å), equipped with a *Pilatus3 X CdTe 2M* area detector. Single crystals of the studied samples were ground to a fine powder and filled with Silicone oil AP100 as pressure transmitting medium into a plastic capillary (Makrolon, inside diameter 1.8 mm) and sealed with Araldyte-2014-1 by heating up to 60 °C for 20 min. Please note that Silicone oil AP100 has been previously applied in hydrostatic pressure experiments and is known to maintain hydrostatic conditions up to pressures of 0.9 GPa. We used an automated high-pressure setup with hydrostatic conditions, as described in detail in the literature.[11,12] To further validate the performance of the high-pressure setup, Nickel dimethylglyoxime ($Ni(dmgH)_2$) was used as a standard, see Chapter 10 of this supporting information. The samples were loaded into a chamber filled with water to transmit the pressure, and a hydraulic gauge pump was used to apply and release pressure. We collected HPPXRD data for all three samples through two diamond windows in the metal block (sample chamber) along beam direction in the range of p = ambient – 0.4 GPa in small p steps (0.02 GPa) with an estimated standard deviation of p = ± 0.003 GPa.

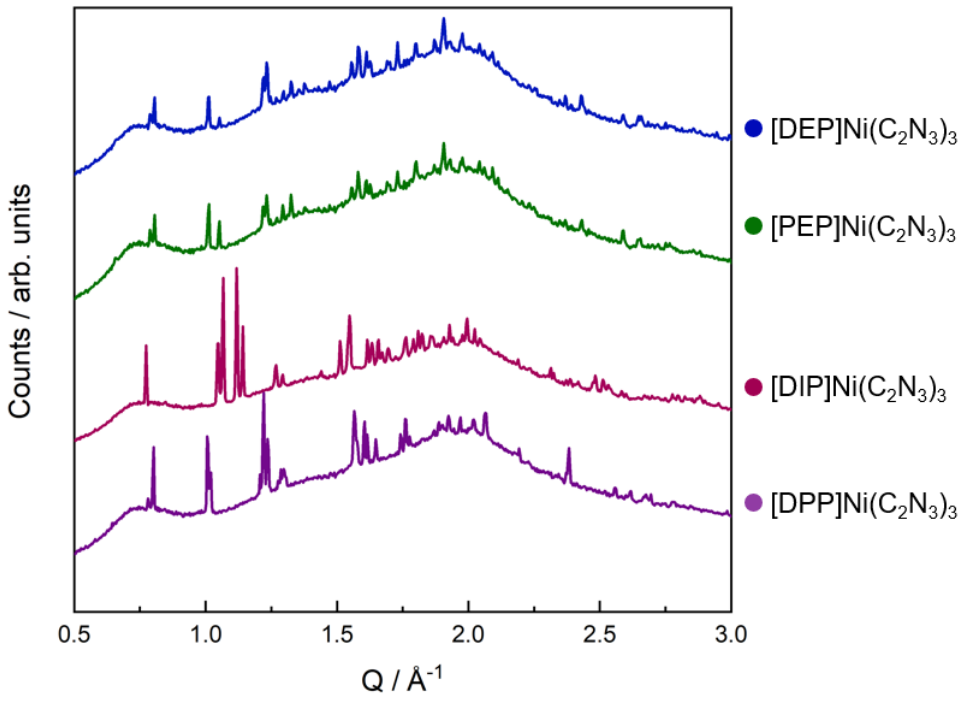

Figure S33: Collection of the normalised PXRD patterns recorded at ambient pressure of all studied $[A]Ni(C_2N_3)_3$ molecular perovskites.

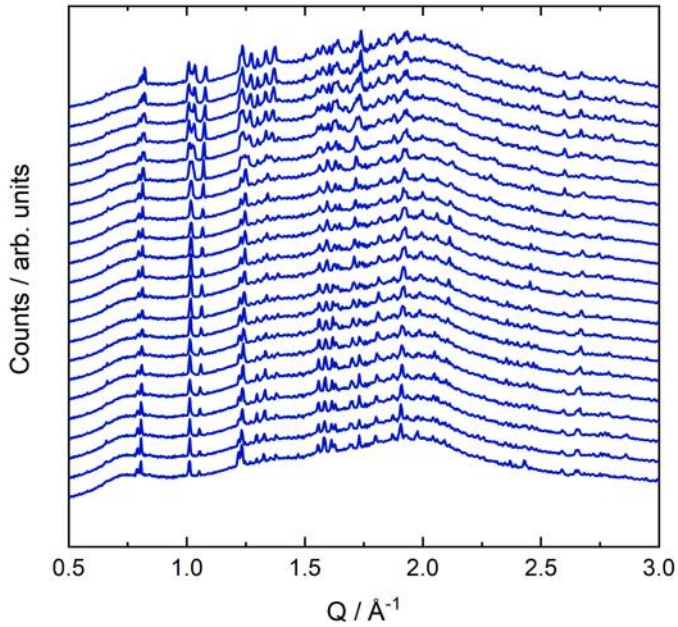

Figure S34: HPPXRD patterns for [DEP]Ni(C_2N_3)$_3$ collected between the pressure range from ambient to 0.4 GPa.

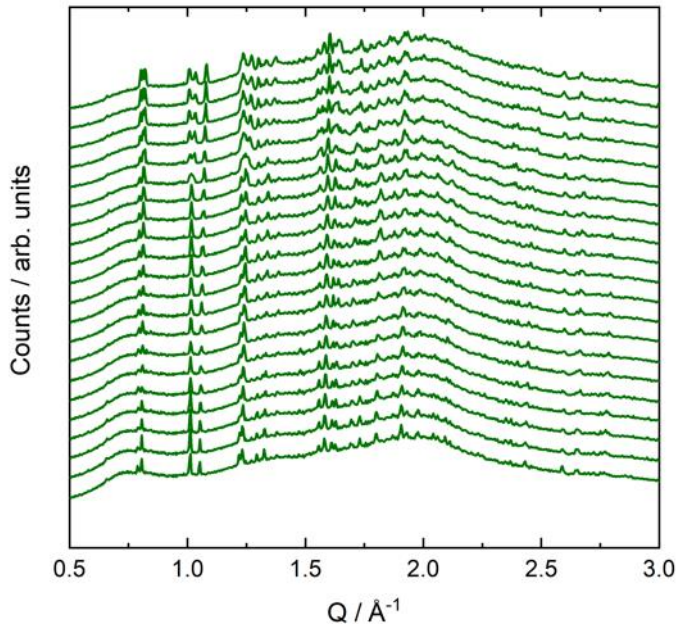

Figure S35: HPPXRD patterns for [PEP]Ni(C_2N_3)$_3$ (within the solid solution solution [PEP]$_{1-x}$[DPP^i]$_x$Ni(C_2N_3)$_3$, x = 0) collected between the pressure range from ambient to 0.4 GPa.

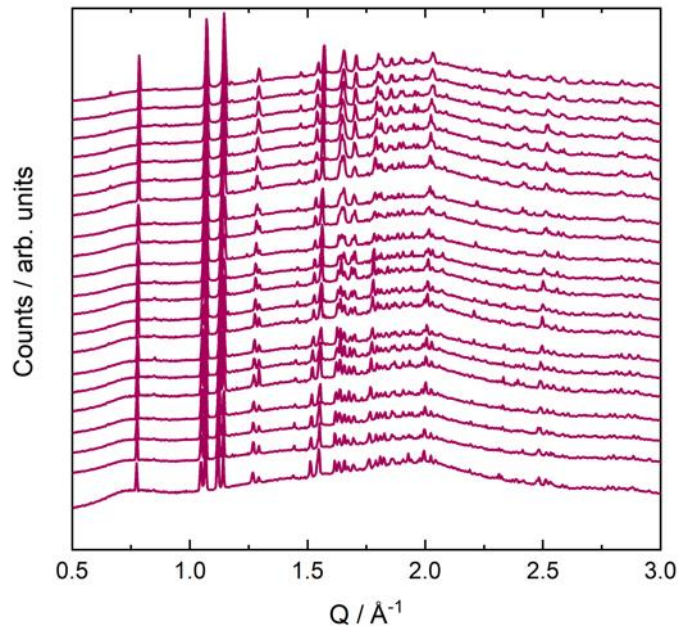

Figure S36: HPPXRD patterns for [DIP]Ni(C_2N_3)$_3$ collected between the pressure range from ambient to 0.4 GPa.

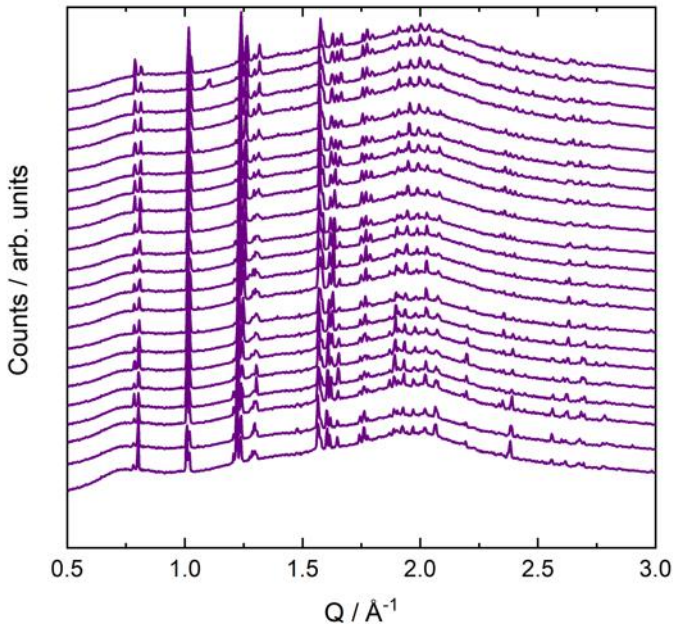

Figure S37: HPPXRD patterns for [DPP]Ni(C_2N_3)$_3$ (within the solid solution [PEP]$_{1-x}$[DPP']$_x$Ni(C_2N_3)$_3$, x = 1) collected between the pressure range from ambient to 0.4 GPa.

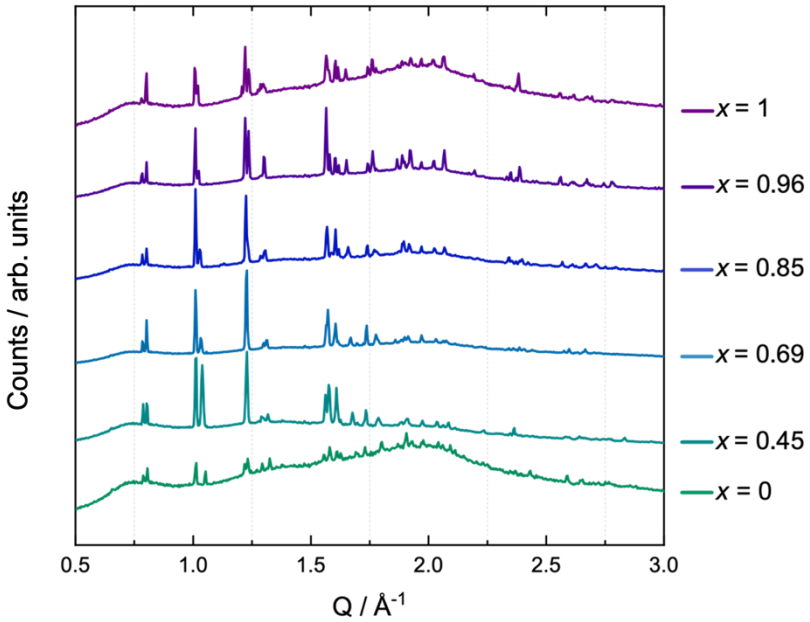

Figure S38: Collection of normalised PXRD patterns recorded at ambient pressure of the series of solid solutions $[PEP]_{1-x}[DPP]_xNi(C_2N_3)_3$ with x = 0, 0.45, 0.69, 0.85, 0.96 and 1.

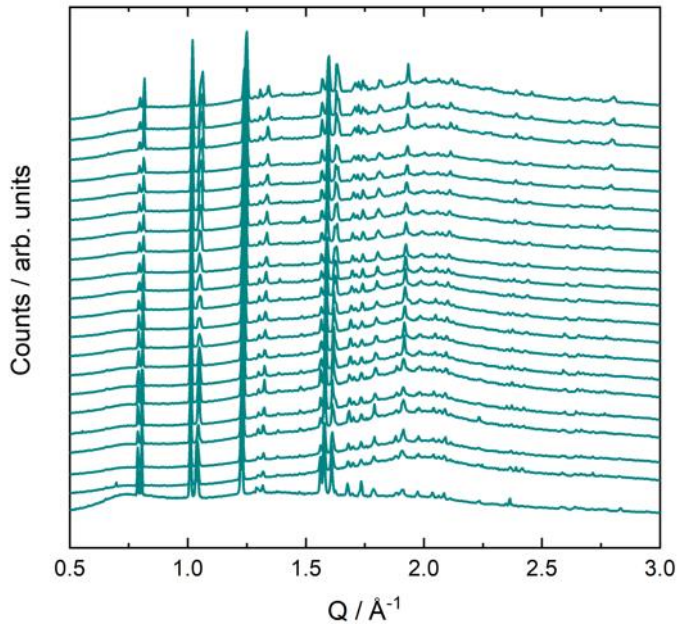

Figure S39: HPPXRD patterns for the solid solution $[PEP]_{1-x}[DPP]_xNi(C_2N_3)_3$ (with x = 0.45) collected between the pressure range from ambient to 0.4 GPa.

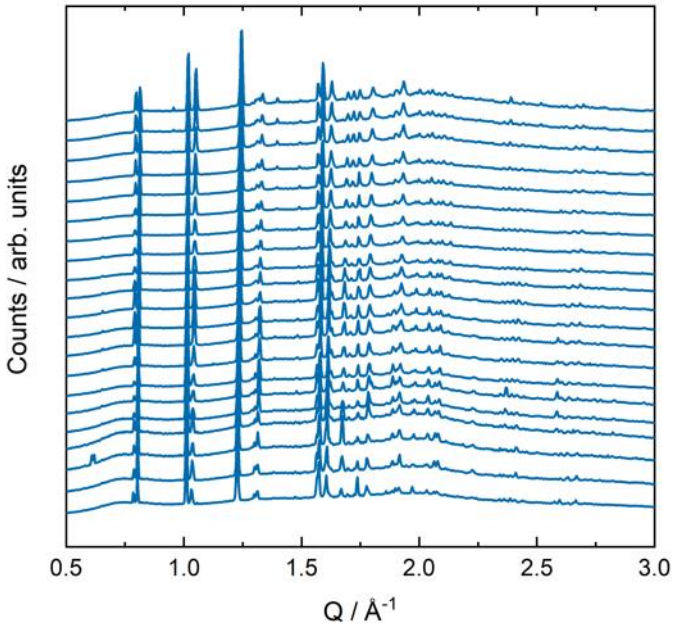

Figure S40: HPPXRD patterns for the solid solution $[PEP]_{1-x}[DPP]_xNi(C_2N_3)_3$ (with $x = 0.69$) collected between the pressure range from ambient to 0.4 GPa.

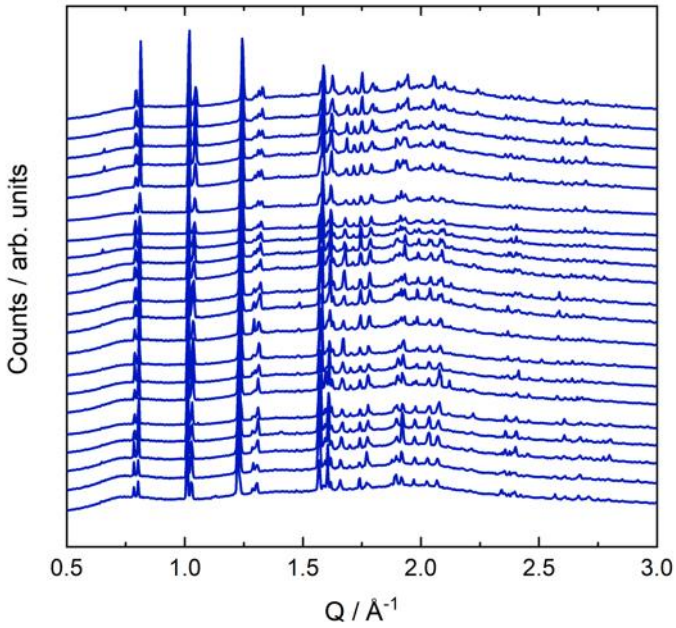

Figure S41: HPPXRD patterns for the solid solution $[PEP]_{1-x}[DPP]_xNi(C_2N_3)_3$ (with $x = 0.85$) collected between the pressure range from ambient to 0.4 GPa.

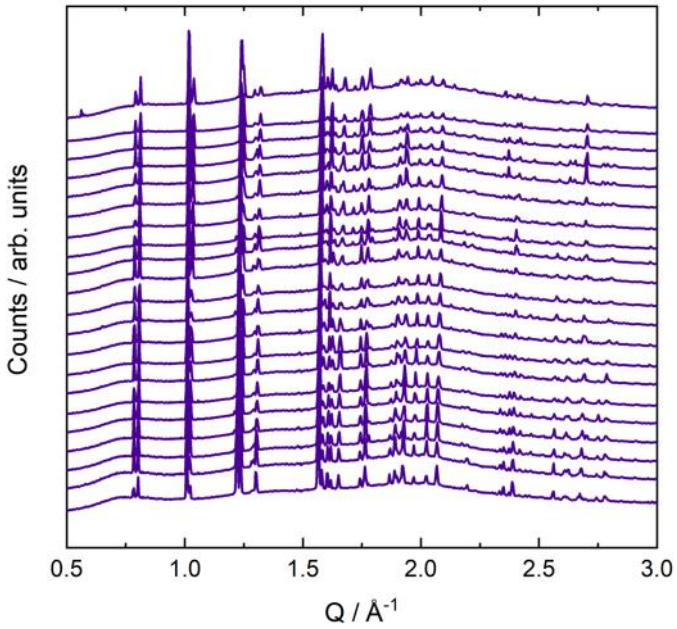

Figure S42: HPPXRD patterns for the solid solution $[PEP]_{1-x}[DPP]_xNi(C_2N_3)_3$ (with x = 0.96) collected between the pressure range from ambient to 0.4 GPa.

8. HPPXRD analysis

The collected HPPXRD detector images were calibrated and integrated using DAWN.[13] Subsequent analysis, *i.e.* Pawley refinements[14] on the HPPXRD data, was performed by sequential refinement of the multipattern datasets of each sample using TOPAS *v6*.[10] Representative Pawley profile fits of the ambient pressure PXRD data show a good fit to the monoclinic space groups as determined by SCXRD experiments at 300 K. We obtained pressure dependent cell parameters with standard deviations and full-width at half maximum (fwhm) using "pv_fwhm" of the average of peak profiles in the Pawley refinement of the diffraction data up to 0.28 GPa for [DIP]Ni(C_2N_3)$_3$, 0.26 GPa for [PEP]Ni(C_2N_3)$_3$ and 0.28 GPa for [DIP]Ni(C_2N_3)$_3$ a pressure-induced phase transition ($p_{trs.}$) is observed and up to 0.4 GPa for [DPP]Ni(C_2N_3)$_3$.

Table S10: Structural parameters (refined lattice parameter *a*, *b*, *c*, *ß*, volume *V* and space group *S.G.*) for all studied [A]Ni(C_2N_3)$_3$ molecular perovskites obtained from Pawley refinement of the ambient pressure PXRD data.

[A]Ni(C_2N_3)$_3$	**[DIP]$^+$**	**[PEP]$^+$**	**[DEP]$^+$**	**[DPP]$^+$**
S.G.	*P2$_1$/c*	*P2$_1$/c*	*P2$_1$/c*	*C2/c*
a / Å	16.337(1)	16.485(2)	16.465(2)	17.309(2)
b / Å	12.005(8)	11.949(1)	11.950(2)	12.330(1)
c / Å	11.031(7)	10.665(1)	10.663(1)	10.479(1)
ß / °	93.729(7)	104.973(8)	104.961(9)	111.790(9)
V / Å^3	2159.1(3)	2029.7(4)	2027.2(5)	2076.9(4)

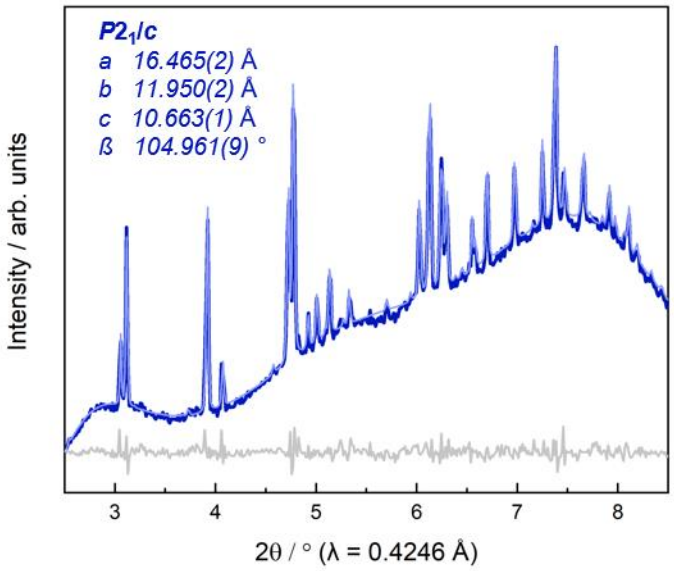

Figure S43: Pawley fit to synchrotron PXRD data at ambient pressure for [DEP]Ni(C_2N_3)$_3$. Experimental data is shown as dark blue line, Pawley fit as light blue line, and the difference curve (fit – data) as grey line.

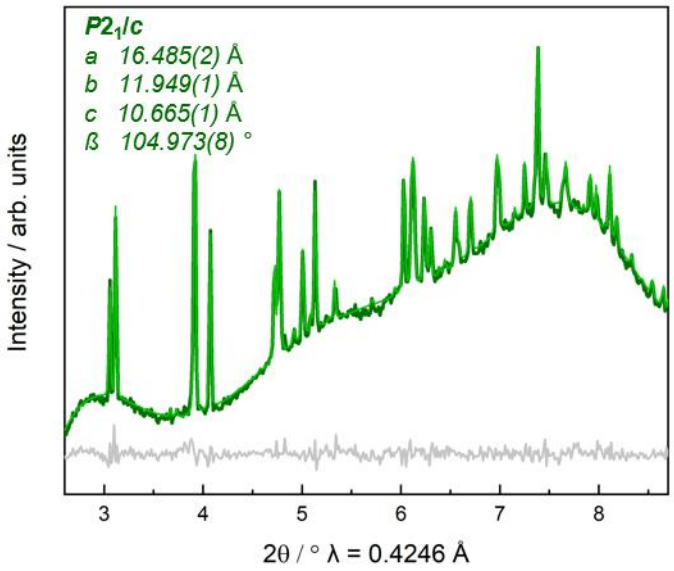

Figure S44: Pawley fit to synchrotron PXRD data at ambient pressure for [PEP]Ni(C_2N_3)$_3$. Experimental data is shown as dark green line, Pawley fit as light green line, and the difference curve (fit – data) as grey line.

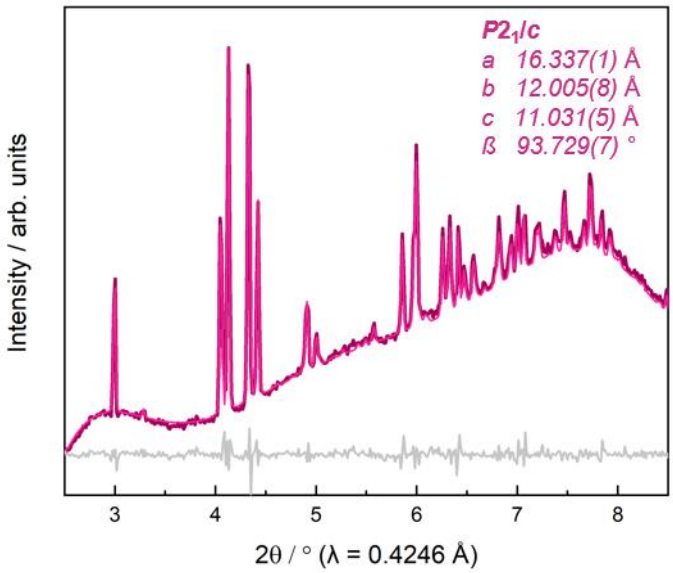

Figure S45: Pawley fit to synchrotron PXRD data at ambient pressure for $[DIP]Ni(C_2N_3)_3$. Experimental data is shown as dark pink line, Pawley fit as light pink line, and the difference curve (fit – data) as grey line.

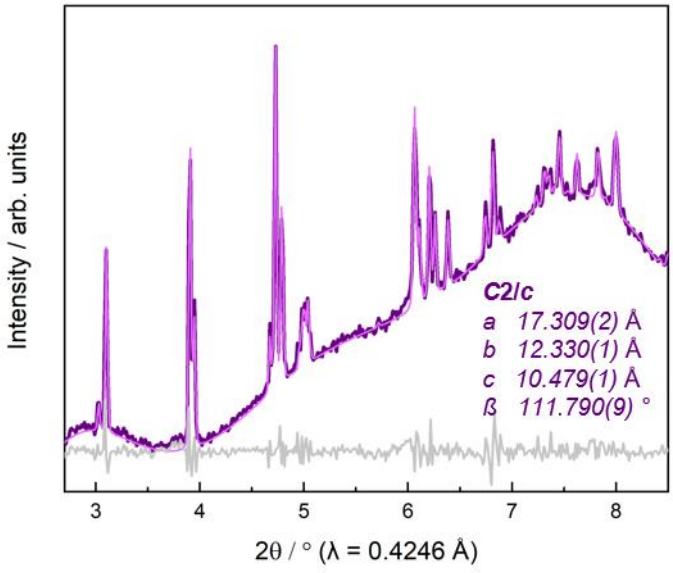

Figure S46: Pawley fit to synchrotron PXRD data at ambient pressure for $[PEP]_{1-x}[DPP^{\cdot}]_xNi(C_2N_3)_3$ (with x = 1). Experimental data is shown as dark purple line, Pawley fit as light purple line, and the difference curve (fit – data) as grey line.

Table S11: Overview of the unit cell parameters and volumes of [DEP]Ni(C_2N_3)$_3$ obtained from Pawley fits of the HPPXRD data up to 0.28 GPa.

p / GPa	R_{wp}	*a* / Å	*b* / Å	*c* / Å	ß / °	*V* / Å^3
ambient	1.66366	16.466(2)	11.952(2)	10.663(1)	104.964(9)	2027.4(5)
0.0194	2.22259	16.456(3)	11.921(3)	10.659(3)	104.88(2)	2020.9(8)
0.0398	1.46792	16.451(2)	11.909(2)	10.653(1)	105.054(8)	2015.6(4)
0.0598	1.60712	16.442(2)	11.906(2)	10.648(1)	105.067(8)	2012.9(4)
0.0794	1.75472	16.436(2)	11.893(2)	10.646(2)	105.105(9)	2009.3(5)
0.0995	1.80946	16.428(3)	11.871(2)	10.636(2)	105.19(1)	2001.8(6)
0.1199	1.69991	16.414(2)	11.866(2)	10.632(2)	105.208(8)	1998.2(6)
0.1399	1.62644	16.412(2)	11.846(2)	10.632(2)	105.20(1)	1994.8(6)
0.1594	1.59567	16.406(3)	11.829(2)	10.629(2)	105.25(1)	1990.3(6)
0.1794	1.53563	16.387(2)	11.822(2)	10.623(2)	105.316(8)	1984.9(6)
0.1996	1.77553	16.381(2)	11.814(2)	10.617(2)	105.35(1)	1981.4(6)
0.2196	1.62587	16.378(2)	11.799(2)	10.624(2)	105.38(1)	1979.5(6)
0.2397	1.69393	16.375(2)	11.778(2)	10.617(2)	105.34(1)	1974.6(6)
0.2597	1.58818	16.357(3)	11.771(2)	10.623(2)	105.51(1)	1971.2(6)
0.2798	1.60136	16.355(3)	11.765(2)	10.614(3)	105.48(1)	1968.1(8)

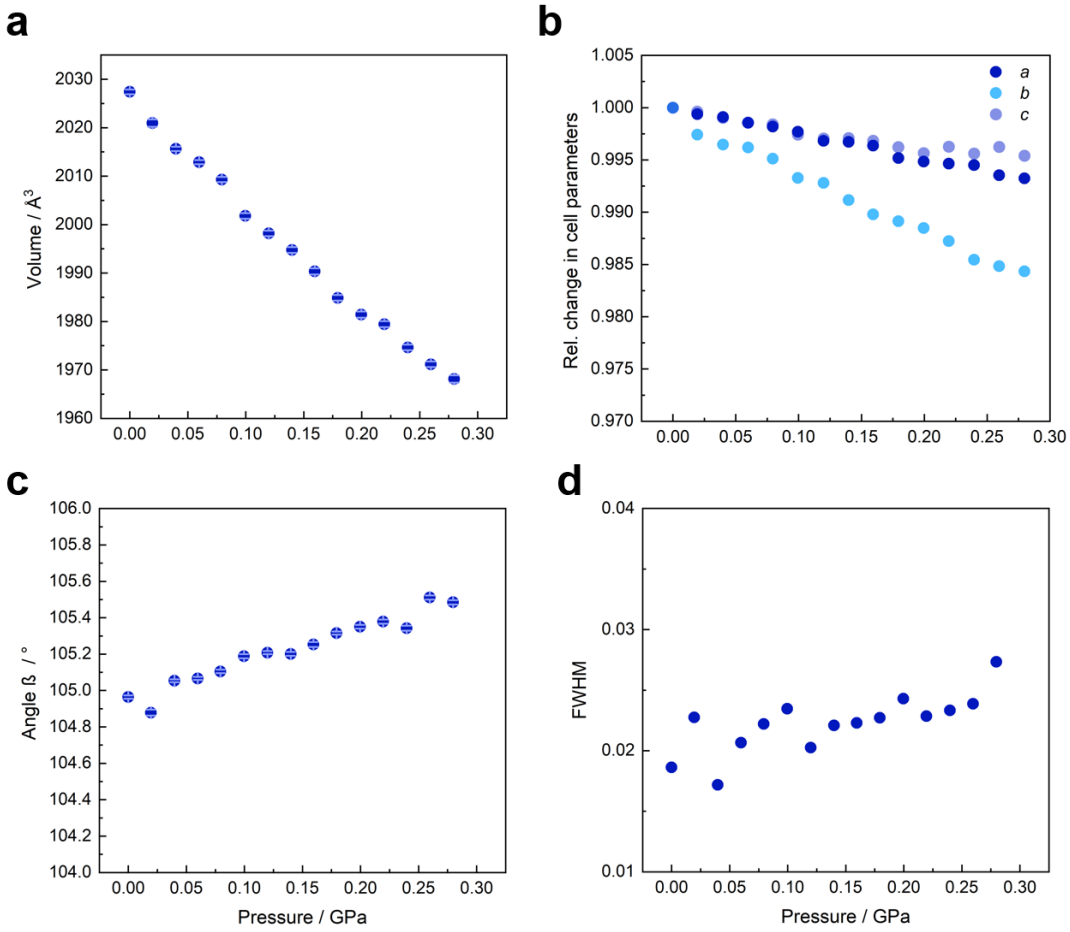

Figure S47: The evolution of unit cell volume (a), parameters (b), angle (c) and fwhm (d) as a function of hydrostatic compression until 0.28 GPa for [DEP]Ni(C_2N_3)$_3$.

Table S12: Overview of the unit cell parameters and volumes of [PEP]Ni(C_2N_3)$_3$ obtained from Pawley fits of the HPPXRD data up to 0.26 GPa.

p / GPa	R_{wp}	*a* / Å	*b* / Å	*c* / Å	ß / °	*V* / Å^3
ambient	1.44525	16.486(2)	11.949(1)	10.667(1)	104.981(8)	2029.9(4)
0.0198	1.53702	16.485(2)	11.941(1)	10.659(1)	105.028(8)	2026.6(4)
0.0398	1.79636	16.478(4)	11.926(1)	10.656(3)	105.03(2)	2022.5(8)
0.0598	1.70747	16.466(5)	11.910(2)	10.665(4)	105.06(2)	2019.7(9)
0.0793	1.48532	16.447(3)	11.889(1)	10.643(3)	105.08(1)	2009.5(7)
0.0999	1.43183	16.424(4)	11.886(2)	10.638(3)	105.10(1)	2004.9(8)
0.1199	1.47878	16.417(3)	11.883(2)	10.631(2)	105.23(1)	2001.1(6)
0.1393	1.51467	16.417(3)	11.865(2)	10.622(2)	105.27(1)	1996.1(7)
0.1594	1.38044	16.414(3)	11.851(2)	10.622(3)	105.335(9)	1992.7(6)
0.1793	1.72835	16.404(3)	11.835(1)	10.627(2)	105.36(1)	1989.5(6)
0.1996	1.96211	16.403(3)	11.822(1)	10.619(3)	105.39(1)	1985.4(7)
0.2195	1.80703	16.381(3)	11.815(1)	10.617(2)	105.395(1)	1981.0(6)
0.2397	1.52922	16.383(2)	11.796(1)	10.612(1)	105.417(9)	1976.9(4)
0.2597	1.84962	16.373(3)	11.791(2)	10.606(2)	105.47(1)	1973.5(6)

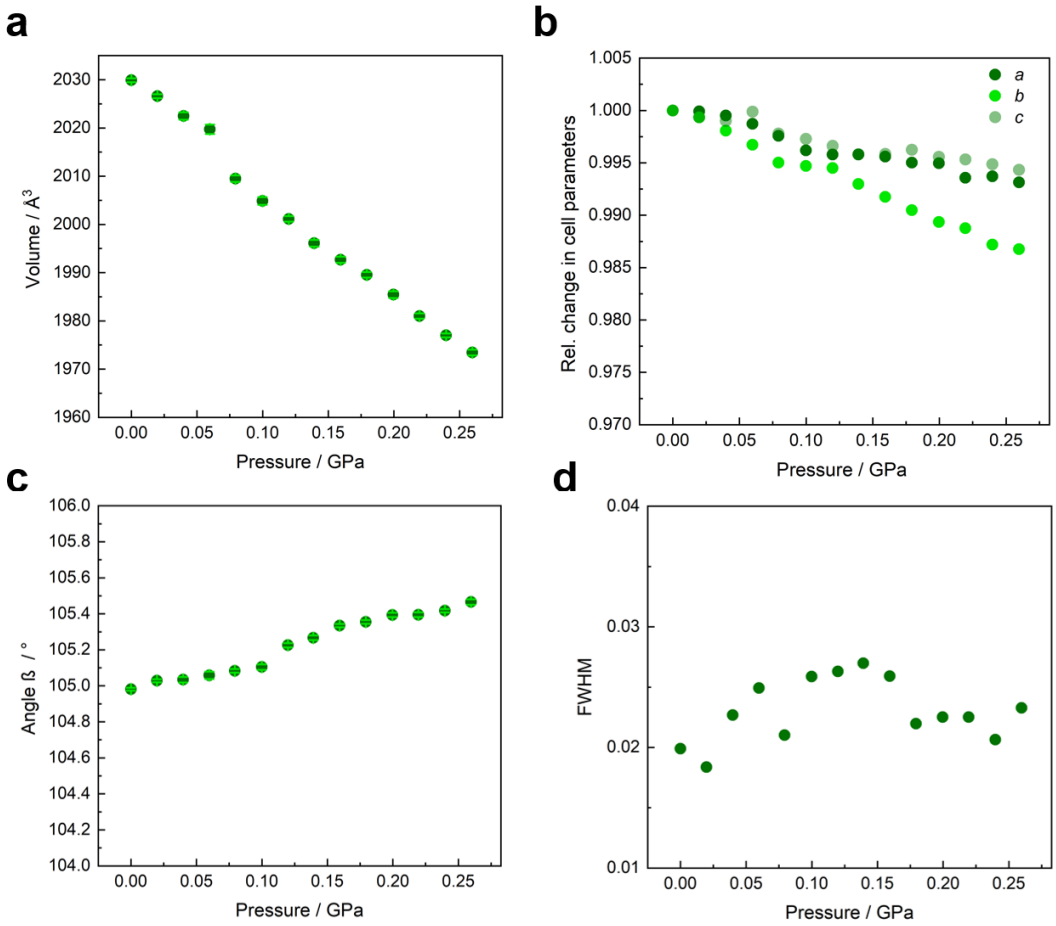

Figure S48: The evolution of unit cell volume (a), parameters (b), angle (c) and fwhm (d) as a function of hydrostatic compression until 0.26 GPa for [PEP]Ni(C_2N_3)$_3$.

Table S13: Overview of the unit cell parameters and volumes of [DIP]Ni(C_2N_3)$_3$ obtained from Pawley fits of the HPPXRD data up to 0.28 GPa.

p / GPa	R_{wp}	*a* / Å	*b* / Å	*c* / Å	ß / °	*V* / Å^3
ambient	1.57572	16.337(1)	12.006(1)	11.031(1)	93.727(7)	2159.1(3)
0.0196	1.54057	16.323(2)	11.989(1)	11.021(1)	93.839(9)	2152.1(3)
0.0398	1.37845	16.307(1)	11.975(1)	11.014(1)	93.883(4)	2145.9(2)
0.0598	1.69156	16.297(2)	11.959(1)	11.011(1)	93.987(9)	2140.9(3)
0.0797	1.54961	16.276(1)	11.957(1)	11.005(1)	94.102(5)	2136.3(2)
0.0993	1.56752	16.271(1)	11.942(1)	11.002(1)	94.158(5)	2132.1(3)
0.1198	1.50498	16.251(1)	11.920(1)	11.001(1)	94.229(5)	2125.1(2)
0.1399	1.33754	16.243(1)	11.913(1)	10.993(1)	94.341(4)	2121.2(2)
0.1594	1.66066	16.223(2)	11.904(1)	10.993(1)	94.437(7)	2116.7(3)
0.1794	1.62171	16.222(1)	11.882(1)	10.987(1)	94.495(6)	2111.3(3)
0.1995	1.5133	16.206(1)	11.872(1)	10.986(1)	94.549(5)	2107.2(3)
0.2195	1.37688	16.197(1)	11.861(1)	10.982(1)	94.643(5)	2102.9(3)
0.2397	1.57011	16.191(1)	11.846(2)	10.982(1)	94.711(6)	2099.3(4)
0.2597	1.31572	16.182(1)	11.828(1)	10.981(1)	94.761(6)	2094.5(3)
0.2798	1.37773	16.164(2)	11.821(1)	10.979(1)	94.872(8)	2090.1(4)

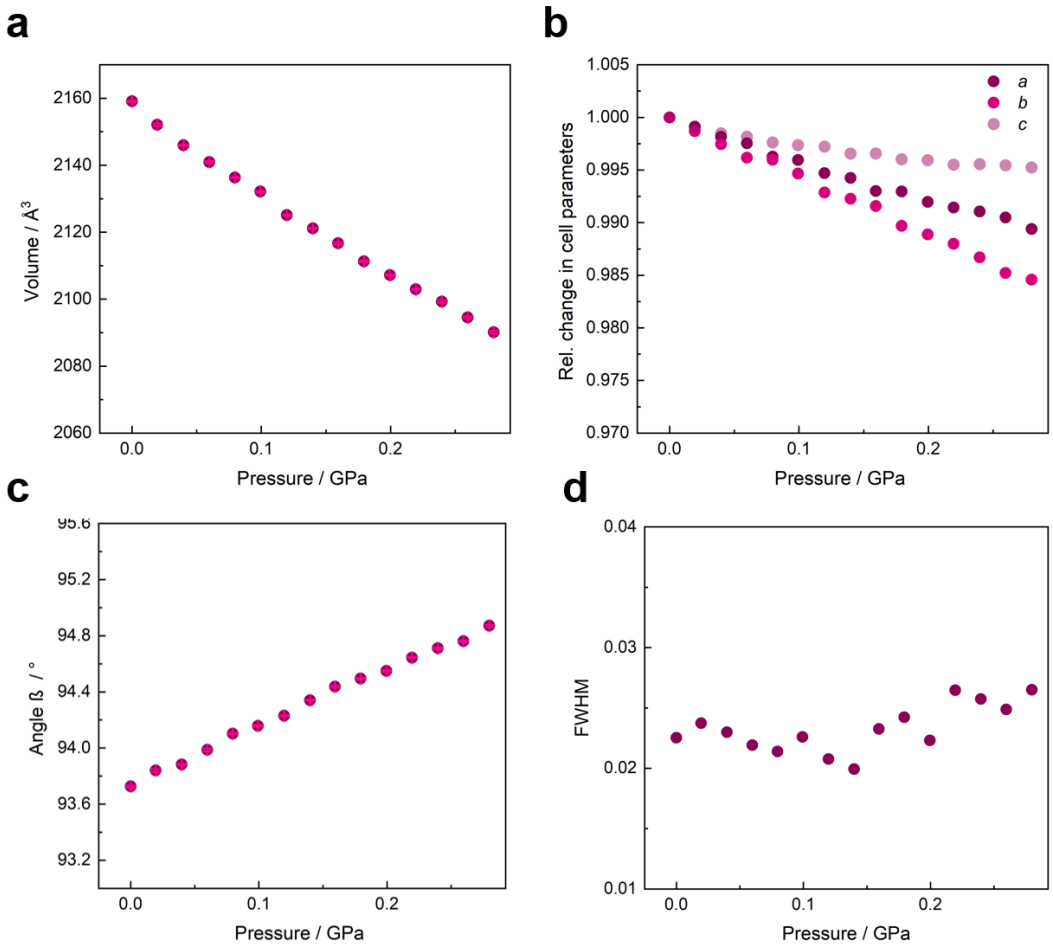

Figure S49: The evolution of unit cell volume (a), parameters (b), angle (c) and fwhm (d) as a function of hydrostatic compression until 0.28 GPa for [DIP]Ni(C_2N_3)$_3$.

Table S14: Overview of the unit cell parameters and volumes of $[PEP]_{1-x}[DPP^{i}]_xNi(C_2N_3)_3$ (with x = 1) obtained from Pawley fits of the HPPXRD data up to 0.4 GPa.

p / GPa	R_{wp}	a / Å	b / Å	c / Å	ß / °	V / Å^3
ambient	1.87831	17.306(2)	12.330(2)	10.482(1)	111.801(9)	2076.9(5)
0.0197	1.55011	17.299(2)	12.326(1)	10.472(1)	111.81(1)	2073.3(4)
0.0398	1.50488	17.266(1)	12.318(1)	10.453(1)	111.825(5)	2063.9(3)
0.0598	1.55784	17.247(1)	12.321(2)	10.442(2)	111.685(8)	2061.9(5)
0.0794	1.53154	17.241(1)	12.311(1)	10.429(1)	111.694(6)	2057.0(3)
0.0999	1.64929	17.224(1)	12.313(1)	10.421(1)	111.674(6)	2053.8(3)
0.1199	1.57977	17.219(1)	12.302(1)	10.412(1)	111.616(5)	2050.6(2)
0.1399	1.8763	17.206(2)	12.298(1)	10.406(1)	111.602(7)	2047.2(4)
0.1593	1.72529	17.196(2)	12.289(1)	10.393(1)	111.543(7)	2042.8(4)
0.1793	2.08452	17.189(2)	12.283(2)	10.383(1)	111.514(1)	2039.6(4)
0.1995	1.58205	17.179(1)	12.277(1)	10.365(1)	111.409(7)	2035.2(3)
0.2196	1.85094	17.171(2)	12.273(2)	10.359(1)	111.397(8)	2032.5(4)
0.2397	1.7263	17.158(2)	12.272(2)	10.345(1)	111.320(7)	2029.2(4)
0.2597	1.58309	17.139(1)	12.266(1)	10.335(1)	111.299(5)	2024.4(3)
0.2798	1.55227	17.131(1)	12.263(1)	10.328(1)	111.264(5)	2022.0(3)
0.2997	1.59153	17.126(1)	12.261(2)	10.316(1)	111.227(6)	2019.2(4)
0.3198	1.70593	17.108(1)	12.260(2)	10.308(1)	111.171(7)	2016.2(4)
0.3397	1.42475	17.098(1)	12.250(1)	10.306(1)	111.181(6)	2012.9(3)
0.3598	1.5862	17.089(2)	12.235(2)	10.297(1)	111.209(8)	2007.2(5)
0.3798	1.82388	17.087(2)	12.233(2)	10.284(1)	111.144(9)	2005.0(5)
0.3998	1.41571	17.082(1)	12.231(2)	10.272(1)	111.112(7)	2002.0(4)

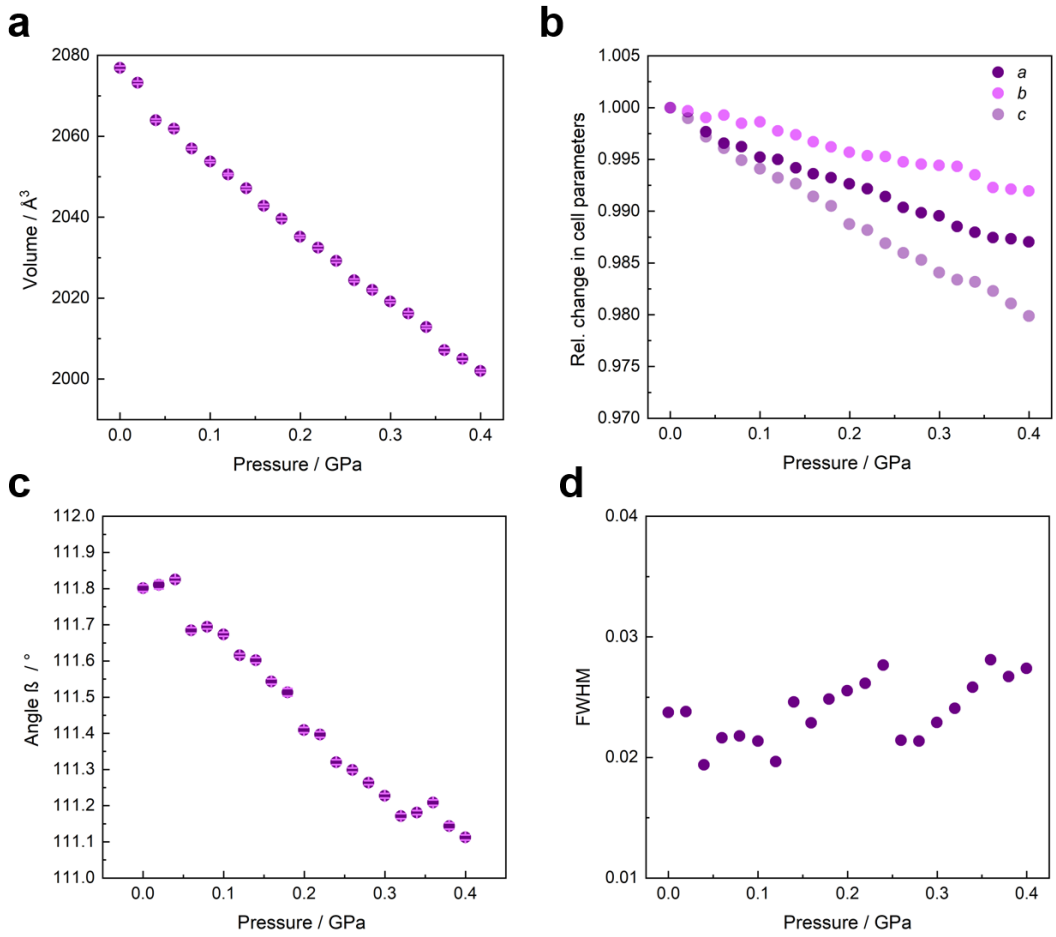

Figure S50: The evolution of unit cell volume (a), parameters (b), angle (c) and fwhm (d) as a function of hydrostatic compression until 0.4 GPa for $[PEP]_{1-x}[DPP^{\cdot}]_xNi(C_2N_3)_3$ (with x = 1).

We determined unit cell volumes, cell parameters, angles and fwhm of all solid solutions $[PEP]_{1-x}[DPP]_xNi(C_2N_3)_3$ (with x = 0.45, 0.69, 0.85 and 0.96) with standard deviations up to 0.4 GPa.

Table S15: Volume (*V*), angle (*ß*) and space group (*S.G.*) for all studied solid solutions $[PEP]_{1-x}[DPP]_xNi(C_2N_3)_3$ (with x = 0, 0.45, 0.69, 0.85, 0.96 and 1) obtained from Pawley fits of the ambient pressure PXRD data.

x	**0**	**0.45**	**0.69**	**0.85**	**0.96**	**1**
S.G.	*P2₁/c*	*P2₁/c*	*P2₁/c*	*P2₁/c*	*P2₁/c*	*C2/c*
ß / °	104.973(8)	104.59(1)	104.446(9)	104.295(6)	104.17(1)	111.790(9)
V / Å³	2029.7(4)	2042.5(7)	2054.3(4)	2060.6(4)	2072.6(5)	2076.9(4)

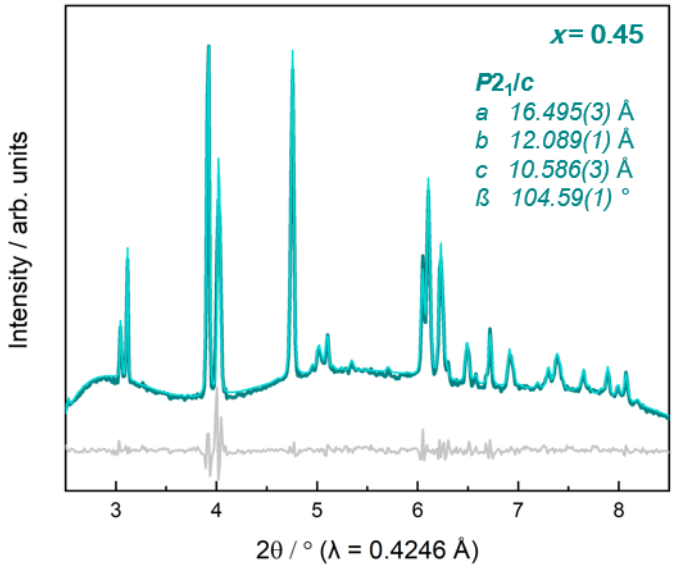

Figure S51: Pawley fit to synchrotron PXRD data at ambient pressure for $[PEP]_{1-x}[DPP]_xNi(C_2N_3)_3$ (with x = 0.45). Experimental data is shown as dark turquoise line, Pawley fit as light turquoise line, and the difference curve (fit – data) as grey line.

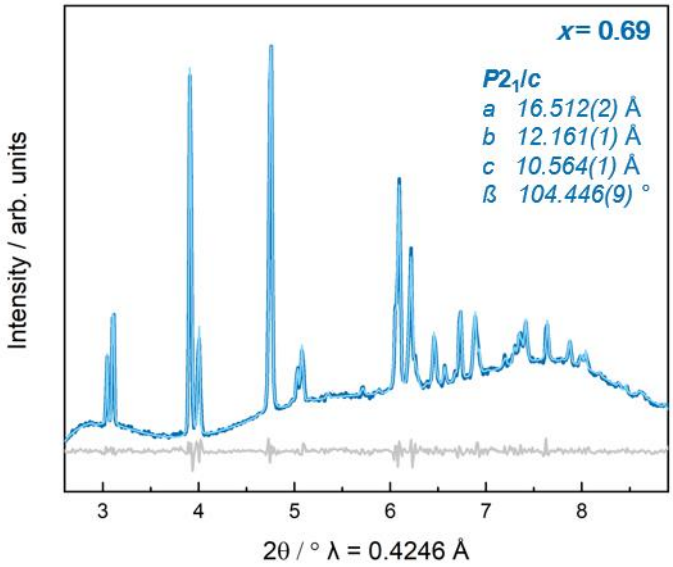

Figure S52: Pawley fit to synchrotron PXRD data at ambient pressure for $[PEP]_{1-x}[DPP]_xNi(C_2N_3)_3$ (with x = 0.69). Experimental data is shown as dark blue line, Pawley fit as light blue line, and the difference curve (fit – data) as grey line.

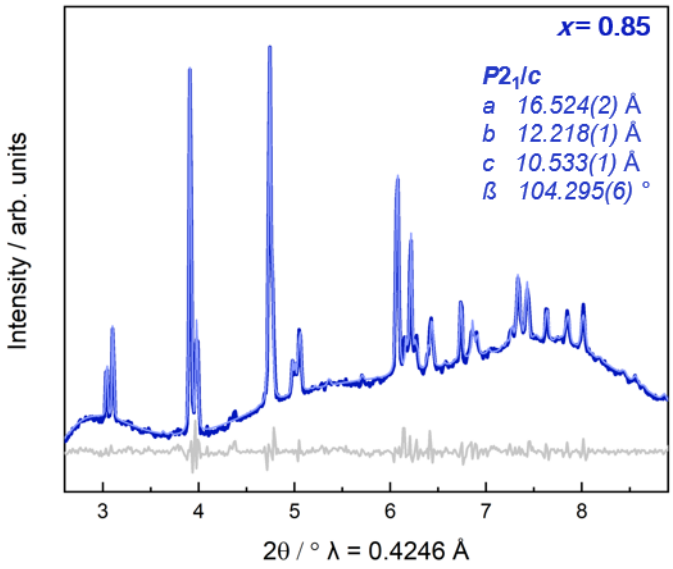

Figure S53: Pawley fit to synchrotron PXRD data at ambient pressure for $[PEP]_{1-x}[DPP]_xNi(C_2N_3)_3$ (with x = 0.85). Experimental data is shown as dark blue line, Pawley fit as light blue line, and the difference curve (fit – data) as grey line.

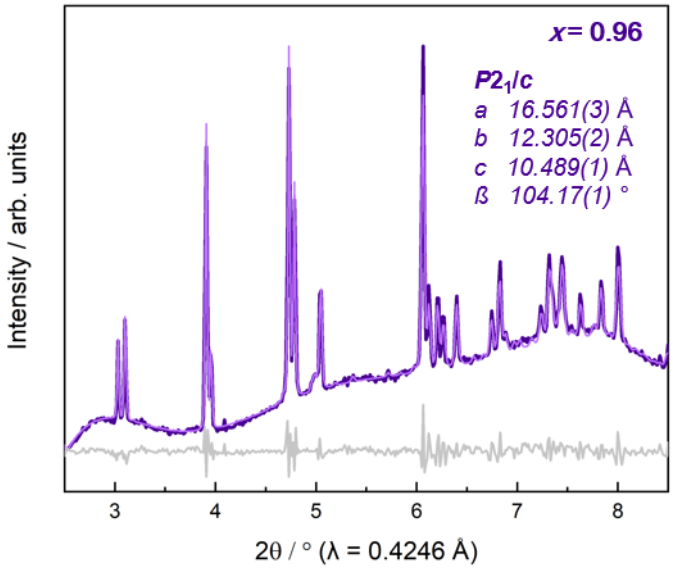

Figure S54: Pawley fit to synchrotron PXRD data at ambient pressure for $[PEP]_{1-x}[DPP]_xNi(C_2N_3)_3$ (with x = 0.96). Experimental data is shown as dark purple line, Pawley fit as light purple line, and the difference curve (fit – data) as grey line.

Table S16: Overview of the unit cell parameters and volumes of $[PEP]_{1-x}[DPP]_xNi(C_2N_3)_3$ (with x = 0.45) obtained from Pawley fits of the HPPXRD data up to 0.4 GPa.

p / GPa	R_{wp}	*a* / Å	*b* / Å	*c* / Å	ß / °	*V* / Å^3
ambient	3.41886	16.493(4)	12.089(1)	10.591(3)	104.58(2)	2043.6(9)
0.0194	2.73906	16.479(3)	12.070(2)	10.601(3)	104.59(1)	2040.4(7)
0.0398	2.53516	16.476(3)	12.058(2)	10.595(3)	104.63(1)	2036.6(7)
0.0598	1.63417	16.481(2)	12.040(1)	10.581(2)	104.757(9)	2030.4(4)
0.0795	2.13199	16.462(2)	12.005(1)	10.589(2)	104.720(9)	2024.0(5)
0.0998	2.2139	16.455(1)	11.998(1)	10.582(2)	104.778(9)	2020.2(5)
0.1199	2.30452	16.444(2)	11.995(1)	10.573(3)	104.82(2)	2016.1(7)
0.1399	2.44387	16.434(2)	11.980(2)	10.574(2)	104.886(9)	2011.9(6)
0.1593	2.35471	16.429(2)	11.970(2)	10.564(3)	104.918(9)	2007.5(7)
0.1794	1.92737	16.423(2)	11.959(1)	10.554(2)	105.006(7)	2002.3(5)
0.1996	2.103	16.413(2)	11.950(2)	10.551(2)	105.007(8)	1998.8(5)
0.2196	2.26691	16.403(2)	11.945(1)	10.547(2)	105.02(1)	1995.9(5)
0.2397	2.71957	16.385(3)	11.945(2)	10.543(3)	105.04(1)	1992.8(7)
0.2597	2.61814	16.381(3)	11.923(1)	10.539(3)	105.08(1)	1987.5(6)
0.2797	2.64843	16.378(2)	11.916(1)	10.528(3)	105.09(1)	1983.8(6)
0.2997	2.95571	16.369(3)	11.913(1)	10.522(3)	105.12(1)	1980.7(6)
0.3198	3.74298	16.355(4)	11.904(2)	10.518(3)	105.15(2)	1976.5(9)
0.3397	2.7522	16.351(3)	11.880(1)	10.518(3)	105.18(1)	1971.8(7)
0.3598	2.81426	16.341(3)	11.874(1)	10.515(3)	105.17(1)	1969.0(8)
0.3798	2.94866	16.332(4)	11.868(2)	10.511(4)	105.19(1)	1965.9(9)
0.3998	3.37968	16.323(4)	11.866(2)	10.504(2)	105.22(2)	1963.1(8)

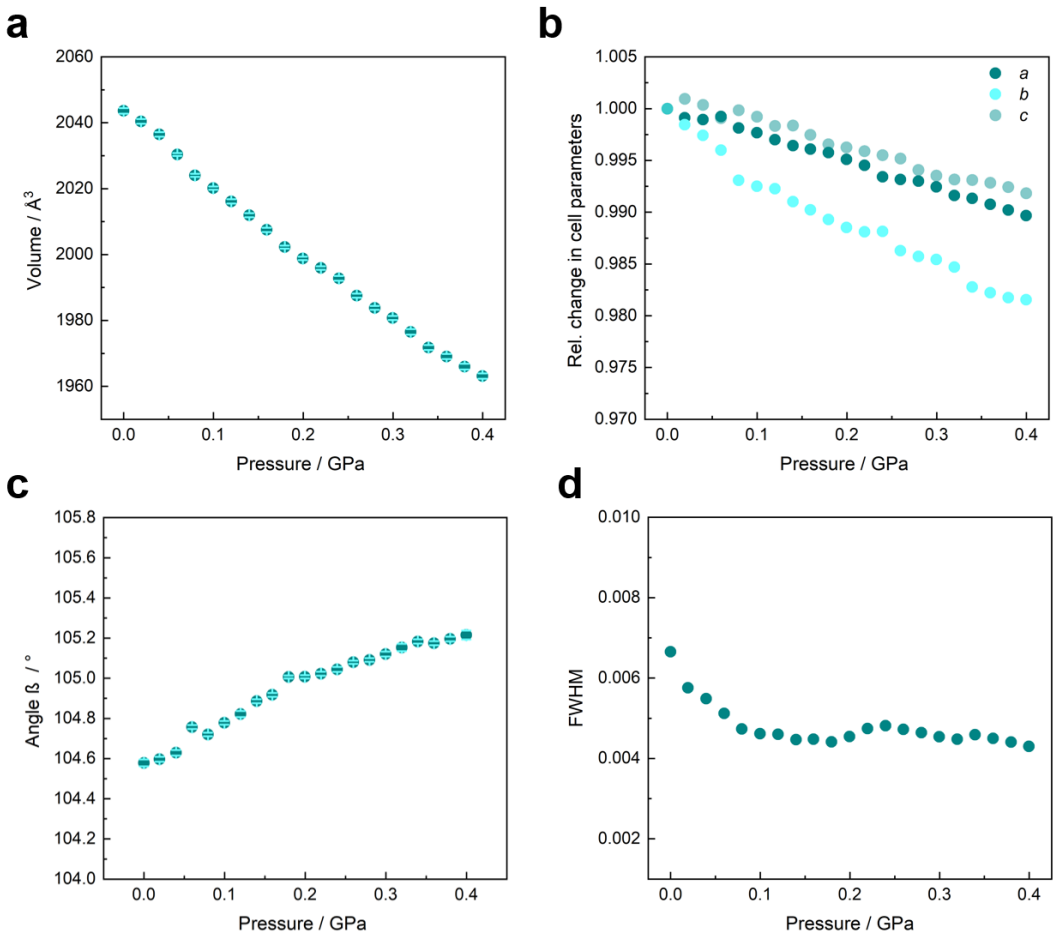

Figure S55: The evolution of unit cell volume (a), parameters (b), angle (c) and fwhm (d) as a function of hydrostatic compression until 0.4 GPa for $[PEP]_{1-x}[DPP]_xNi(C_2N_3)_3$ (with x = 0.45).

Table S17: Overview of the unit cell parameters and volumes of $[PEP]_{1-x}[DPP]_xNi(C_2N_3)_3$ (with x = 0.69) obtained from Pawley fits of the HPPXRD data up to 0.4 GPa.

p / GPa	R_{wp}	*a* / Å	*b* / Å	*c* / Å	ß / °	*V* / Å³
ambient	1.64036	16.512(2)	12.162(1)	10.564(1)	104.449(9)	2054.2(4)
0.0194	2.12111	16.494(3)	12.130(1)	10.569(1)	104.46(1)	2047.7(5)
0.0398	1.51596	16.492(2)	12.121(1)	10.562(1)	104.52(1)	2043.7(4)
0.0598	1.89252	16.481(3)	12.114(2)	10.558(3)	104.58(2)	2040.0(7)
0.0795	1.95462	16.485(2)	12.098(2)	10.554(2)	104.69(1)	2035.9(5)
0.0998	2.58579	16.475(3)	12.092(2)	10.548(2)	104.69(2)	2032.5(7)
0.1199	2.33094	16.458(3)	12.073(1)	10.549(2)	104.72(1)	2027.4(6)
0.1399	2.18724	16.447(2)	12.068(1)	10.541(2)	104.74(1)	2023.4(5)
0.1593	2.18776	16.442(2)	12.047(1)	10.539(2)	104.75(1)	2018.9(4)
0.1794	2.77814	16.433(2)	12.041(1)	10.533(1)	104.798(7)	2015.1(4)
0.1996	2.71619	16.425(2)	12.038(1)	10.524(1)	104.81(1)	2011.8(5)
0.2196	2.43792	16.416(2)	12.033(1)	10.515(2)	104.81(1)	2008.1(5)
0.2397	2.26279	16.409(3)	12.026(1)	10.509(1)	104.84(1)	2004.7(5)
0.2597	2.11972	16.401(2)	12.012(1)	10.506(1)	104.869(8)	2000.3(4)
0.2797	2.2051	16.392(2)	12.002(1)	10.499(1)	104.88(1)	1996.2(4)
0.2997	2.05911	16.385(3)	11.991(1)	10.494(1)	104.91(1)	1992.4(5)
0.3198	2.09096	16.376(2)	11.979(1)	10.487(1)	104.992(8)	1987.5(3)
0.3397	1.8482	16.373(1)	11.968(1)	10.484(1)	105.031(7)	1984.1(3)
0.3598	1.91531	16.369(1)	11.960(1)	10.481(1)	105.058(7)	1981.4(3)
0.3798	2.04331	16.362(1)	11.955(1)	10.474(1)	105.071(8)	1978.3(3)
0.3998	2.15417	16.356(1)	11.948(1)	10.468(2)	105.085(8)	1975.1(4)

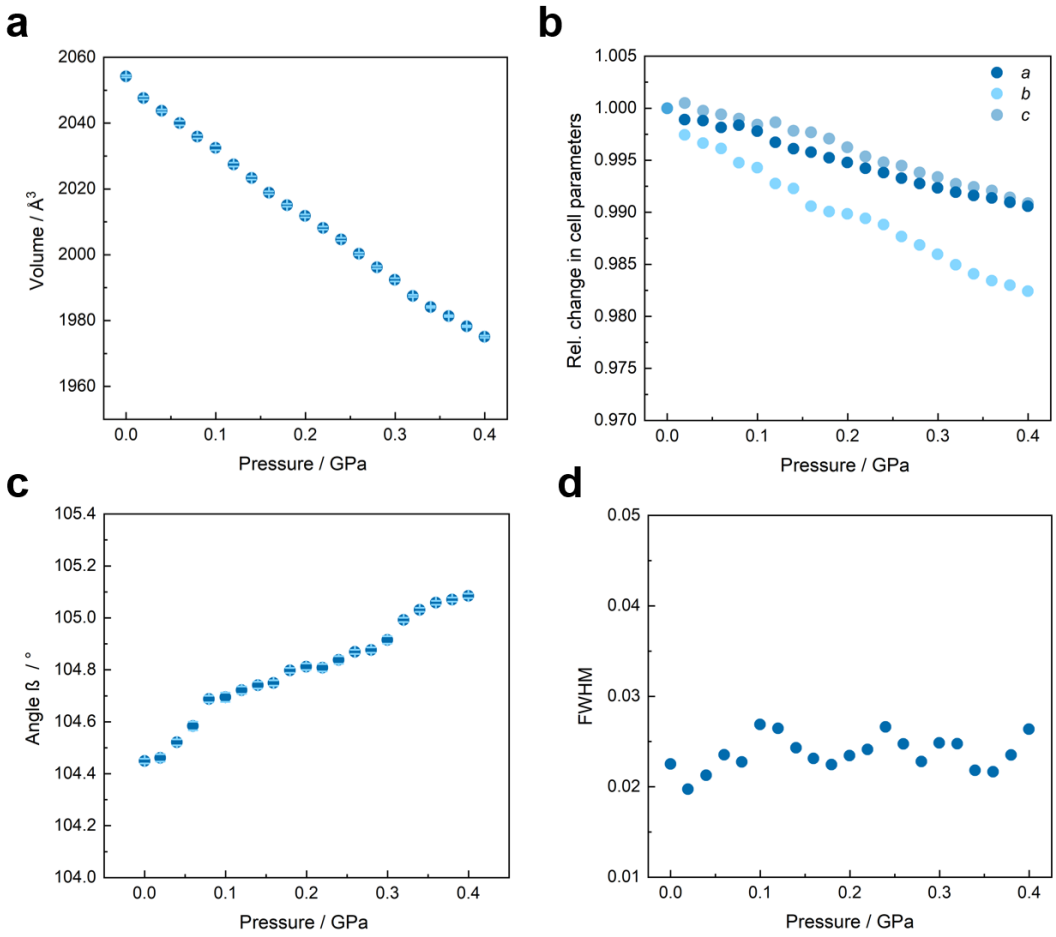

Figure S56: The evolution of unit cell volume (a), parameters (b), angle (c) and fwhm (d) as a function of hydrostatic compression until 0.4 GPa for $[PEP]_{1-x}[DPP]_xNi(C_2N_3)_3$ (with x = 0.69).

Table S18: Overview of the unit cell parameters and volumes of $[PEP]_{1-x}[DPP]_xNi(C_2N_3)_3$ (with x = 0.85) obtained from Pawley fits of the HPPXRD data up to 0.4 GPa (0.24 GPa was not used for further analysis of the *V(p)* data due to the R_{wp} value).

p / GPa	R_{wp}	*a* / Å	*b* / Å	*c* / Å	ß / °	*V* / Å³
ambient	2.08697	16.527(2)	12.221(1)	10.526(1)	104.298(6)	2060.1(4)
0.0194	2.00284	16.525(2)	12.217(1)	10.516(1)	104.318(7)	2057.1(4)
0.0398	2.2769	16.509(1)	12.213(1)	10.512(1)	104.356(6)	2053.2(4)
0.0598	2.20888	16.502(1)	12.206(1)	10.506(1)	104.427(6)	2049.3(4)
0.0795	2.15894	16.491(2)	12.197(1)	10.499(1)	104.485(7)	2044.8(4)
0.0998	2.01669	16.489(2)	12.170(1)	10.499(1)	104.518(7)	2039.8(3)
0.1199	2.0015	16.469(1)	12.161(1)	10.497(1)	104.521(9)	2035.1(4)
0.1399	2.65996	16.459(2)	12.158(1)	10.482(2)	104.536(9)	2031.1(5)
0.1593	1.78337	16.459(2)	12.131(1)	10.491(1)	104.54(1)	2027.7(4)
0.1794	2.20132	16.446(2)	12.126(1)	10.480(2)	104.600(8)	2022.5(4)
0.1996	2.30149	16.439(2)	12.122(1)	10.473(1)	104.611(7)	2019.4(4)
0.2196	2.08851	16.438(2)	12.114(1)	10.471(1)	104.653(7)	2017.4(4)
0.2597	1.92212	16.418(1)	12.079(1)	10.472(1)	104.714(8)	2008.6(4)
0.2797	2.21099	16.419(1)	12.069(1)	10.469(1)	104.750(9)	2006.1(4)
0.2997	1.87295	16.409(2)	12.051(1)	10.475(1)	104.77(1)	2002.8(4)
0.3198	1.97827	16.393(2)	12.042(1)	10.467(1)	104.77(1)	1997.9(4)
0.3397	2.05381	16.386(2)	12.039(1)	10.453(1)	104.73(1)	1994.3(3)
0.3598	2.26418	16.382(2)	12.031(1)	10.444(1)	104.71(1)	1991.1(4)
0.3798	2.42483	16.379(2)	12.025(1)	10.438(1)	104.807(9)	1987.7(4)
0.3998	1.96896	16.368(2)	12.008(1)	10.442(1)	104.85(1)	1983.8(4)

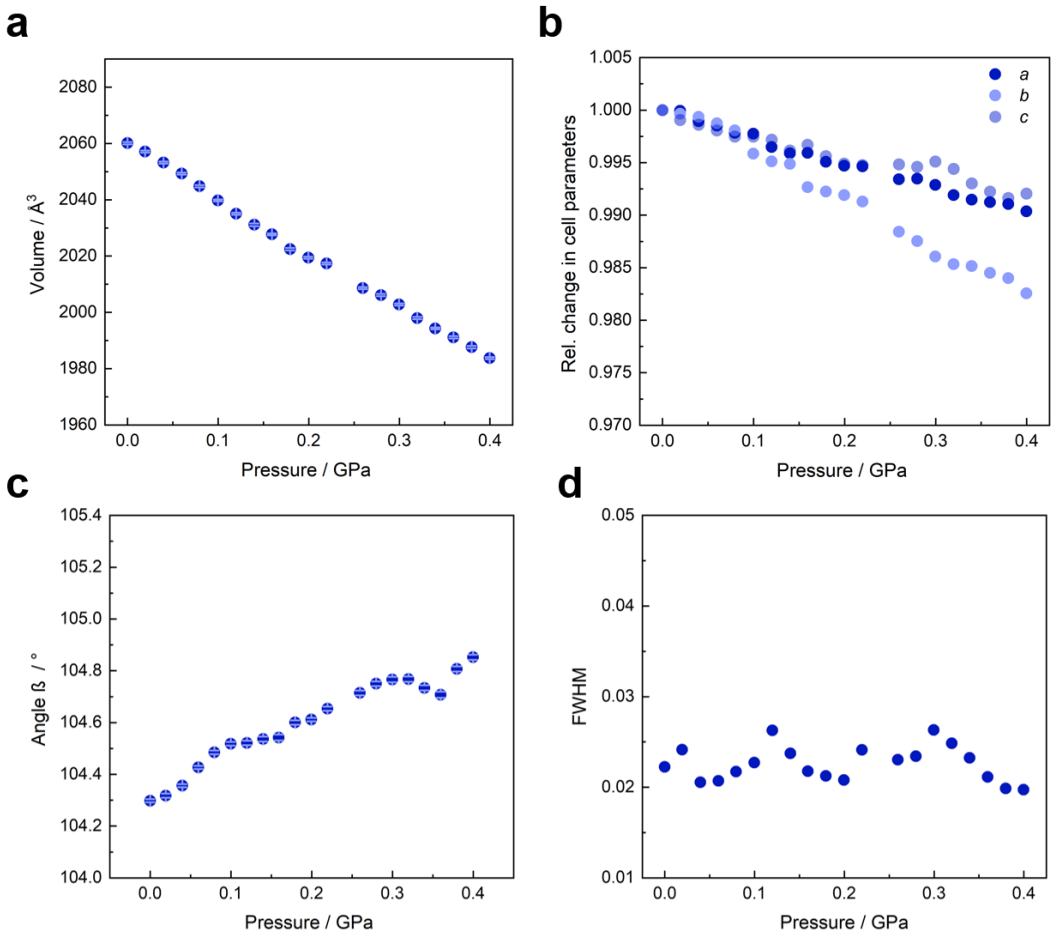

Figure S57: The evolution of unit cell volume (a), parameters (b), angle (c) and fwhm (d) as a function of hydrostatic compression until 0.4 GPa (without 0.24 GPa) for $[PEP]_{1-x}[DPP]_xNi(C_2N_3)_3$ (with x = 0.85).

Table S19: Overview of the unit cell parameters and volumes of $[PEP]_{1-x}[DPP]_xNi(C_2N_3)_3$ (with x = 0.96) obtained from Pawley fits of the HPPXRD data up to 0.4 GPa.

p / GPa	R_{wp}	*a* / Å	*b* / Å	*c* / Å	ß / °	*V* / Å^3
ambient	1.64612	16.559(1)	12.307(1)	10.488(1)	104.158(5)	2072.5(3)
0.0194	1.69902	16.547(1)	12.297(1)	10.478(1)	104.151(6)	2067.3(3)
0.0398	1.81976	16.535(1)	12.295(1)	10.469(1)	104.172(5)	2063.5(2)
0.0598	1.88344	16.529(1)	12.286(1)	10.466(1)	104.225(5)	2060.2(2)
0.0795	1.85947	16.524(1)	12.279(1)	10.455(1)	104.275(6)	2055.8(3)
0.0998	1.9511	16.522(1)	12.264(1)	10.447(1)	104.307(6)	2051.2(3)
0.1199	1.88938	16.516(1)	12.259(1)	10.438(1)	104.346(6)	2047.5(3)
0.1399	2.20804	16.509(2)	12.251(1)	10.430(1)	104.372(8)	2043.4(3)
0.1593	2.28441	16.506(2)	12.247(1)	10.423(1)	104.436(8)	2040.5(4)
0.1794	1.76172	16.490(2)	12.231(2)	10.422(1)	104.469(7)	2035.3(4)
0.1995	1.59709	16.486(1)	12.220(1)	10.418(1)	104.489(6)	2031.9(3)
0.2195	1.94357	16.474(2)	12.197(1)	10.418(1)	104.485(7)	2026.9(4)
0.2397	2.18806	16.459(2)	12.197(2)	10.408(1)	104.506(7)	2022.7(4)
0.2596	2.00007	16.446(2)	12.174(1)	10.412(1)	104.534(6)	2017.7(3)
0.2798	1.66219	16.445(1)	12.163(1)	10.408(1)	104.559(6)	2014.9(3)
0.2998	1.8349	16.438(2)	12.159(1)	10.402(1)	104.623(6)	2012.1(3)
0.3198	2.08299	16.422(1)	12.154(1)	10.403(1)	104.631(6)	2009.0(3)
0.3397	1.78474	16.419(1)	12.136(1)	10.402(1)	104.673(6)	2005.1(3)
0.3598	1.75927	16.416(1)	12.128(1)	10.401(1)	104.682(5)	2003.2(3)
0.3798	1.85032	16.404(1)	12.116(1)	10.390(1)	104.681(6)	1997.7(3)
0.3998	1.86516	16.397(1)	12.096(1)	10.389(1)	104.692(5)	1993.2(3)

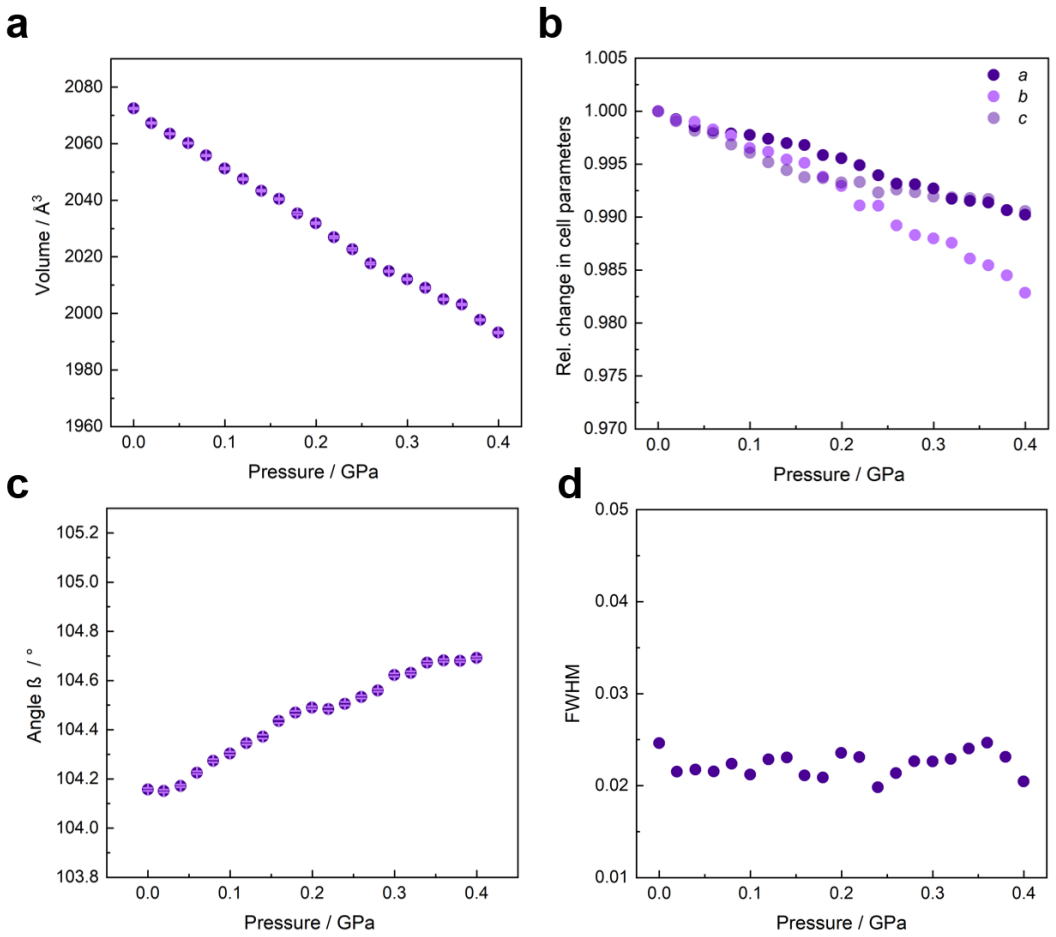

Figure S58: The evolution of unit cell volume (a), parameters (b), angle (c) and fwhm (d) as a function of hydrostatic compression until 0.4 GPa for $[PEP]_{1-x}[DPP]_xNi(C_2N_3)_3$ (with x = 0.96).

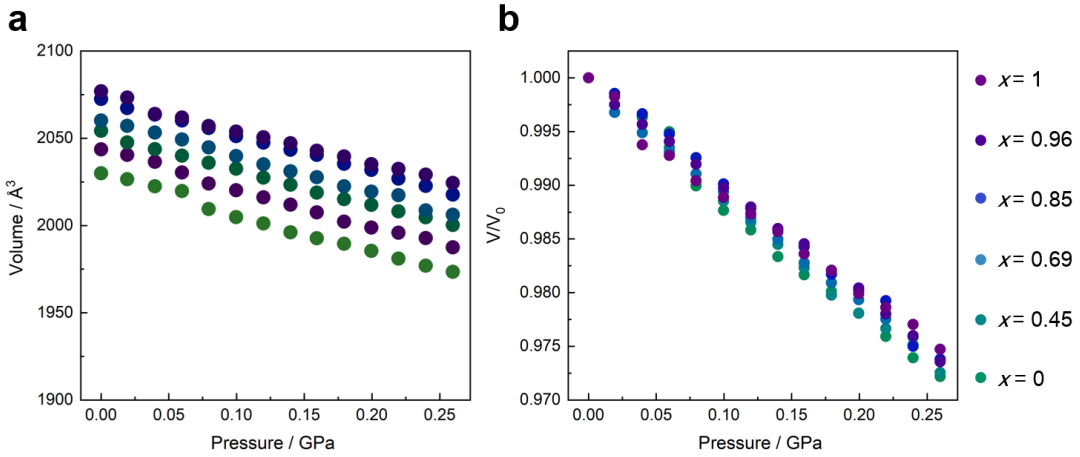

Figure S59: (a) The extracted unit cell volume including error bars as a function of pressure along the series of A-site solid solutions $[PEP]_{1-x}[DPP]_xNi(C_2N_3)_3$ with x = 0, 0.45, 0.69, 0.85, 0.96 and 1 and (b) relative volumes (V/V_0) as a function of hydrostatic compression until 0.26 GPa.

Rietveld refinements of solid solution samples. We have performed Rietveld refinements of the PXRD patterns at p = ambient with the goal of analysing tilt distortions across the solid solution $[PEP]_{1-x}[DPP]_xNi(C_2N_3)_3$ structures. This was done by using routines as implemented in TOPAS *v6* software.[10]

In detail, we have used the single crystal structure of $[PEP]Ni(C_2N_3)_3$ (monoclinic, $P2_1/c$) as a starting structural model. The unit cell parameters, as obtained from Pawley profile fits (Fig. S51-S54), were applied in the refinement (Rietveld method) and fixed. The structure models for $[PEP]_{1-x}[DPP]_xNi(C_2N_3)_3$ (x = 0.45, 0.69, 0.85 and 0.96) were refined against ambient pressure PXRD data (λ = 0.4246 Å) in the 2θ range from 2.5° to 9.0°. The peak shapes were refined using "TCHZ_Peak_Type" (modified Thompson-Cox-Hastings pseudo-Voigt function with U, V, W and Y as refined parameters). Notably, the A-site cation has been refined as a rigid body. The A-site cation, *i.e.* $[PEP]_{1-x}[DPP]_x^+$, was modelled by starting from the structure of $[PEP]^+$ and adding one carbon atom at a chemically sensible position with a fixed occupancy. During the refinement, the A-site cation was allowed to move and rotate freely without conformational changes. Furthermore, distance and angle restraints were applied within the $(C_2N_3)^-$ units, and NiN_6 octahedra as a chemically informed guess for guiding the refinement.

We expect that this approach won't deliver an accurate model of the A-site cation but will enable us to analyse structural distortions of the $[Ni(C_2N_3)_3]^-$ network to an accuracy level that we can estimate A_p and, overall, draw conclusions between A_p and B; however, we would like to mention that a custom-built high-pressure diffraction setup was applied for data collection, where the background (water, plastic capillary and diamond windows) and a relatively large capillary diameter of (~ 1mm) decreased the quality of PXRD data for a quantitative structural analysis based on a Rietveld refinement. Furthermore, non-uniform Bragg rings were visible on the 2D detector with spots of high intensities. By applying intensities cut-off during data integration, we attempted to reduce these intensity inaccuracies to a minimum; however, these are certainly additional error sources for wrong intensities. Lastly, we would like to mention that we have tried several approaches (with and without restraints, with several different rigid bodies, etc.), where all structural refinements led to A_p values between 2 – 4 for the solid solution series ($0 \leq x \leq 1$). Given the various sources for inaccuracies, however, we only provide structural models of the input for the ISODISTORT[15,16] analysis to avoid false interpretation, *i.e.* overinterpretation of the obtained structures.

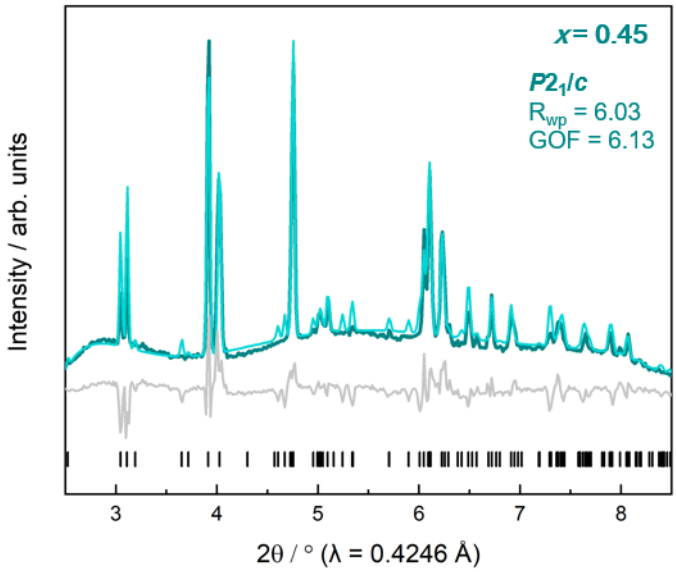

Figure S60: Rietveld fit of high-resolution PXRD data for $[PEP]_{1-x}[DPP]_xNi(C_2N_3)_3$ (with x = 0.45). Experimental data is shown as dark turquoise line, Rietveld fit as light turquoise line, reflection positions as black vertical tick marks, and the difference curve (fit – data) as grey line.

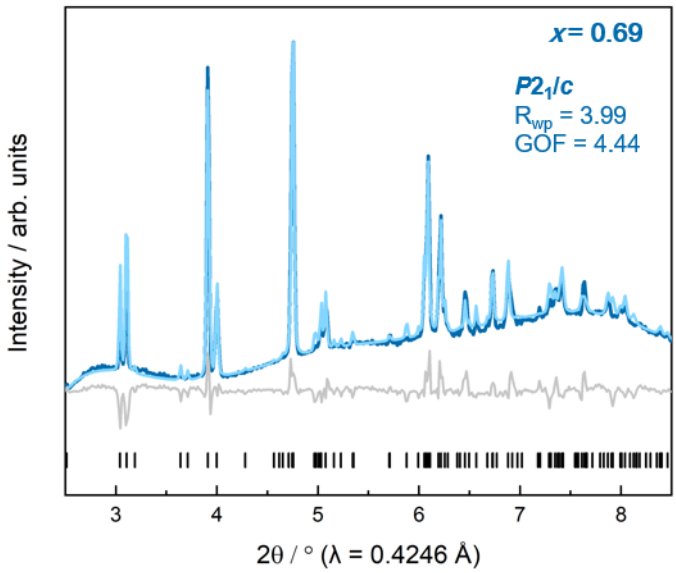

Figure S61: Rietveld fit of high-resolution PXRD data for $[PEP]_{1-x}[DPP]_xNi(C_2N_3)_3$ (with x = 0.69). Experimental data is shown as dark blue line, Rietveld fit as light blue line, reflection positions as black vertical tick marks, and the difference curve (fit – data) as grey line.

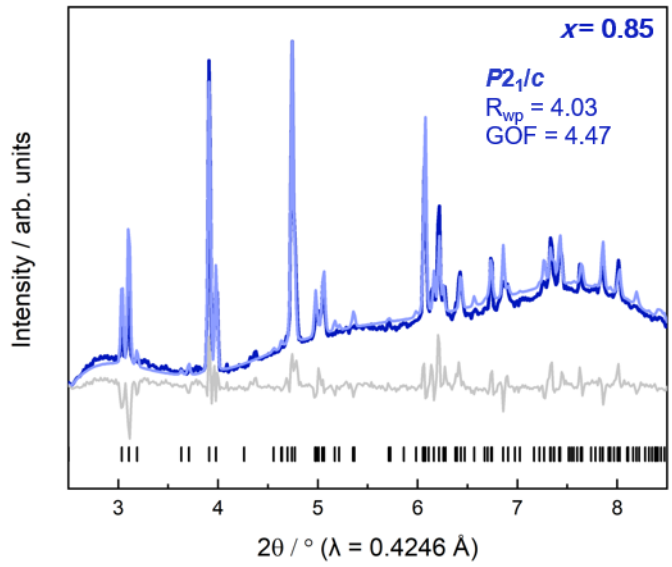

Figure S62: Rietveld fit of high-resolution PXRD data for $[PEP]_{1-x}[DPP]_xNi(C_2N_3)_3$ (with x = 0.85). Experimental data is shown as dark purple line, Rietveld fit as light blue purple, reflection positions as black vertical tick marks, and the difference curve (fit – data) as grey line.

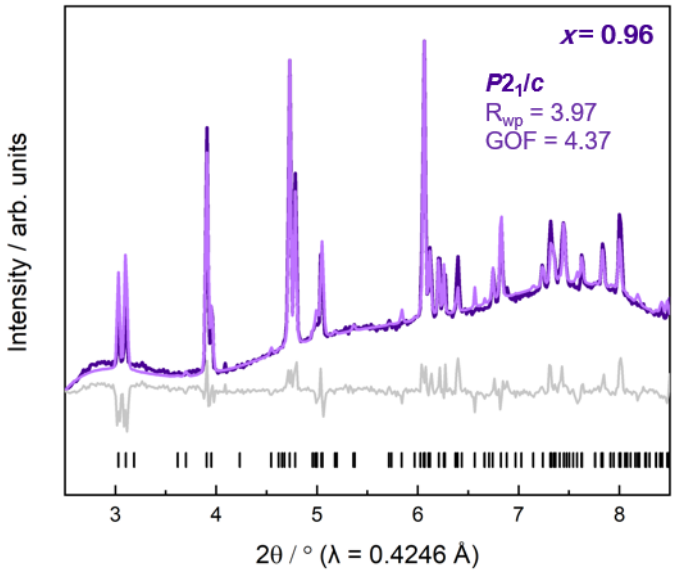

Figure S63: Rietveld fit of high-resolution PXRD data for $[PEP]_{1-x}[DPP]_xNi(C_2N_3)_3$ (with x = 0.96). Experimental data is shown as dark purple line, Rietveld fit as light purple line, reflection positions as black vertical tick marks, and the difference curve (fit – data) as grey line.

9. Bulk modulus

The unit cell volume changes obtained by HPPXRD throughout the hydrostatic regime were fitted to a 2nd order Birch-Murnaghan (B-M) equation of states using the software EoSFit7-Gui to estimate each material's bulk modulus (*B*).[17] The standard deviations of the volumes extracted by Pawley fits and a standard pressure error (p = ± 0.003 GPa) were included in the B-M fitting procedure. Additionally, 2nd and 3rd order calculations are given in Table S20 and Chapter 14 of this supporting information.

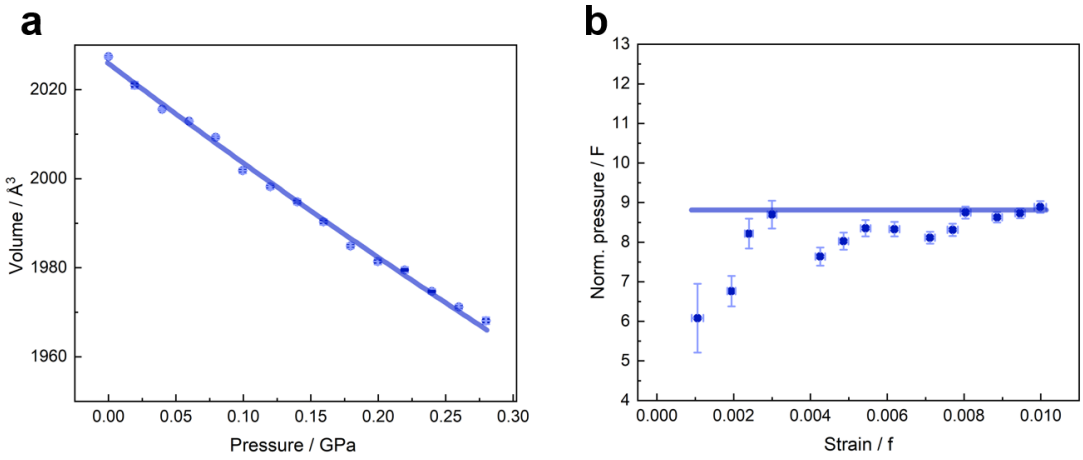

Figure S64: The change in unit cell volume of [DEP]Ni(C_2N_3)$_3$ is fitted using 2nd order B-M equation of state shown as blue line in the *V*(*p*)-plot (a) and *F*(*f*)-plot (b), confirming the applicability of the 2nd order fit to calculate *B*.

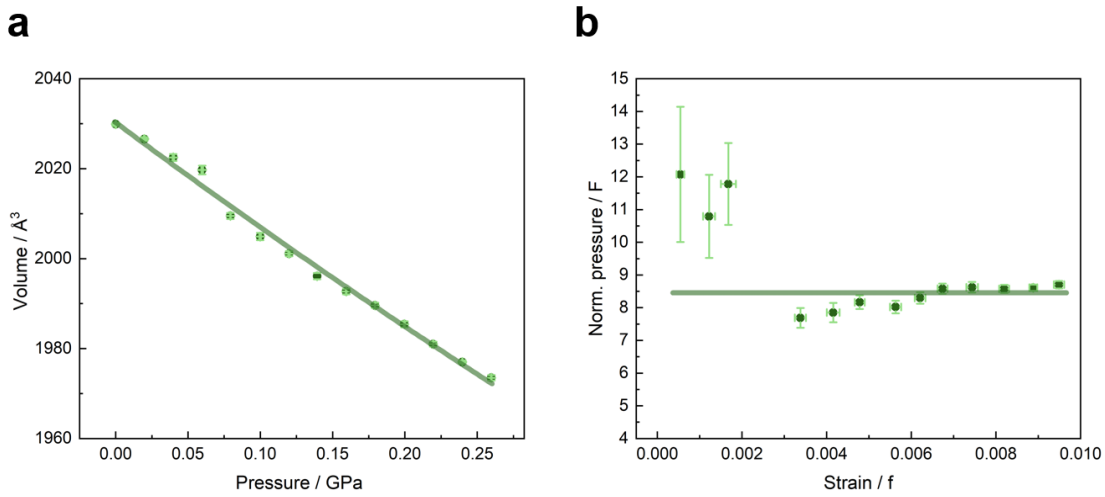

Figure S65: The change in unit cell volume of [PEP]Ni(C_2N_3)$_3$ (within the solid solution x = 0) is fitted using 2nd order B-M equation of state shown as green line in the *V*(*p*)-plot (a) and *F*(*f*)-plot (b), confirming the applicability of the 2nd order fit to calculate *B*.

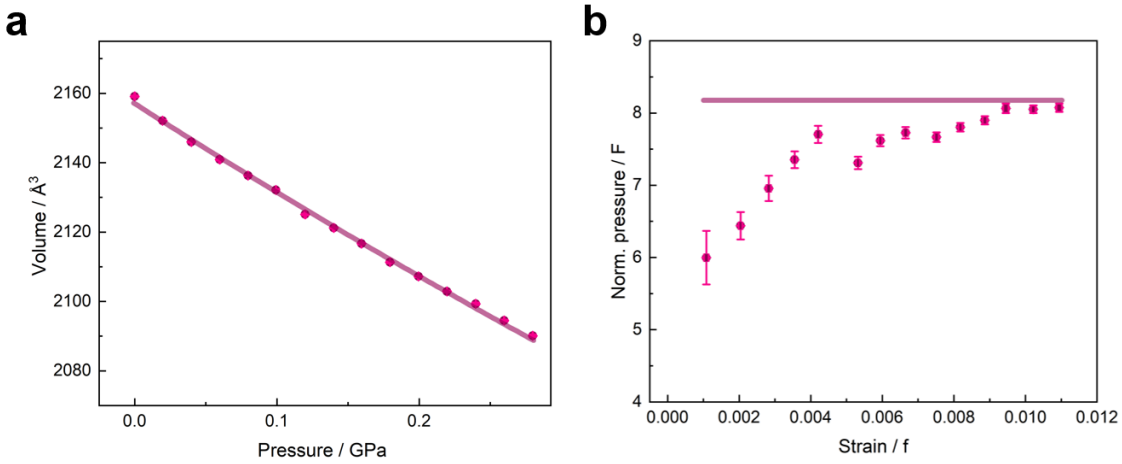

Figure S66: The change in unit cell volume of $[DIP]Ni(C_2N_3)_3$ is fitted using 2nd order B-M equation of state shown as blue line in the *V*(*p*)-plot (a) and *F*(*f*)-plot (b), confirming the applicability of the 2nd order fit to calculate *B*.

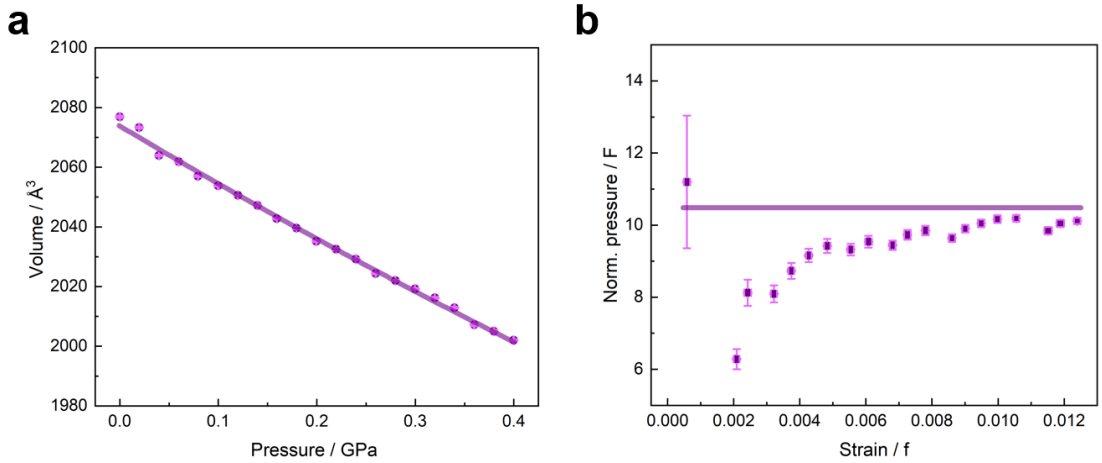

Figure S67: The change in unit cell volume of $[DPP]Ni(C_2N_3)_3$ (within the solid solution $x = 1$) is fitted using 2nd order B-M equation of state shown as blue line in the *V*(*p*)-plot (a) and *F*(*f*)-plot (b), confirming the applicability of the 2nd order fit to calculate *B*.

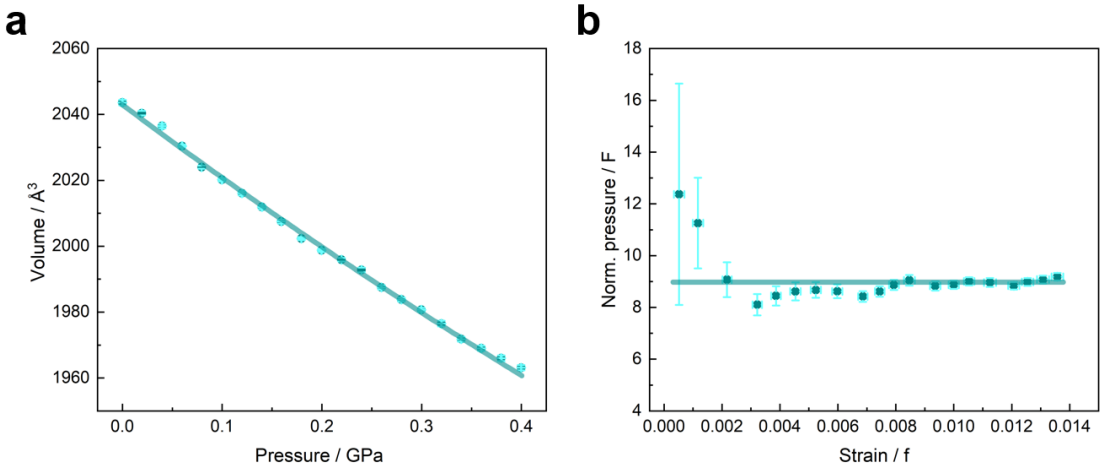

Figure S68: The change in unit cell volume of $[PEP]_{1-x}[DPP]_xNi(C_2N_3)_3$ (with $x = 0.45$) is fitted using 2nd order B-M equation of state shown as blue line in the *V*(*p*)-plot (a) and *F*(*f*)-plot (b), confirming the applicability of the 2nd order fit to calculate *B*.

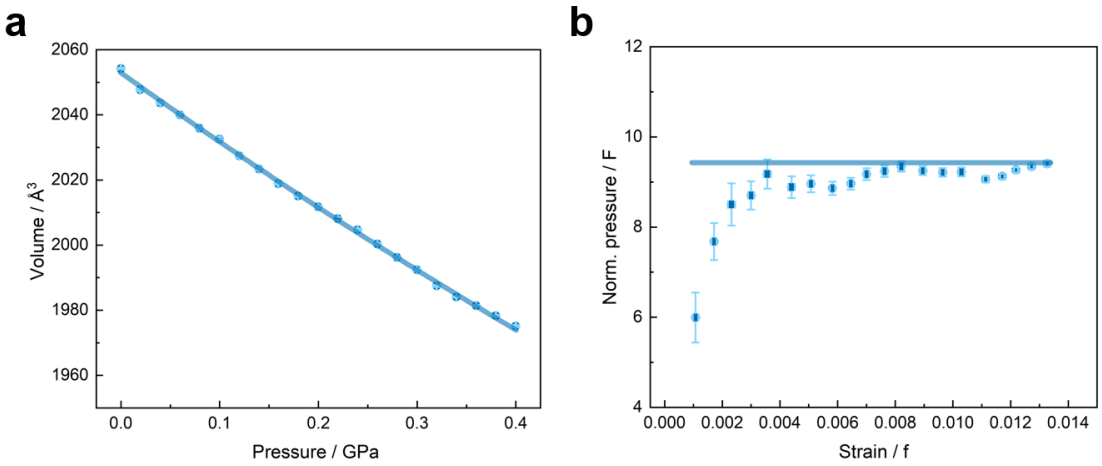

Figure S69: The change in unit cell volume of $[PEP]_{1-x}[DPP]_xNi(C_2N_3)_3$ (with $x = 0.69$) is fitted using 2nd order B-M equation of state shown as blue line in the $V(p)$-plot (a) and $F(f)$-plot (b), confirming the applicability of the 2nd order fit to calculate B.

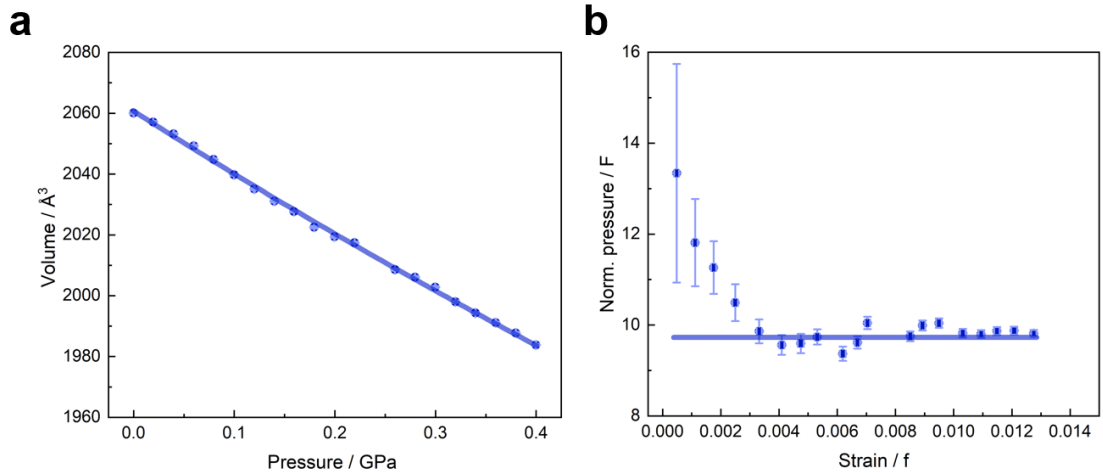

Figure S70: The change in unit cell volume of $[PEP]_{1-x}[DPP]_xNi(C_2N_3)_3$ (with $x = 0.85$) is fitted using 2nd order B-M equation of state shown as blue line in the $V(p)$-plot (a) and $F(f)$-plot (b), confirming the applicability of the 2nd order fit to calculate B.

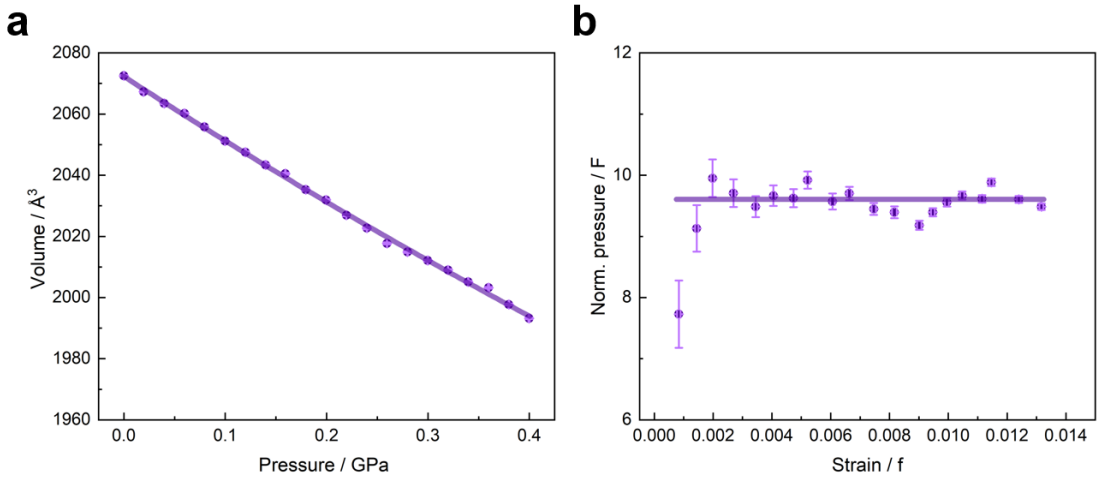

Figure S71: The change in unit cell volume of $[PEP]_{1-x}[DPP]_xNi(C_2N_3)_3$ (with $x = 0.96$) is fitted using 2nd order B-M equation of state shown as blue line in the $V(p)$-plot (a) and $F(f)$-plot (b), confirming the applicability of the 2nd order fit to calculate B.

Table S20: Bulk moduli (B) of $[PEP]_{1-x}[DPP]_xNi(C_2N_3)_3$ calculated from 2nd and 3rd order B-M equation of state fits to the HPPXRD data using EOSFit.

x	**0.45**	**0.69**	**0.85**	**0.96**
B (2nd) / GPa	8.9	9.4	9.7	9.6
σB (2nd) / GPa	0.1	0.1	0.1	0.1
V_0 (2nd) / Å^3	2042.9	2052.9	2060.7	2072.3
σV_0 (2nd) / Å^3	0.5	0.4	0.4	0.3
B (3rd) / GPa	7.7	9.1	9.3	9.6
σB (3rd) / GPa	0.3	0.3	0.3	0.3
V_0 (3rd) / Å^3	2045.1	2053.4	2061.3	2072.3
σV_0 (3rd) / Å^3	0.6	0.5	0.5	0.5

10. $Ni(dmgH)_2$ as reference material

We used $Ni(dmgH)_2$ (Nickel dimethylglyoxime) as reference material with well-known reported variable pressure behaviour to verify the applied pressure cell setup.[18,19] The sample was prepared similiarly as described above in Chapter 7, including HPPXRD experimental details. The HPPXRD data was collected in the same pressure regime (ambient pressure to 0.4 GPa) with the same pressure step size of 0.02 GPa (Fig. S72). Pawley refinement of the PXRD data at ambient pressure shows unit cell parameters *a* = 16.5717(6) Å, *b* = 10.4331(3) Å, *c* = 6.4621(2) Å and *V* = 1117.28(6) Å^3, which is in great accordance across variable pressure PXRD data with the reported structure.[20] The calculated bulk moduli, *i.e. B* = 8.43±0.15 GPa (derived from the 3rd order B-M equation of state fit) and *B* = 9.57±0.09 GPa (derived from the 2nd B-M order equation of state fit) are in line with reported data, confirming the applicability of the setup (Fig. S74).[21]

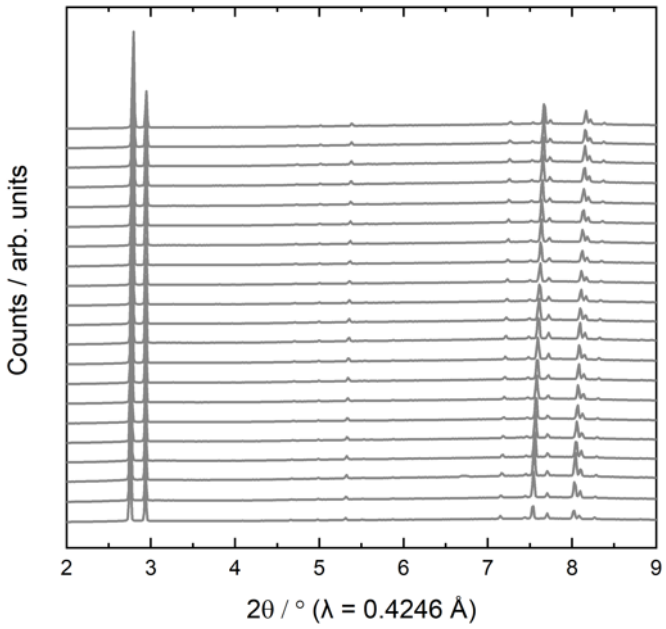

Figure S72: Collection of HPPXRD data of $Ni(dmgH)_2$ up to 0.4 GPa.

Table S21: Overview of the unit cell parameters and volumes $Ni(dmgH)_2$ obtained from Pawley fits of the HPPXRD data up to 0.4 GPa.

p/bar	R_{wp}	*a* / Å	*b* / Å	*c* / Å	*V* / Å^3
ambient	2.95280	16.5717(6)	10.4331(3)	6.4621(2)	1117.28(6)
0.0197	3.58596	16.5718(9)	10.4265(5)	6.4539(4)	1115.16(10)
0.0398	2.99285	16.5677(7)	10.4105(4)	6.4483(3)	1112.21(8)
0.0598	2.96639	16.5690(8)	10.4004(4)	6.4412(3)	1109.99(9)
0.0793	2.97736	16.5615(9)	10.3890(5)	6.4345(3)	1107.11(10)
0.0999	2.87619	16.5635(8)	10.3808(6)	6.4283(3)	1105.31(10)
0.1199	2.95232	16.5562(6)	10.3677(5)	6.4217(4)	1102.29(9)
0.1399	2.49250	16.5566(6)	10.3571(4)	6.4157(3)	1100.16(7)
0.1594	3.03165	16.5552(8)	10.3482(6)	6.4108(2)	1098.30(11)
0.1795	2.52741	16.5501(6)	10.3387(4)	6.4045(2)	1095.86(7)
0.1996	3.04075	16.5497(8)	10.3310(5)	6.3991(4)	1094.11(10)
0.2196	2.55868	16.5480(6)	10.3221(4)	6.3934(2)	1092.07(7)
0.2397	2.66187	16.5446(6)	10.3129(4)	6.3890(3)	1090.12(7)
0.2597	2.66473	16.5418(8)	10.3073(6)	6.3828(3)	1088.29(9)
0.2798	2.61754	16.5367(7)	10.2969(4)	6.3774(3)	1085.93(8)
0.2997	2.37638	16.5330(7)	10.2919(5)	6.3722(3)	1084.28(9)
0.3198	2.96540	16.5287(7)	10.2873(6)	6.3673(3)	1082.68(9)
0.3397	2.72334	16.5242(9)	10.2765(6)	6.3609(4)	1080.17(10)
0.3598	2.86385	16.5198(7)	10.2708(5)	6.3565(3)	1078.52(9)
0.3798	2.57641	16.5161(6)	10.2624(5)	6.3514(3)	1076.54(8)
0.3998	2.58556	16.5147(6)	10.2581(4)	6.3463(2)	1075.14(7)

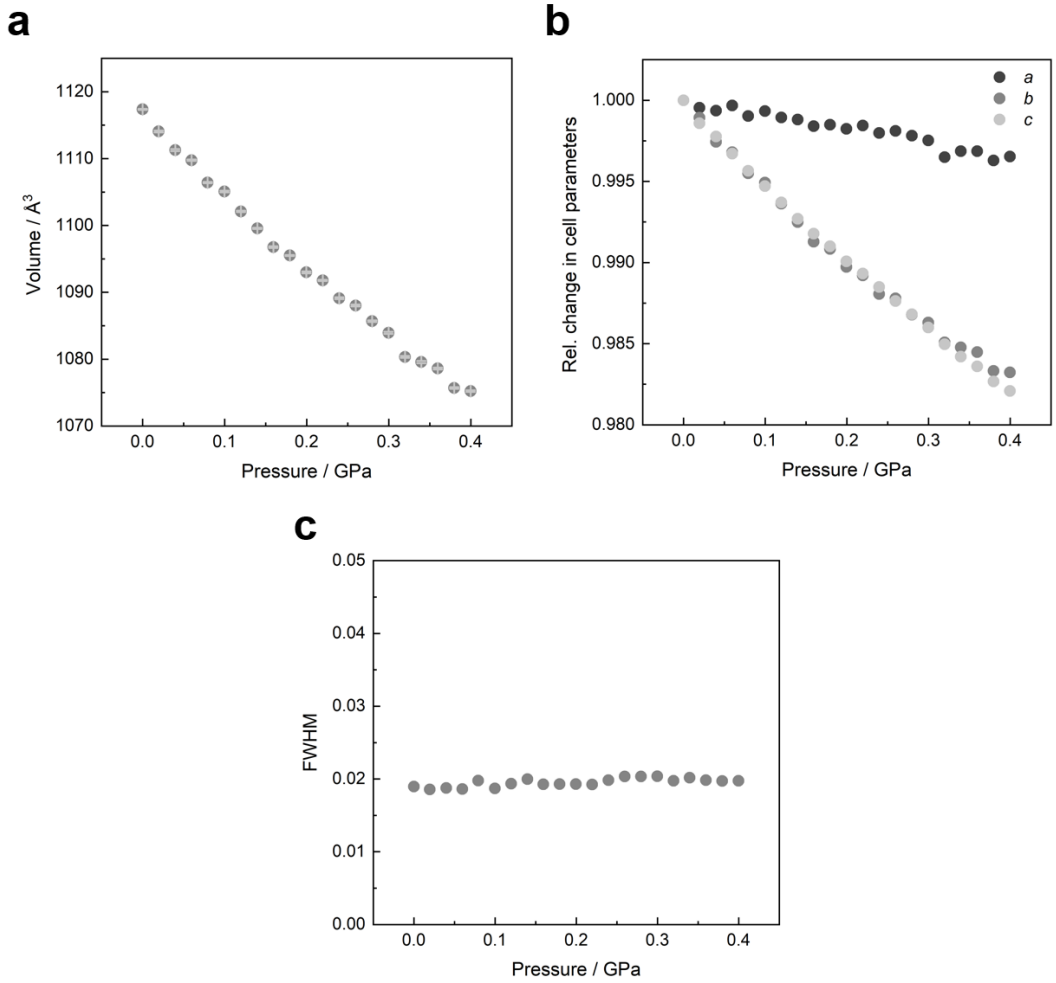

Figure S73: Change in volume (a), relative changes of the lattice parameters *a, b*, and *c* (b) and fwhm (c) for $Ni(dmgH)_2$ as a function of hydrostatic pressure.

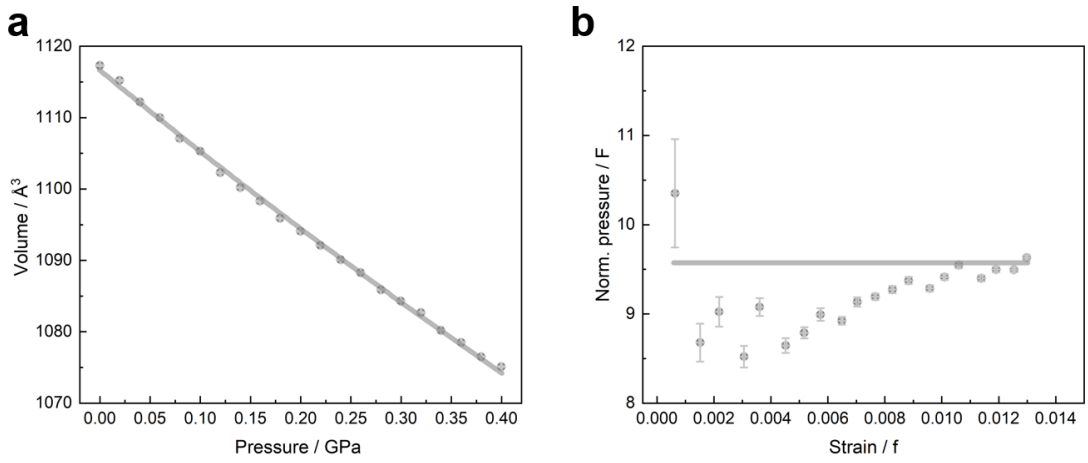

Figure S74: Variable pressure unit cell volume of $Ni(dmgH)_2$ is fitted using 2nd order B-M equation of state shown as grey line in the *V*(*p*)-plot (a) and *F*(*f*)-plot (b), confirming the applicability of the 3rd order fit to calculate *B*.

11. Tilt analysis of molecular perovskites

We used the web-based software tool ISODISTORT[15,16] to explore the active framework distortion modes of the $[Ni(C_2N_3)_3]^-$ framework. Herein, group theoretical analysis was applied to SCXRD data of 300 K to describe network distortions compared to a hypothetical cubic $[MX_3]^-$ network. In a first step, we created a hypothetical highly symmetric parent perovskite structure (aristotype) from two atom sites (***Ni*** *1.0 0.500000 0.50000 0.500000 Biso 1.000000 Ni* and ***N*** *1.0 0.250000 0.500000 0.500000 Biso 1.000000 N*) in *Pm*-3*m* cubic symmetry with unit cell parameters $a = b = c = 8$ Å and $\alpha = \beta = \gamma = 90$ °. This parent structure was used for all compounds and uploaded as a cif structure file to start the structural distortion mode analysis in ISODISTORT. After simplifying the low-symmetry crystal structure (hettotype) by removing the respective A^+ atom coordinates, resulting in the $[Ni(C_2N_3)_3]^-$ network structure composed of linear dicyanamide linkers, we subsequently uploaded all the distorted cif files to proceed with Method 4: "Mode decomposition of a distorted structure" implemented in ISODISTORT. Here, the mode decomposition of the distorted structure was analysed with respect to the cubic parent framework, identifying all active distortion modes corresponding to octahedral tilts and columnar shifts, as well as the overall distortion mode amplitude (A_p). These active distortions were assigned to a combination of irreducible representations (irreps) for conventional (R_5^- and M_2^+), unconventional tilts (Γ_4^+, X_5^- and M_5^+) and columnar shifts (Γ_5^+).

To showcase how A_p can be calculated, we present the procedure on the example of $[DPP]Ni(C_2N_3)_3$ in the following. In a first step, we simplified the cif file by removing all atom coordinates of $[DPP]^+$ and atom coordinates of $(C_2N_3)^-$ despite the N atoms of the NiN_6 octahedra. This cif file contains the distorted octahedral network structure from four atom sites (***Ni1*** *1.0 0.250000 0.250000 0.500000 Uiso 0.034915 Ni,* ***N1*** *1.0 0.1264(2) 0.2917(4) 0.4062(4) Uiso 0.058012 N,* ***N2*** *1.0 0.2812(2) 0.4008(4) 0.4472(4) Uiso 0.056581 N* and ***N4*** *1.0 0.2540(2) 0.6843(4) 0.1851(4) Uiso 0.056376 N*) with space group symmetry *C*2/*c* (*a* = 17.3196(5) Å, *b* = 12.3357(3) Å, *c* = 10.4909(3) Å and $\alpha = \gamma = 90$ ° $\beta = 111.917(1)$ °). Our next step was to start the analysis in the web-based software ISODISTORT and import our chosen high symmetry structure as a cif file. Important here, both cif files must contain the same types of atoms (*e.g.* ***Ni*** and ***N***). Then, we used Method 4: "Mode decomposition of a distorted structure", and uploaded our modified cif file of the distorted structure. Here, a specified sublattice basis must be provided, *i.e.* a set of basis vectors specified as a transformation matrix (a' (211) b' (01-1) and c' (011) for the crystallographic basis vectors of the modified cif file of $[DPP]Ni(C_2N_3)_3$). This basis is chosen with real-space lattice vectors of the distorted structure in relation to the lattice vectors of the undistorted structure. In this case, the "nearest-site method" to match each atom of the parent structure to the nearest atom in the distorted structure failed. Therefore, the "more robust but slower method: $d_{max} = 3$ Å" is chosen, mapping an atom in the

parent structure to every atom in the distorted structure within the chosen distance, *e.g.* here, 3 Å. The distortion page then appears, giving complete mode details with displacive mode amplitudes for each active irrep and an overall amplitude (A_p) normalised to the parent cell.[15,16]

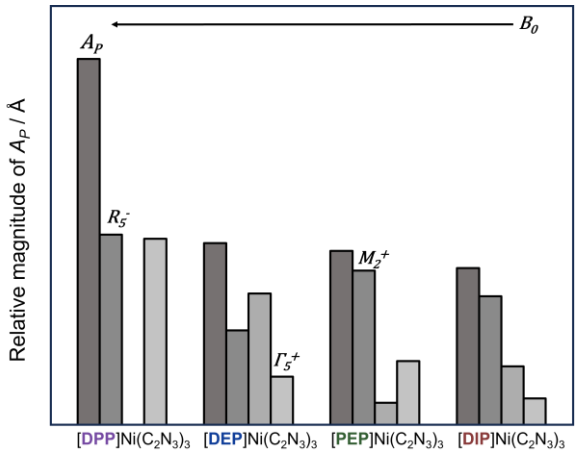

Figure S75: Relative magnitude of the overall parent-cell normalised amplitude (A_p) and the framework distortion modes with the largest amplitude associated with the irreducible representations (irreps) for conventional tilting (R_5^- and M_2^+) and columnar shifts (Γ_5^+) derived from the mode decomposition analysis of the distorted [A]Ni(C_2N_3)$_3$ structures along the series with varying A^+. The colour saturation corresponds to a higher magnitude within the respective primary order parameters.

Table S22: Group theoretical analysis of AMX_3 materials for the crystal structures obtained at 100 and 300 K, showing the strongest irreps from the left to right in order of decreasing relative magnitude and a possible set (not a unique set, one of several possible sets) of distortions accounting for the symmetry with the largest magnitude, giving the primary order parameters (POPs).

Compounds	**Temperature / K**	**Irreps**	**S.G.**	***POPs***
[DIP]Ni(C_2N_3)$_3$	100	$R_5^- M_2^+ M_5^+ \Gamma_5^+ X_5^- \Gamma_4^+$	$P2_1/c$	$\Gamma_4^+ R_3^- X_2^-$
[PEP]Ni(C_2N_3)$_3$	100	$R_5^- \Gamma_5^+ M_5^+ M_2^+ X_5^- \Gamma_4^+$	$P2_1/c$	$\Gamma_4^+ R_3^- X_2^-$
[DEP]Ni(C_2N_3)$_3$	100	$M_2^+ R_5^- \Gamma_5^+ X_5^- M_5^+ \Gamma_4^+$	$P2_1/c$	$\Gamma_4^+ R_3^- X_2^-$
[DPP]Ni(C_2N_3)$_3$	100	$\Gamma_4^+ R_5^- \Gamma_5^+$	$C2/c$	$\Gamma_4^+ R_3^-$
[DIP]Ni(C_2N_3)$_3$	300	$R_5^- M_2^+ M_5^+ X_5^- \Gamma_5^+ \Gamma_4^+$	$P2_1/c$	$\Gamma_4^+ R_3^- X_2^-$
[PEP]Ni(C_2N_3)$_3$	300	$R_5^- \Gamma_5^+ M_5^+ X_5^- M_2^+ \Gamma_4^+$	$P2_1/c$	$\Gamma_4^+ R_3^- X_2^-$
[DEP]Ni(C_2N_3)$_3$	300	$M_2^+ R_5^- \Gamma_5^+ X_5^- M_5^+ \Gamma_4^+$	$P2_1/c$	$\Gamma_4^+ R_3^- X_2^-$
[DPP]Ni(C_2N_3)$_3$	300	$\Gamma_4^+ R_5^- \Gamma_5^+$	$C2/c$	$\Gamma_4^+ R_3^-$

Table S23: Mode decomposition of the distorted [A]Ni(C_2N_3)$_3$ structures (obtained from SCXRD of 100 K) with displacive mode amplitudes displaying the parent-cell normalised amplitude (A_p) for each active mode. Displacive modes are given in Angstrom units.

	[DIP]Ni(C_2N_3)$_3$	**[PEP]Ni(C_2N_3)$_3$**	**[DEP]Ni(C_2N_3)$_3$**	**[DPP]Ni(C_2N_3)$_3$**
S.G.	*P2$_1$/c*	*P2$_1$/c*	*P2$_1$/c*	*C2/c*
R_5^-	1.67136	1.91172	1.17738	2.39294
M_2^+	0.74040	0.33760	1.64960	-
Γ_4^+	0.23561	0.12105	0.19103	2.86078
X_5^-	0.37122	0.25950	0.56322	-
M_5^+	0.69707	0.45264	0.44891	-
Γ_5^+	0.42617	0.83306	0.60846	2.09049
A_p / Å	2.08543	2.19858	2.27946	4.39524

Table S24: Mode decomposition of the distorted [A]Ni(C_2N_3)$_3$ structures (obtained from SCXRD of 300 K) with displacive mode amplitudes displaying the parent-cell normalised amplitude (A_p) for each active mode. Displacive modes are given in Angstrom units.

	[DIP]Ni(C_2N_3)$_3$	**[PEP]Ni(C_2N_3)$_3$**	**[DEP]Ni(C_2N_3)$_3$**	**[DPP]Ni(C_2N_3)$_3$**
S.G.	*P2$_1$/c*	*P2$_1$/c*	*P2$_1$/c*	*C2/c*
R_5^-	1.48752	1.78415	1.09421	2.20013
M_2^+	0.67680	0.25480	1.51840	-
Γ_4^+	0.10579	0.07128	0.14934	2.76733
X_5^-	0.33173	0.29571	0.54472	-
M_5^+	0.55209	0.31201	0.39960	-
Γ_5^+	0.30552	0.73871	0.55841	2.15237
A_p / Å	1.81201	2.01309	2.10231	4.23220

Table S25: Mode decomposition of the distorted $[Pr_3NMe]M(C_2N_3)_3$ structures with varying M^{2+} (for SCXRD data of 300 K accessed from the CCDC) with displacive mode amplitudes displaying the parent-cell normalised amplitude (A_p) for each active mode. Displacive modes are given in Angstrom units.

$[Pr_3NMe]M(C_2N_3)_3$ (reference[22])	**Mn^{2+}**	**Co^{2+}**	**Ni^{2+}**
CCDC number	2068843	2068842	2068716
S.G.	*Pnma*	*Pnma*	*Pnma*
R_5^-	1.68563	1.55756	1.50846
M_2^+	1.02984	0.99776	0.97728
Γ_4^+	-	-	-
X_5^-	1.04105	0.90069	0.84449
M_5^+	-	-	-
Γ_5^+	0.65560	0.57760	0.54528
POP	R_5^-	R_5^-	R_5^-
A_p / Å	2.35863	2.16636	2.09184

Table S26: Mode decomposition of the distorted $[PEP]_{1-x}[DPP]_xNi(C_2N_3)_3$ structures (obtained from Rietveld refinement data at ambient pressure) with displacive mode amplitudes displaying the parent-cell normalised amplitude (A_p) for each active mode. Displacive modes are given in Angstrom units.

x	**0.45**	**0.69**	**0.85**	**0.96**
S.G.	$P2_1/c$	$P2_1/c$	$P2_1/c$	$P2_1/c$
R_5^-	1.83227	1.97842	1.97021	2.70344
M_2^+	0.40800	0.62800	0.04000	0.22400
Γ_4^+	0.12445	0.16405	0.46386	0.09051
X_5^-	0.64647	0.62405	0.57822	0.26242
M_5^+	0.67090	0.68071	0.23786	0.51480
Γ_5^+	0.92413	0.88532	1.25633	0.89385
POP	R_5^-	R_5^-	R_5^-	R_5^-
A_p / Å	2.32350	2.46623	2.51368	2.93780

12. DFT calculations

All density functional theory (DFT) calculations were performed using the Gaussian16 software[23] at the B3LYP/6-311+G** level of theory to approximate the molecular geometry of A^+, *i.e.* molecular volumes (V_{A+}) and radius (r_{A+}), that were used in the model study of $[A]Ni(C_2N_3)_3$ materials. Therefore, the polarisable continuum model (PCM) was used and we chose the simplified crystal structure data (of 300 K) of $[A]Ni(C_2N_3)_3$ materials reduced to the atom coordinates of the organic A^+ molecules as a basis.

Table S27: DFT calculations using the PCM model based on SCXRD data from 300 K to describe the A^+ geometry and shape incorporated in the $[A]Ni(C_2N_3)_3$ series, including the volume (V^*_{A+}), the surface ($S_{m,A+}$), the surface derived from the volume of sphere ($S_{sp,A+}$) and the globularity factor ($G' = S_{sp,A+}/S_{m,A+}$).

A^+	**$[DIP]^+$**	**$[PEP]^+$**	**$[DEP]^+$**	**$[DPP]^+$**
V^*_{A+} / Å^3	270.986	242.984	235.791	271.266
$S_{m,A+}$ / Å^2	241.078	234.653	219.225	259.426
$S_{sp,A+}$ / Å^2	202.068	188.205	184.335	203.078
G'	0.838	0.802	0.841	0.783

13. PASCal calculations

To verify the calculation of *B* as described in Chapter 9, we used the web-based tool PASCal to fit the HPPXRD data to a 2nd and 3rd order B-M equation of states.[24] The calculated *B* of $Ni(dmgH)_2$, *i.e.* *B* = 9.26±0.12 GPa (derived from 2nd order B-M equation of state fit) and *B* = 7.89±0.28 GPa (derived from 3rd order B-M equation of state fit) are in line with the obtained values as described in Chapter 10.

Table S28: Bulk moduli (*B*) calculated from 2nd and 3rd order B-M equation of state fits to the HPPXRD data using PASCal.

	[DIP]Ni(C_2N_3)$_3$	**[PEP]Ni(C_2N_3)$_3$**	**[DEP]Ni(C_2N_3)$_3$**	**[DPP]Ni(C_2N_3)$_3$**
B (2nd) / GPa	8.2	8.4	8.9	10.4
σB (2nd) / GPa	0.1	0.2	0.2	0.1
V_0 (2nd) / Å^3	2156.9	2030.5	2025.5	2074.2
σV_0 (2nd) / Å^3	0.5	0.9	0.7	0.6
B (3rd) / GPa	7.8	6.7	7.4	9.3
σB (3rd) / GPa	0.3	0.8	0.5	0.5
V_0 (3rd) / Å^3	2157.6	2032.6	2027.2	2075.5
σV_0 (3rd) / Å^3	0.7	1.5	0.9	0.8

Table S29: Bulk moduli (*B*) of the solid solutions calculated from 2nd and 3rd order B-M equation of state fits to the HPPXRD data using PASCal.

x	**0.45**	**0.69**	**0.85**	**0.96**
B (2nd) / GPa	9.0	9.4	9.7	9.6
σB (2nd) / GPa	0.5	0.1	0.1	0.1
V_0 (2nd) / Å^3	2043.0	2052.8	2060.6	2072.4
σV_0 (2nd) / Å^3	0.5	0.3	0.4	0.6
B (3rd) / GPa	7.9	9.2	9.0	9.5
σB (3rd) / GPa	0.3	0.3	0.3	0.3
V_0 (3rd) / Å^3	2044.8	2053.1	2061.4	2072.4
σV_0 (3rd) / Å^3	0.6	0.5	0.6	0.6

14. Data overview of $[A]Ni(C_2N_3)_3$ materials

Table S30: Crystallographic data of the $[A]Ni(C_2N_3)_3$ series at 100 and 300 K. Differences of the A^+ were captured by the volume (V_{A+}) enclosed by the "promolecule electron density isosurface" and the globularity factor (G) obtained by Crystal Explorer17 based on 300 K SCXRD data. Additionally, the volume (V^*_{A+}) and surface ($S_{m,A+}$) of all A^+ were determined using Gaussian16 based on 300 K SCXRD data. Here, the surface was derived from the spherical volume ($S_{sp,A+}$) to obtain a second globularity factor defined as ($G' = S_{sp,A+}/S_{m,A+}$) to provide a comprehensive data set of A^+'s size and shape. The overall parent-cell normalised amplitude (A_p), as determined from group theoretical analysis, is given based on 300 K SCXRD data. The calculated bulk moduli (B, calculated from 2nd and 3rd order B-M equation of state fits *via* EOSFit) and volumes (V_0 at zero pressure and temperature obtained from experimental HPPXRD) are given below.

$[A]Ni(C_2N_3)_3$	A^+ = $[DIP]^+$	$[DEP]^+$	$[PEP]^+$	$[DPP]^+$
V_{A+} / Å^3	227.25	190.56	202.18	225.87
G	0.872	0.879	0.831	0.807
V^*_{A+} / Å^3	270.986	235.791	242.984	271.266
$S_{m,A+}$ / Å^2	241.078	219.225	234.653	259.426
$S_{sp,A+}$ / Å^2	202.068	184.335	188.205	203.078
G'	0.838	0.841	0.802	0.783
T/ K	100	100	100	100
Space group	$P2_1/c$	$P2_1/c$	$P2_1/c$	$C2/c$
a / Å	16.1247(8)	16.3161(17)	16.3743(14)	17.1198(15)
b / Å	11.9812(5)	12.1389(13)	11.9171(9)	12.3344(10)
c / Å	10.8829(5)	10.1679(11)	10.4761(8)	10.2007(9)
β / °	95.986(2)	101.691(3)	105.903(4)	110.800(3)
V / Å^3	2091.04(17)	1972.1(4)	1966.0(3)	2013.6(3)
A_p / Å	2.085	2.279	2.199	4.395
T / K	300	300	300	300
Space group	$P2_1/c$	$P2_1/c$	$P2_1/c$	$C2/c$
a / Å	16.346(2)	16.3871(7)	16.4756(7)	17.3196(5)
b / Å	12.0065(16)	12.2076(5)	11.9516(5)	12.3357(3)
c / Å	11.0462(17)	10.2673(4)	10.6587(4)	10.4909(3)
β / °	93.708(6)	100.250(2)	104.9160(10)	111.9170(10)
V_{cell} / Å^3	2163.4(5)	2021.16(14)	2028.08(14)	2079.38(10)
A_p / Å	1.812	2.102	2.013	4.232
B (2nd) / GPa	8.2±0.1	8.8±0.2	8.5±0.1	10.5±0.2
V_0 (2nd) / Å^3	2157.1±0.5	2025.9±0.2	2030.3±0.6	2073.8±0.6

B (3rd) / GPa	7.1±0.2	7.5±0.5	7.3±0.6	9.0±0.5
V_0 (3rd) / Å^3	2158.5±0.5	2027.2±0.8	2031.1±0.7	2075.6±0.8

15. References

1 S. Burger, S. Kronawitter, H. L. B. Boström, J. K. Zaręba and G. Kieslich, *Dalton Trans.*, 2020, **49**, 10740–10744.
2 Bruker AXS Inc., Madison, Wisconsin, USA, *APEX suite of crystallographic software*, **2015**, SADABS, Version 2014/15.
3 Bruker AXS Inc., Madison, Wisconsin, USA, *APEX suite of crystallographic software*, 2015, APEX 3, Version 2015–5.2.
4 Bruker AXS Inc., Madison, Wisconsin, USA, *APEX suite of crystallographic software*, 2014, SAINT, Version 8.34A.
5 G. M. Sheldrick, *Acta Crystallogr. C Struct. Chem.*, 2015, **71**, 3–8.
6 G. M. Sheldrick, *Acta Cryst. A*, 2015, **71**, 3–8.
7 O. V. Dolomanov, L. J. Bourhis, R. J. Gildea, J. A. K. Howard and H. Puschmann, *J. Appl. Crystallogr.*, 2009, **42**, 339–341.
8 K. Momma and F. Izumi, *J. Appl. Crystallogr.*, 2011, **44**, 1272–1276.
9 G. R. Fulmer, A. J. M. Miller, N. H. Sherden, H. E. Gottlieb, A. Nudelman, B. M. Stoltz, J. E. Bercaw and K. I. Goldberg, *Organometallics*, 2010, **29**, 2176–2179.
10 A. A. Coelho, *J. Appl. Crystallogr.*, 2018, **51**, 210–218.
11 N. J. Brooks, B. L. L. E. Gauthe, N. J. Terrill, S. E. Rogers, R. H. Templer, O. Ces and J. M. Seddon, *Rev. Sci. Instrum.*, 2010, **81**, 64103.
12 S. Dissegna, P. Vervoorts, C. L. Hobday, T. Düren, D. Daisenberger, A. J. Smith, R. A. Fischer and G. Kieslich, *J. Am. Chem. Soc*, 2018, **140**, 11581–11584.
13 J. Filik, A. W. Ashton, P. C. Y. Chang, P. A. Chater, S. J. Day, M. Drakopoulos, M. W. Gerring, M. L. Hart, O. V. Magdysyuk, S. Michalik, A. Smith, C. C. Tang, N. J. Terrill, M. T. Wharmby and H. Wilhelm, *J. Appl. Crystallogr.*, 2017, **50**, 959–966.
14 G. S. Pawley, *J. Appl. Crystallogr.*, 1981, **14**, 357–361.
15 B. J. Campbell, H. T. Stokes, D. E. Tanner and D. M. Hatch, *J. Appl. Crystallogr.*, 2006, **39**, 607–614.
16 H. T. Stokes, D. M. Hatch, and B. J. Campbell, *ISODISTORT, ISOTROPY Software Suite, iso.byu.edu*.
17 J. Gonzalez-Platas, M. Alvaro, F. Nestola and R. Angel, *J. Appl. Crystallogr.*, 2016, **49**, 1377–1382.
18 I. F. Bruce-Smith, B. A. Zakharov, J. Stare, E. V. Boldyreva and C. R. Pulham, *J. Phys. Chem. C*, 2014, **118**, 24705–24713.
19 K. Takeda, J. Hayashi, I. Shirotani, H. Fukuda and K. Yakushi, *Mol. Cryst. Liq.*, 2006, **460**, 131–144.
20 D. E. Williams, G. Wohlauer and R. E. Rundle, *J. Am. Chem. Soc*, 1959, **81**, 755–756.
21 K. Takeda, T. Sasaki, J. Hayashi, S. Kagami, I. Shirotani and K. Yakushi, *J. Phys.: Conf. Ser.*, 2010, **215**, 12065.
22 S. Burger, S. Grover, K. T. Butler, H. L. B. Boström, R. Grau-Crespo and G. Kieslich, *Mater. Horiz.*, 2021, **8**, 2444–2450.
23 M. J. Frisch, G. W. Trucks and H. B. Schlegel, *Gaussian 16 Rev. B.01*, Wallingford, CT, 2016.
24 M. J. Cliffe and A. L. Goodwin, *J. Appl. Crystallogr.*, 2012, **45**, 1321–1329.